MAY 2 1991

ORNL
MASTER COPY

ORNL/ATD-42

ornl

OAK RIDGE
NATIONAL
LABORATORY

MARTIN MARIETTA

COMPOSITE HEAT DAMAGE SPECTROSCOPIC ANALYSIS

PART 1. MECHANICAL TESTING OF IM6/3501-6 LAMINATES

PART 2. LASER-PUMPED FLUORESCENCE SPECTROSCOPIC STUDIES ON IM6/3501-6 LAMINATES

PART 3. DIFFUSE REFLECTANCE INFRARED FOURIER TRANSFORM SPECTROSCOPIC STUDIES ON IM6/3501-6 LAMINATES

C. J. Janke
J. D. Muhs
E. A. Wachter
R. E. Ziegler

Oak Ridge National Laboratory

G. L. Powell
N. R. Smyrl

Oak Ridge Y-12 Plant

H. E. Philpot

Oak Ridge Gaseous Diffusion Plant

September 1990

OPERATED BY
MARTIN MARIETTA ENERGY SYSTEMS, INC.
FOR THE UNITED STATES
DEPARTMENT OF ENERGY

This report has been reproduced directly from the best available copy.

Available to DOE and DOE contractors from the Office of Scientific and Technical Information, P.O. Box 62, Oak Ridge, TN 37831; prices available from (615) 576-8401, FTS 626-8401.

Available to the public from the National Technical Information Service, U.S. Department of Commerce, 5285 Port Royal Rd., Springfield, VA 22161.
NTIS price codes—Printed Copy: A05 Microfiche A01

This report was prepared as an account of work sponsored by an agency of the United States Government. Neither the United States Government nor any agency thereof, nor any of their employees, makes any warranty, express or implied, or assumes any legal liability or responsibility for the accuracy, completeness, or usefulness of any information, apparatus, product, or process disclosed, or represents that its use would not infringe privately owned rights. Reference herein to any specific commercial product, process, or service by trade name, trademark, manufacturer, or otherwise, does not necessarily constitute or imply its endorsement, recommendation, or favoring by the United States Government or any agency thereof. The views and opinions of authors expressed herein do not necessarily state or reflect those of the United States Government or any agency thereof.

ORNL/ATD-42

COMPOSITE HEAT DAMAGE SPECTROSCOPIC ANALYSIS

PART 1. MECHANICAL TESTING OF IM6/3501-6 LAMINATES

PART 2. LASER-PUMPED FLUORESCENCE SPECTROSCOPIC STUDIES ON IM6/3501-6 LAMINATES

PART 3. DIFFUSE REFLECTANCE INFRARED FOURIER TRANSFORM SPECTROSCOPIC STUDIES ON IM6/3501-6 LAMINATES

C. J. Janke
J. D. Muhs
E. A. Wachter
R. E. Ziegler

Oak Ridge National Laboratory

G. L. Powell
N. R. Smyrl

Oak Ridge Y-12 Plant

H. E. Philpot

Oak Ridge Gaseous Diffusion Plant

Date Published–September 1990

MARTIN MARIETTA ENERGY SYSTEMS, INC.
operating the
Oak Ridge National Laboratory Oak Ridge Y-12 Plant
Oak Ridge Gaseous Diffusion Plant
for the
U.S. DEPARTMENT OF ENERGY
under contract DE-AC05-84OR21400

CONTENTS

LIST OF FIGURES iv

LIST OF TABLES vii

ABSTRACT viii

SUMMARY 1

INTRODUCTION 2

TGDDM-DDS CURE REACTIONS 3

TGDDM-DDS THERMAL OXIDATIVE DEGRADATION REACTIONS 4

MOISTURE EFFECTS ON POLYMER-MATRIX COMPOSITES 5

PART 1. MECHANICAL TESTING OF IM6/3501-6 LAMINATES 7

SUMMARY 7

EXPERIMENTAL 7
SAMPLE MATERIALS 7
PANEL FABRICATION 7
PRECONDITIONING OF SPECIMENS 8
HEAT EXPOSURE OF SPECIMENS 10

MECHANICAL PROPERTY TESTING 10
COMPRESSION TESTING 10
SHORT-BEAM-SHEAR TESTING 11
PERCENT WEIGHT LOSS TESTING 11
FLEXURAL TESTING 14
LAMINATE-THICKNESS-MEASUREMENT TESTING 14
SHORE-D-HARDNESS TESTING 14

STATISTICAL t TESTING 15

RESULTS AND DISCUSSION 15
STATISTICS 15
SHORE D AND COMPRESSION 15
SHORT-BEAM SHEAR AND FLEXURE 16
VISUAL/MICROSCOPIC/THICKNESS 17
PERCENT WEIGHT LOSS 17
USE OF COATINGS ON POLYMER-MATRIX COMPOSITES 18

PART 2: LASER-PUMPED FLUORESCENCE 20

SUMMARY 20

EXPERIMENTAL 26

RESULTS AND DISCUSSION 27

CONCLUSIONS 29

PART 3: DIFFUSE REFLECTANCE INFRARED FOURIER TRANSFORM .. 29

INTRODUCTION 29

EXPERIMENTAL 30

EVACUABLE CELL RESULTS ON A SINGLE SAMPLE 31

BARREL ELLIPSOID RESULTS ON 0° IM6/3501-6 FLEXURAL SPECIMENS 33

CONCLUSIONS 34

RECOMMENDATIONS FOR FUTURE WORK 34

REFERENCES 74

LIST OF FIGURES

		Page
1	Panel fiber orientation	36
2	Geometry of specimens for (a) compression, (b) flexure/shore-D, (c) short-beam-shear testing	37
3	Preconditioning profile of wet and dry IM6/3501-6 specimens, panel 5 data	38
4	Specimen heating chamber	39
5	Close-up view of specimen heating chamber	40
6	Temperature monitoring of IM6/3501-6 specimens during heat exposure	41
7	Testing procedures for compression, short beam shear and flexure	42
8	Test results for IM6/3501-6: ASTM D3410	43
9	Test results for IM6/3501-6: ASTM D2344	44
10	Test results for IM6/3501-6: ASTM D2344	45
11	Test results for IM6/3501-6: weight loss	46
12	Test results for IM6/3501-6: ASTM D790	47
13	Test results for IM6/3501-6: ASTM D790	48
14	Test results for IM6/3501-6: thickness	49
15	Test results for IM6/3501-6: ASTM D2240	50
16	Laser-pumped fluorescence using 482.5-nm excitation	51
17	Laser-pumped fluorescence using 482.5-nm excitation	52
18	Laser-pumped fluorescence using 488.0-nm excitation	53
19	Laser-pumped fluorescence using 488.0-nm excitation	54
20	Laser-pumped fluorescence using 488.0-nm excitation	55

Page

21 Laser-pumped fluorescence using 488.0-nm excitation 56

22 Laser-pumped fluorescence using 488.0-nm excitation 57

23 Optical geometries used for laser-pumped fluorescence 58

24 ORNL field laser Spectrometer system 59

25 Potential laser-pumped fluorescence instruments 60

26 An evacuable cell for use with a Harrick DRA-3CQ praying mantis diffuse reflectance cell. 61

27 An evacuable cell for use with a Harrick DRA-3CQ praying mantis diffuse reflectance cell showing the sample stage through the beam exit window. 62

28 An evacuable cell for use with a Harrick DRA-3CQ praying mantis diffuse reflectance cell mounted in the praying-mantis sample compartment optics 63

29 An artist concept of the barrel-ellipsoid diffuse-reflectance inspection accessory 64

30 A diffuse reflectance spectrum of a 0° IM6/3501-6 flexural specimen using the barrel ellipsoid inspection accessory using resin-free IM6 graphite fibers as a background spectrum 65

31 Diffuse reflectance spectra showing the carbonyl region of the spectrum obtained from an IM6/3501-6 laminate specimen in the evacuable cell at the indicated time intervals in flowing air at 553°F 66

32 Diffuse reflectance spectra showing the C-H, N-H, O-H region of the spectrum obtained from an IM6/3501-6 laminate specimen in the evacuable cell at the indicated time intervals in flowing air at 553°F 67

33 Normalized reduced spectral data as a function of time for the oxidation of an IM6/3501-6 laminate specimen reacting with air at 553°F at early times 68

34 Normalized reduced spectral data as a function of time for the oxidation of an IM6/3501-6 laminate specimen reacting with air at 553°F at medium times 69

Page

35 Normalized reduced spectral data as a function of time for the oxidation of an IM6/3501-6 laminate specimen reacting with air at 553°F at long times 70

36 Flexural strength data for 0° IM6/3501-6 laminate specimens as a function of the 1775 wave number band edge intensity. 71

37 Flexural strength data for 0° IM6/3501-6 laminate specimens as a function of the normalized carbonyl (C=O) band integral. 72

38 Flexural strength data for 0° IM6/3501-6 laminate specimens as a function of the normalized hydrocarbon band integral. 73

39 Flexural strength data for 0° IM6/3501-6 laminate specimens as a function of the 3520 wave number (hydroxyl, O-H) band edge intensity. 74

LIST OF TABLES

		Page
1	Preconditioning Data of IM6/3501-6 Specimens	9
2	Composite heat damage test results	12
3	Composite heat damage test results	12
4	Composite heat damage test results	13
5	Composite heat damage test results	13
6	Laser-pumped fluorescence test results using 482.5-nm excitation	21
7	Laser-pumped fluorescence test results using 482.5-nm excitation with logarithmic intensity data	22
8	Laser-pumped fluorescence test results using 488.0-nm excitation	23
9	Laser-pumped fluorescence test results using 488.0-nm excitation with logarithmic intensity data	24
10	Dual comparison study - 488.0-nm excitation	25

ABSTRACT

The Oak Ridge National Laboratory/Applied Technology Division (ORNL/ATD) has successfully demonstrated the unique applicability of two spectroscopic techniques that possess the capability of detecting heat damage in IM6/3501-6 laminates and correlation of this damage with the residual mechanical-strength properties. The results on the diffuse reflectance infrared fourier transform (DRIFT) and laser-pumped fluorescence (LPF) spectroscopic techniques, which are capable of rapid, in-service, nondestructive detection and quantitation of heat damage in IM6/3501-6 laminates, is presented. Both of these techniques have been shown to be quite effective at probing the elusive and complex molecular changes that take place in IM6/3501-6 laminates subjected to varying degrees of thermal degradation. Using LPF or DRIFT techniques, it has been shown that laminates having different thermal histories can be readily differentiated from one another due to their characteristic "fingerprint" spectral features. The effects of short-term, elevated temperature heating on the room-temperature, compressive, interlaminar-shear, and flexural strengths and room-temperature shore-D hardness properties of "dry" and "wet" preconditioned IM6/3501-6 laminates are discussed. Additionally, the geometrical changes and percent-weight-loss measurements of IM6/3501-6 laminates that accompany heat damage are also examined. Results from an earlier ORNL/ATD study indicate that these laminates suffer significant and irreversible reduction in their room-temperature mechanical-strength properties after subjection to temperatures beyond the recommended 350°F upper-service temperature. It was found that below a certain temperature/time exposure threshold, these laminates visually and microscopically appeared to be undamaged but, in fact, may have lost a significant percentage of their original strength. In addition, laminates that were exposed above the temperature/time exposure threshold suffered dramatic geometrical changes and large amounts of weight loss.

SUMMARY

An extensive study was published in May 1990 by the Oak Ridge National Laboratory/Applied Technology Division (ORNL/ATD) for the Navy Aviation Depot in Cherry Point, North Carolina.[1] This study focused on the effects of short-term, elevated-temperature heating on the matrix-dominated mechanical properties of "dry" and "wet" preconditioned IM6/3501-6 composite laminates. Results from this investigation demonstrated that these laminates suffered significant and irreversible reduction in their room-temperature, compressive, interlaminar-shear, and flexural-strength properties after being subjected to temperatures beyond the recommended 350°F upper service temperature specified for this material. In addition, it was found that below a certain temperature/time exposure threshold, 650°F for 5 min, there appeared to be no visual or microscopic differences whatsoever between heat-damaged and nonheat-damaged IM6/3501-6 laminates. Therefore, IM6/3501-6 laminates that have been exposed in the vicinity of the temperature/time threshold may appear to be undamaged but, in fact, may have lost the majority (>60%) of their original interlaminar shear and flexural strength.

Currently, a nondestructive test method having the capability of detecting and quantifying various levels of heat degradation in polymer matrix composites does not exist. Nondestructive evalution (NDE) techniques, based on ultrasonic methods, including digital pulse (broadband), tone burst (monochromatic) and ultrasonic-C scanning have been investigated by ORNL/ATD and determined not to lend themselves to detecting heat damage in IM6/3501-6 laminates.[1] It is believed that the reason why heat damage cannot be detected by conventional NDE techniques is because the size of the damage is on the molecular scale, which is well below the practical detection limits for these techniques.

The present work was performed by ORNL/ATD for the Naval Air Systems Command. The objective of this work was to investigate various state-of-the-art spectroscopic techniques and identify those techniques that possess the capability of detecting and quantifying various levels of heat damage in IM6/3501-6 composite laminates subjected to progressively higher temperatures. It was also the intent of this study to establish whether a definitive correlation could be developed between the degree of heat damage in IM6/3501-6 laminates and their residual mechanical strengths.

The spectroscopic techniques investigated in this study included

1. Diffuse Reflectance Infrared Fourier Transform (DRIFT)
2. Laser-Pumped Fluorescence (LPF)
3. Attenuated Total Reflectance (ATR)
4. Fluorescence
5. Specular Reflectance
6. Fourier Transform - Raman
7. Diffuse Reflectance Visible (400 to 700 nm)
8. Ultraviolet-Visible Diffuse Reflectance (200 to 800 nm)

Of these techniques, DRIFT and LPF demonstrated the highest degree of success in terms of potential lightweight or field portability and composite heat damage distinguishing capability.

The unique applicability of the DRIFT and LPF spectroscopic techniques that possess the novel capability of detecting heat damage in IM6/3501-6 laminates and correlating this damage with the residual mechanical strength properties has been successfully demonstrated. Both of these techniques have the particular advantage of allowing one to probe the elusive and complex molecular changes resulting from elevated temperature exposure on the polymer matrix resin. In addition, both the DRIFT and LPF techniques have the potential capability of being made into lightweight or field portable inspection devices and could be used successfully for the rapid, in-service, nondestructive detection and quantitation of heat damage in large composite structures fabricated from IM6/3501-6.

The authors of this report anticipate that there also exists a high probability, particularly with the DRIFT technique, for using these heat-damage-detection techniques on other polymer matrix composites incorporating various thermoset and thermoplastic resin systems, including bismaleimides, polyimides, polyether ether ketone (PEEK), and others. A very large wealth of information has been accumulated on infrared and fluorescence based techniques because both have been used extensively for many years by chemists for identifying, characterizing and determining the composition of chemical compounds, in general, and organic polymers, in particular.

The remainder of the report will focus on the results obtained with the DRIFT and LPF spectroscopic techniques.

INTRODUCTION

Fiber-reinforced polymer-matrix composites (PMCs) have been gaining, in recent years, increasingly wider acceptance by the aerospace industry as manifested by their increased usage in both aircraft and space applications. Significant research and development activities by advanced composite material suppliers have resulted in an onslaught to the marketplace of a myriad of innovative polymer-matrix resins, reinforcement fibers, and various prepreg forms. These materials are continually being optimized and tailored, in terms of strength, stiffness, weight, and environmental durability, for use in specific applications.

Numerous studies have appeared in the literature over the past several years concerning the damaging environmental effects of temperature, moisture, and thermal spiking on the mechanical, chemical, and physical properties of PMCs.[2-20] A survey of these studies suggests that significant and irreversible degradation of the mechanochemical properties of these materials can result from being subjected to elevated temperatures for short periods of time.

An inherent problem with all-organic polymer-matrix resins used in the manufacture of advanced composites is their susceptibility to thermal oxidative degradation following subjection to temperatures above their recommended upper service temperatures or for extended periods of time at temperatures within a narrow window of their respective service temperatures. Polymer-matrix composite materials that are exposed to temperatures sufficiently high enough to cause resin degradation experience a drop in the glass transition temperature (T_g), which serves to effectively lower the upper service temperature and

significantly reduce the mechanical-strength properties of the composite.[15,20] In addition, embrittlement and cracking of the surface causes a loss in the impact strength of the material. Therefore, aircraft that are fabricated from PMCs and exposed to high-temperature heating can suffer irreversible and catastrophic damage in a very short time. Typical situations causing such deleterious effects would be heating that occurs during a fire, a supersonic dash, from exposure to hot gases from missile efflux, or from the engines of a vertical or short-takeoff-and-landing (V/STOL) aircraft reflected from the ground during low level hover and/or during take-off and landing.[2,17] Military aircraft that have the potential to succumb to composite heat damage include the AV-8B Harrier jumpjet,[2,17] the newly developed V-22 Osprey, the F-18, and any other types of PMC aircraft that are likely to experience temperatures around or exceeding the recommended upper service temperature that is specified for the polymer matrix resin.

One particular prepreg resin system that has enjoyed, since its inception in the 1970s, a somewhat dominating position in the fabrication of high-technology advanced composites is the diaminodiphenyl sulfone (DDS)-cured tetraglycidyl 4,4'diaminodiphenyl methane (TGDDM) epoxy-resin system. The commercially available prepreg resins, such as BASF/Narmco 5208, Hercules 3501-6, and ICI's Fiberite 934, all primarily consist of the TGDDM-DDS epoxy-resin system; the latter two resin systems also contain boron trifluoride catalysts.[21] In addition to its relatively high hot and wet mechanical strength properties, compared with other epoxy matrices, it offers a recommended upper service temperature of 350°F.[22]

TGDDM-DDS CURE REACTIONS

Recent studies appearing in the literature on the chemical cure and thermal oxidative degradation reactions of the TGDDM-DDS resin system will be discussed.[20,21]

There are basically three chemical cure reactions that operate at the 350°F (177°C) cure temperature for the TGDDM-DDS resin system. These reactions involve the primary amine-epoxide, the secondary amine-epoxide, and the epoxide-hydroxyl reactions, and all three are catalyzed similarly by boron trifluoride monoethyl amine. The primary amine-epoxide-addition cure reaction occurs at a rate ten times faster then the other two reactions, dominating the initial stages of cure and therefore having the greatest influence on the composite processing conditions. The chemistry of the primary amine-epoxide reaction is shown in reaction (1), with the arrows indicating potential sites for further reactions via the epoxide-hydroxyl (a) and secondary amine-epoxide (b) reactions.[20,21]

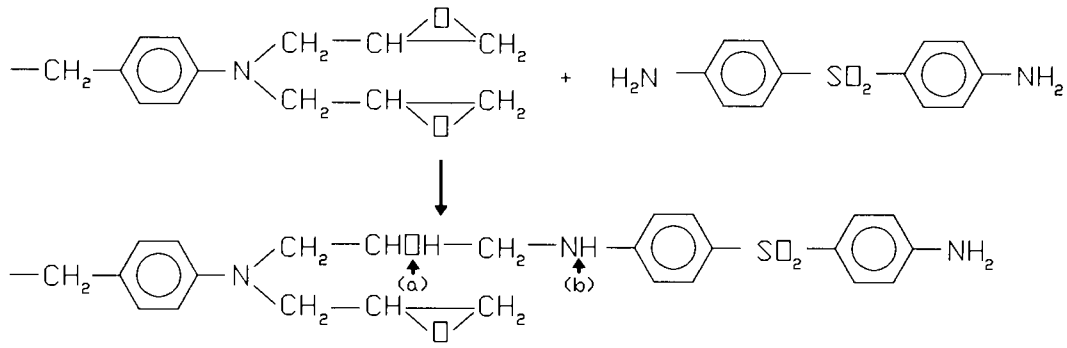

(1)

At the later stages of cure when all the primary amine has been consumed, the epoxide-hydroxyl reaction becomes the dominating reaction. Illustrated in reaction (2) are both the epoxide-hydroxyl (a) and the secondary amine-epoxide (b) cure reactions, which are believed to occur intermolecularly to form cross linked networks or intramolecularly to form internal rings that are not cross-linked, with diffusion and steric restrictions favoring internal-ring formation at the later stages of cure. It has been shown by molecular modeling and statistical studies that 75% of the epoxide-hydroxyl (a) and secondary amine-epoxide (b) reactions occur via the intramolecular route.[20,21]

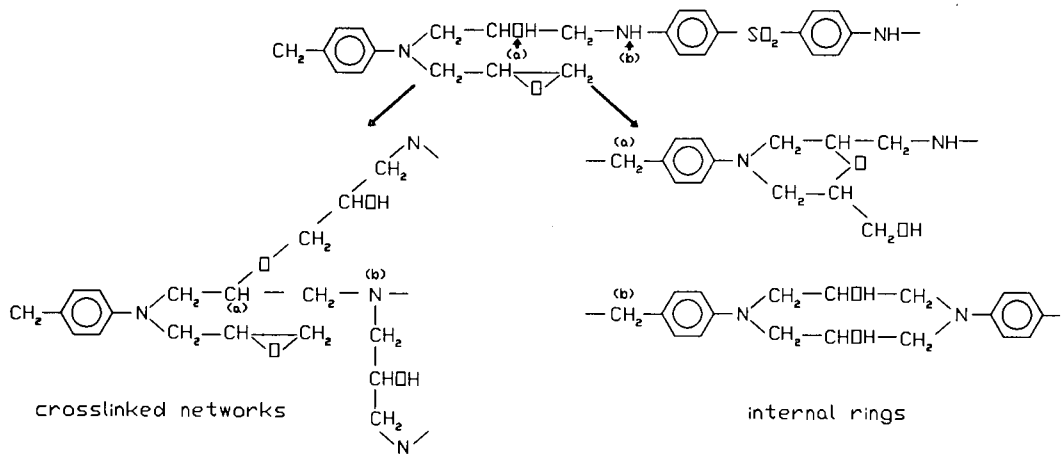

(2)

TGDDM-DDS THERMAL OXIDATIVE DEGRADATION REACTIONS

The thermal oxidative degradation reactions that result from exposing the TGDDM-DDS epoxy resin system to temperatures beyond the 350°F cure temperature or for prolonged periods of time proximate to the cure temperature can be divided into three distinct groups: (1) oxidation reactions, (2) hydrolysis or photooxidation reactions, and (3) dehydration reactions.[20,21]

The oxidation reactions appear to take place on specific sites of the resin backbone that are formed during the curing of the epoxy resin. Numerous studies suggest that carbonyl compounds, including amide products, are generated as a result of oxidation of the epoxy resin. These carbonyl-containing groups undergo subsequent degradation to form propenal. Propenal has also been reported to occur by the decomposition of noncyclized epoxide-hydroxyl [reaction (3)] and cyclized epoxide-hydroxyl [reaction(4)] cure reaction products.[20,21]

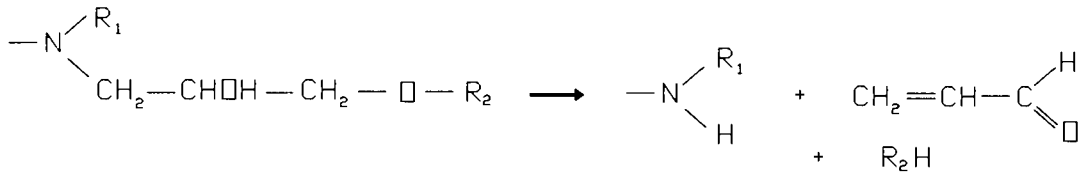

(3)

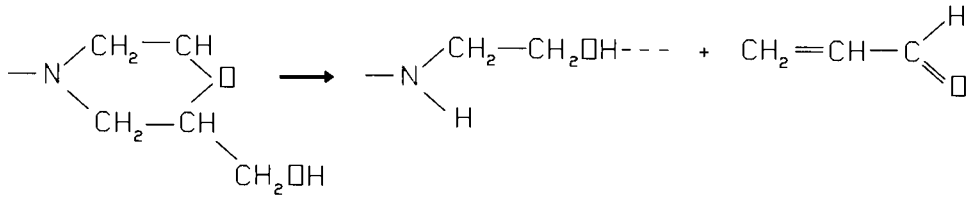

(4)

The hydrolysis or photooxidation reactions is thought to occur on portions of the molecule that are not related to the formation of epoxy-amine linkages. Infrared (IR) studies seem to indicate that these degradation reactions occur between the aromatic ring and the tertiary nitrogen of the TGDDM portion of the molecule. As a result of this reaction, structures that resemble iminium ions are produced. Upon further degradation through hydrolysis or free radical reactions, the resin undergoes a dark color change forming phenone or phenol groups in addition to a free secondary amine. This reaction is assumed to be catalyzed by light and/or oxygen. Two possible reaction mechanisms for forming iminium ions and phenone or phenol compounds are shown in reaction (5).[20,21]

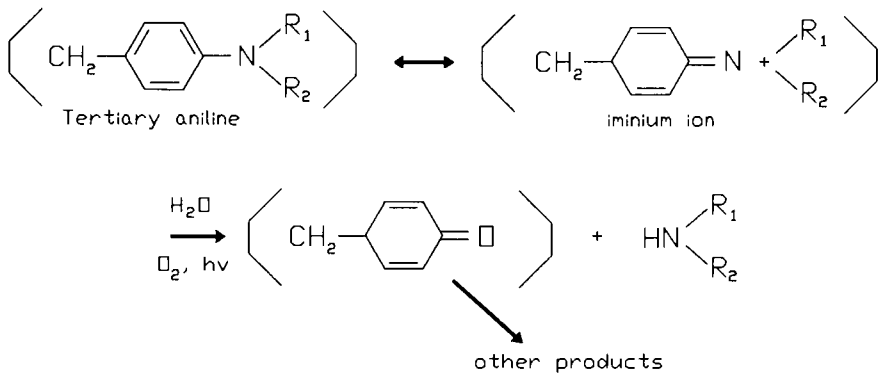

(5)

The dehydration degradation reactions are reported to occur with the secondary alcohols that are formed during the curing reactions. The water that is generated as a result of this reaction can be substantial.[20,21]

MOISTURE EFFECTS ON POLYMER-MATRIX COMPOSITES

A survey of numerous reports appearing in the literature was performed by Wright[19] concerning the effects of absorbed moisture on the mechanical properties of PMCs. The following conclusions were reached:

1. On the effect of absorbed moisture on the room-temperature mechanical properties of PMCs, 67% of the reports indicate that these properties are not significantly altered.

2. On the effect of realistic quantities of absorbed water on the elevated temperature properties of PMCs, there seems to be a consensus on the fact that absorbed moisture does lower the elevated-temperature strength properties. These losses range from 15 to 60% for interlaminar shear and 0 to 60% for the flexural strengths.

3. On the question of whether or not the effect of moisture absorption can be regarded as being reversible in PMCs, the literature seems to support the notion that there is are no chemical reactions occurring with the composites. It is believed that the small permanent loss in mechanical properties results from the swelling stresses and microvoids that are present within the laminate. For example, the interlaminar shear strength of composites generally decreases 7% for every 1% increase in void content. The swelling stresses are believed to be in opposition to the residual stresses that are generated during cure, thus a certain level of moisture absorption can result in an almost stess-free state for the composite.

4. Moisture absorption by PMCs under stress at ambient conditions has shown little effect on the room-temperature mechanical properties. The effect of moisture on the elevated temperature properties of PMCs while under stress requires further study.

5. The fatique resistance measured under ambient conditions has been reported to suffer as a consequence of absorbed moisture. The effect of moisture on the fatigue properties at elevated temperatures requires futher study.

Reports on PMCs have shown that after several moisture-absorption and thermal-spiking cycles have occured, reductions in some of the matrix-dominated properties (i.e., flexural and interlaminar shear strength) can result.[2,7,10,12] Apparently, this loss in strength results from the additional free volume that becomes available after undergoing many thermal cycles. These empty sites allow for greater moisture absorption to occur, creating greater moisture-induced swelling stresses within the laminate.[23]

The remaining sections of this report will focus on the following:

Part 1. A summary of the background information on the Composite Heat Damage project conducted by ORNL/ATD concerning the mechanical testing of heat-damaged IM6/3501-6 laminates.

Part 2. A discussion on the current work that was performed and the results that were obtained on the LPF composite heat-damage detection technique.

Part 3. A discussion on the current work that was performed and the results that were obtained on the DRIFT composite-heat-damage detection technique.

PART 1. MECHANICAL TESTING OF IM6/3501-6 LAMINATES

SUMMARY

This section of the report provides background information from work that was completed in June 1989 by ORNL/ATD for the Navy Aviation Depot, Cherry Point, North Carolina.[1] The focus of this work dealt with the effects of preconditioning and elevated temperature/time on the matrix-dominated, room-temperature mechanical properties of IM6/3501-6 composite laminates.

A series of 21-ply, symmetrical laminate test specimens, having one of two orientations, were separated into two groups—one group was preconditioned in a humid or "wet" environment, and the other group was preconditioned in a "dry" environment, then allowed to weight stabilize according to American Society for Testing and Materials (ASTM) D570-81. Subsequent to the preconditioning phase, the specimens were exposed on one side, without load, to elevated temperatures for preset periods of time, followed by a cool-down to ambient conditions. After the specimens were cooled to room temperature, they were mechanically tested in compression, flexure, short-beam shear (SBS), and shore D. Additionally, the percent weight loss and the laminate thickness were measured subsequent to various thermal treatments.

The mechanical properties were tested in accordance with ASTM standards and included compression, ASTM D3410-87; flexure, ASTM D790-87; SBS, ASTM D2344-84; and shore D, ASTM D2240-86.

EXPERIMENTAL

SAMPLE MATERIALS

All investigative work was performed on laminate specimens that were cut from fabricated panels composed of Hercules IM6G/3501-6 unidirectional prepreg tape (12 in. wide, 147 to 148 g/m^2, and 36 wt % resin content).

PANEL FABRICATION

The IM6/3501-6 prepreg tapes were cut into plies with the desired fiber orientations and dimensions shown in Fig. 1. The 5.5- to 6-mil-thick plies were then laid up by hand into 30- by 10-in.-sized panels (nominal thickness = 0.125 in.) according to the following 21-ply stacking sequence, which is representative of the aft-spar lay-up on the V-22 Osprey: $[+45°, 90°, (-45°, +45°)_4, 0°, (+45°, -45°)_4, 90°, +45°]$.

The IM6/3501-6 prepreg panels were vacuum-bag cured in an autoclave according to the following process specification, which is based on Hercules' recommendations for this material.

1. Place vacuum-bagged lay-up in autoclave.

2. Apply full vacuum.

3. Apply 100 psi.

4. At a rate of 3 to 5°F/min, raise the laminate temperature to 240°F ± 10°F. Hold for 60 to 70 min.

5. At a rate of 3 to 5°F/min, raise the laminate temperature to 350°F ± 10°F. Hold for 110 to 130 min.

6. Allow laminate to cool at a maximum rate of 5°F/min to below 200°F. Release vacuum and autoclave pressure.

7. Remove lay-up from autoclave and unbag.

Following cure, the panels were cut, using a diamond-impregnated saw, into appropriately sized test specimens, having one of two orientations, 0° or 90°. The 0° specimens having the lay-up [+45°, 90°, $(-45°, +45°)_4$, 0°, $(+45°, -45°)_4$, 90°, +45°] included a 90° ply at the second and 20th ply positions and a 0° ply in the middle of the laminate. The 90° specimens having the lay-up [-45°, 0°, $(+45°, -45°)_4$, 90°, $(-45°, +45°)_4$, 0°, -45°] included a 0° ply at the second and 20th ply positions and a 90° ply in the middle of the laminate. The geometry of the actual-sized test specimens for compression, flexure/shore-D and SBS are shown in Fig. 2.

PRECONDITIONING OF SPECIMENS

To compare the effects of moisture on the composite mechanical properties, both dry and wet preconditioned test specimens were prepared. Prior to heat exposure, one-half of the specimens were preconditioned in a vacuum oven at 120°F (dry), while the other half were placed in a humidity chamber at 120°F and 98% relative humidity (wet). Selected samples from each group were monitored weekly to determine when the specimens were saturated according to ASTM D570-81. Figure 3 is representative of the percent weight gain (wet specimens) or percent weight loss (dry specimens) vs time of one series of test specimens during the preconditioning phase. Table 1 is a compilation of the preconditioning data for the test specimens from a given panel that were tested in flexure (FLEX), shore D, and SBS.

The specimens that were tested in compression were also closely monitored according to ASTM D570-81 but are not included in Table 1 due to the potential erroneous data resulting from the concomitant absorption or desorption of moisture from both the composite and the fiberglass tab material that occurred during the preconditioning phase. The average percent weight gain or weight loss of the compression specimens during the preconditioning phase is assumed to be in close approximation to the flexure and shore-D specimens.

Table 1. Preconditioning data of IM6/3501-6 specimens

Panel number	Preconditioning time (days)	Average percent weight gain for "wet" specimens (5-spec./panel)	Average percent weight loss for "dry" specimens (5 spec./panel)	Mechanical property
2	56	0.75	0.28	Flex/shore
3	56	1.12	0.16	Flex/shore
5	56	0.81	0.24	Flex/shore
8	56	0.84	0.27	Flex/shore
Average	56	0.87	0.24	
16	56	0.85	0.27	SBS
18	36	0.74	0.06	Flex/shore
19	36	0.89	0.08	Flex/shore
20	36	0.64	0.06	Flex/shore
21	36	0.77	0.08	Flex/shore
Average	36	0.76	0.07	
22	28	0.99	0.10	SBS
23	28	0.97	0.04	SBS
10	28	0.87	0.32	SBS
Average	28	0.94	0.15	
19	82	1.2 (1 spec.)	0.11 (2 spec.)	Flex
20	82	0.93 (1 spec.)	0.08 (2 spec.)	Flex
21	82	1.0 (2 spec.)	0.11 (3 spec.)	Flex
Average	82	1.05	0.10	

HEAT EXPOSURE OF SPECIMENS

Radiant-heat exposure was performed on only one face of the wet and dry preconditioned test specimens at a fixed temperature for a specified time without load. Groups of the preconditioned test specimens, except the room-temperature control specimens, were exposed to one of the following conditions of temperature and exposure times.

1. 350, 450, 550, and 650°F for 60 min;

2. 550, 650, and 750°F for 5 and 30 min; and

3. 750°F for 10 min.

Following heat exposure, the specimens were removed from the heating chamber to a room-temperature environment and allowed to cool to ambient conditions prior to mechanical testing. The heat source was a manually controlled, radiant-quartz heater (Figs. 4 and 5) equipped with six thermocouples (six thermocouples were bonded to the top, middle, and bottom heat-exposed faces of two test specimens located on opposite sides of the heating chamber) and was used to simulate a sudden one-sided heat blast from a jet engine. The ramp-up to the exposure temperature was achieved as quickly as possible. Figure 6 is a representative example of the ramp-up rate and temperature control of one series of test specimens during heat exposure. The dry and wet room-temperature control specimens were removed from the environmental chambers and allowed to cool to ambient conditions before mechanical testing.

MECHANICAL PROPERTY TESTING

The mechanical property testing was performed by the Mechanical Testing Laboratory at the Oak Ridge Gaseous Diffusion Plant. The mechanical property tests that were dominated by the matrix or matrix/fiber interface were the ones investigated because these properties would probably be the first influenced by heat damage.

All testing was carried out in accordance with ASTM test constraints, including ambient pressure, 73.4 ± 3.6°F ambient temperature, and 50 ± 5% relative humidity. The various test procedures and test fixtures for compression, SBS, and flexure are shown in Fig. 7. Data on individual test specimens are contained in Ref. 1.

COMPRESSION TESTING

Nominal 5.5- by 1-in.-sized fiberglass-tabbed 0° specimens were tested according to ASTM D3410-87, procedure B, using the IITRI fixture.

The specimens had a gage length of 0.50 in., and testing was performed on an Instron machine at a rate of 0.05 in./min. Five specimens were tested to yield an average

compression strength. Prior to heat exposure, the tabbed section of the specimens was wrapped with reflective aluminum tape to protect the tabs against heat damage and from delaminating from the composite.

Tables 2, 3, 4 and 5 summarize the average room temperature 0° compressive strength, percent strength retention, percent coefficient of variation (CV), and the number of specimens tested at a given temperature/time for the dry and wet IM6/3501-6 test specimens according to ASTM D3410-87.

The percent CV is numerically equal to the sample standard deviation divided by the sample mean and multiplied by 100. This number provides a relative measure of the deviation of the sample data about the sample mean.

Figure 8 is a plot of the average room temperature 0° compressive strength and percent strength retention versus temperature/time for the dry and wet IM6/3501-6 test specimens according to ASTM D3410-87. The percent strength retention for the dry and wet averages was calculated based on the highest average strength (dry, 350°F/60 min), having 100% strength retention.

SHORT-BEAM-SHEAR TESTING

A three-point bend test was conducted on 0° and 90° 0.75- by 0.25-in.-sized specimens to quantify the interlaminar shear strength by the short-beam method according to ASTM D2344-84.

Testing was carried out on an Instron machine at a rate of 0.05 in./min on specimens having a span:depth ratio of 4:1 (support span = 0.50 in.; nominal depth = 0.125 in.). The specimens were tested with the heat-exposed side down to obtain an average SBS strength.

Tables 2, 3, 4 and 5 summarize the average room temperature 0° and 90° SBS strength, percent strength retention, percent CV, and the number of specimens tested at a given temperature/time for the IM6/3501-6 test specimens according to ASTM D2344-84. It is important to note that all of the SBS specimens that were exposed to temperatures equal to and/or above 650°F separated into fragments upon removal from the heating chamber and could not be tested.

Figures 9 and 10 are plots of the average room temperature 0° and 90° SBS strength and percent strength retention vs temperature/time for the dry and wet IM6/3501-6 test specimens according to ASTM D2344-84. The percent strength retention for the dry and wet averages was calculated based on the highest average strength (wet room temperature) having 100% strength retention.

PERCENT-WEIGHT-LOSS TESTING

Percent-weight-loss data were generated on heat-damaged 0° IM6/3501-6 SBS specimens by weighing, using a Mettler analytical balance, immediately before and after heat exposure in an attempt to correlate interlaminar shear strength degradation with weight loss

DWG. NO. K/G 90-968
(U)

Table 2. Composite heat damage test results
Room temperature strength (ksi)

Exposure conditions: temp/time	Compression (0°)		SBS (0°)		SBS (90°)		Flexural (0°)		Flexural (90°)	
°F/min	Dry	Wet	Dry	Wet	Dry	Wet	Dry	Wet	Dry	Wet
73/NA	44.8	43.7	6.1	6.2	8.7	10	51.7	53.3	87.0	89.7
350/60	46.2	42.9	6.1	5.9	9.4	8.9	52.8	50.8	93.6	87.3
450/60	41.3	39.9	5.7	5.8	8.8	7.4	47.4	46.0	79.6	71.9
550/5	43.8	39.3	5.5	4.8	8.9	6.5	42.6	42.8	57.6	58.4
550/30	40.8	38.4	4.1	3.3	4.6	4.3	30.8	31.7	28.7	34.9
550/60	32.1	26.6	3.2	2.1	2.1	2.4	19.9	23.1	17.5	21.2
650/5	40.9	33.8	1.5	1.1	2.5	3.4	10.9	6.0	7.8	10.0
650/30	18.7	20.6	0.3	0.3	0.0	0.0	3.4	2.4	3.1	3.1
650/60	4.5	3.7	0.3	0.3	0.0	0.0	2.7	2.5	2.2	2.5
750/5	18.8	22.1	0.0	0.0	0.0	0.0	3.1	3.0	1.9	1.9
750/10	12.1	10.7	0.0	0.0	0.0	0.0	2.9	3.1	2.2	2.4
750/30	4.1	2.8	0.0	0.0	0.0	0.0	2.1	3.9	3.7	4.2

Table 3. Composite heat damage test results
Percent strength retention

Exposure conditions: temp/time	Compression (0°)		SBS (0°)		SBS (90°)		Flexural (0°)		Flexural (90°)	
°F/min	Dry	Wet	Dry	Wet	Dry	Wet	Dry	Wet	Dry	Wet
73/NA	97	100	100	100	92	100	98	100	93	100
350/60	100	98	100	95	100	89	100	95	100	97
450/60	90	91	94	93	94	74	90	86	85	80
550/5	95	90	91	77	94	65	81	80	62	65
550/30	88	88	67	52	48	43	58	60	31	39
550/60	70	61	53	34	22	24	38	43	19	24
650/5	89	77	25	18	26	34	21	11	8	11
650/30	41	47	5	4	0	0	6	4	3	3
650/60	10	8	5	5	0	0	5	5	2	3
750/5	41	51	0	0	0	0	6	6	2	2
750/10	26	24	0	0	0	0	6	6	2	3
750/30	9	6	0	0	0	0	4	7	4	5

DWG. NO. K/G 90-969
(U)

Table 4. Composite heat damage test results
Coefficient of variation (%)

Exposure conditions: temp/time	Compression strength (0°)		SBS strength (0°)		SBS strength (90°)		Flexural strength (0°)		Flexural strength (90°)	
°F/min	Dry	Wet	Dry	Wet	Dry	Wet	Dry	Wet	Dry	Wet
73/NA	7	6	4	3	9	8	3	5	11	7
350/60	9	5	4	4	15	10	2	1	9	2
450/60	6	4	4	2	13	5	7	5	6	13
550/5	5	8	7	12	10	6	10	1	15	18
550/30	9	8	16	20	15	17	12	28	30	20
550/60	16	7	22	30	17	20	24	39	28	28
650/5	8	10	85	90	33	25	47	33	33	43
650/30	28	18	31	14	0	0	23	17	21	15
650/60	40	24	19	10	0	0	13	15	16	34
750/5	27	18	0	0	0	0	44	39	24	18
750/10	37	37	0	0	0	0	18	13	18	9
750/30	35	42	0	0	0	0	17	20	16	23

Table 5. Composite heat damage test results
Number of specimens

Exposure conditions: temp/time	Compression strength (0°)		SBS strength (0°)		SBS strength (90°)		Flexural strength (0°)		Flexural strength (90°)	
°F/min	Dry	Wet	Dry	Wet	Dry	Wet	Dry	Wet	Dry	Wet
73/NA	5	5	10	10	10	10	9	8	10	9
350/60	5	5	10	10	10	10	5	6	4	4
450/60	5	5	10	10	10	10	7	11	9	9
550/5	5	5	10	10	10	10	11	6	9	9
550/30	5	5	10	10	10	10	11	5	9	9
550/60	5	5	10	10	8	9	11	11	9	9
650/5	5	5	10	9	10	10	8	9	9	9
650/30	5	5	10	10	10	10	9	9	9	8
650/60	5	5	10	10	10	10	9	9	9	9
750/5	5	5	10	10	10	10	9	4	9	9
750/10	5	5	10	10	10	10	8	8	9	9
750/30	5	5	10	10	10	10	9	9	9	9

as a function of temperature/time. Figure 11 summarizes the average percent weight loss for the 0° SBS IM6/3501-6 specimens after exposure to various temperature/time treatments.

FLEXURAL TESTING

A four-point bend test was performed on nominal 3- by 1-in.-sized 0° and 90° specimens according to ASTM D790-87, method 2, procedure A. The flexural specimens had a span:depth ratio of 16:1 (support span = 2 in., load span = 0.67 in., nominal depth = 0.125 in.), and testing was done on an Instron machine at a rate of 0.06 in./min. The specimens were tested with the heat-exposed side down (in tension) to yield average flexural strength results. Tables 2, 3, 4 and 5 summarize the average room temperature 0° and 90° flexural strength, percent strength retention, percent CV, and the number of specimens tested at a given temperature/time for the IM6/3501-6 test specimens according to ASTM D790-87.

Figures 12 and 13 are plots of the average room temperature 0° and 90° flexural strength and percent strength retention vs temperature/time for the dry and wet IM6/3501-6 test specimens according to ASTM D790-87. The percent strength retention for the dry and wet averages was calculated based on the highest average strength (wet room temperature or dry 350°F/60 min) having 100% strength retention

LAMINATE-THICKNESS-MEASUREMENT TESTING

Thickness measurements were performed on both wet and dry preconditioned 3- by 1-in-sized IM6/3501-6 specimens that were exposed to various temperature/time treatments. Micrometer thickness readings were taken between opposite faces of the specimens at their thickest section. Readings were performed on specimens from panels 2, 3, 5, 8, 17, 18, 19, 20, and 21. Figure 14 summarizes the average micrometer measurements at maximum thickness on the IM6/3501-6 specimens after heat exposure.

SHORE-D-HARDNESS TESTING

A Shore digital durometer hardness tester, Model 71600, was utilized to obtain shore-D hardness values on nominal 3- by 1-in.-sized specimens to determine the effects of heat exposure on composite hardness according to ASTM D2240-86. An average shore-D hardness value was obtained for ten specimens at each temperature/time set point. Each specimen was tested at six different locations, at least 0.25 in. apart, on the heat-exposed side, and an average specimen reading was calculated.

Figure 15 is a plot of the average room temperature shore-D- hardness means and percent strength retention vs temperature/time for the dry and wet IM6/3501-6 test specimens according to ASTM D2440-86. The percent shore-D-hardness retention for the dry and wet averages was calculated based on the highest average shore-D hardness (wet, 350°F/60 min) having 100% hardness retention.

STATISTICAL t TESTING

To determine whether there was any statistically significant difference between the mechanical strength averages of the wet and dry preconditioned IM6/3501-6 specimens, statistical t tests were conducted from the values obtained at each specific temperature/time for compression, flexure, SBS, and shore D.

Large values of t (experimental) (all equations and critical values for t are given in Appendix I of reference 1) occur when the difference in the sample averages is large compared with the standard deviation for this difference. A large value for t (experimental) indicated that the observed difference in sample averages was too large to be explained by sampling error alone. Therefore, when t (experimental) was larger than t (critical) in absolute value, there was a statistically significant difference (at the 95% confidence level) between the strength averages of the wet and dry preconditioned test specimens.

The notation, (a), appearing at the top of some of the rectangular data blocks in Figures 8 through 15 denotes that the wet and dry strength averages have been calculated to be statistically significantly different at the 95% confidence level. Additional statistical information can be found in Appendix I of Ref. 1.

RESULTS AND DISCUSSION

STATISTICS

The results from the ORNL/ATD study did not demonstrate a large statistically significant difference between the room temperature tested, mean strengths of the wet and dry preconditioned compressive, SBS, flexural, and shore-D hardness IM6/3501-6 specimens, except for the statistical differences noted in Figs. 8, 9, 10, 12, 13, and 15.

A total of 64 combined wet and dry strength/hardness means were determined. Of these, 9.4% of the wet, and 21.9% of the dry means were statistically significantly greater (at the 95% confidence level) than their corresponding dry and wet means at the same temperature/time, respectively.

SHORE D AND COMPRESSION

Shore-D hardness and 0° compressive strength properties were the least affected and least sensitive to elevated temperature exposure. The shore-D hardness is a very rough measure of the elastic modulus of a material. Data from our studies indicate that shore D is a very poor indicator for relating loss in IM6/3501-6 mechanical strength to heat damage. No significant decrease in shore-D hardness manifests itself until ~ 650°F, but by the time the material has reached that temperature, it has lost ~ 65 to 98% of its original 0° and 90° interlaminar shear and flexural strength. These findings seem to support the belief that the shore-D and compressive properties are less influenced by the matrix compared with the SBS and flexural properties.

SHORT-BEAM SHEAR AND FLEXURE

The interlaminar shear and flexural strength properties of the IM6/3501-6 specimens were the most sensitive to heat damage. These properties dropped dramatically after exposure to 550°F, retaining only about 20 to 90% of their original room-temperature strength. At elevated temperatures, the 0° SBS and 0° flexural specimens retained a larger percentage of their room temperature strengths, compared with the 90° SBS and 90° flexural specimens, especially above exposure temperatures of 450°F.

The data clearly show a significant difference in the percent strength retention for the 90° compared with the 0° SBS specimens or the 90° compared with the 0° flexural specimens. These differences are particularly evident below exposure temperatures of 650°F. The results from the IM6/3501-6 strength data reveal that the percent strength retention for the 0° SBS and flexural specimens is higher than those of the corresponding 90° SBS and flexural specimens, respectively, at the same temperature/time. As a matter of fact, the strengths for the room-temperature 90° SBS and flexural specimens are initially about 70% higher than the corresponding 0° SBS and flexural specimens, respectively. At elevated temperatures though, the strengths for the 90° specimens dramatically drop off relative to the strengths for the 0° specimens.

The strengths for the 90° and 0° SBS or the 90° and 0° flexural laminates are essentially equal to each other after being exposed to 550°F for 30 min. Additionally, after exposure to temperatures of ~ 650°F and higher, the percent strength retention for both the 90° and 0° SBS or the 90° and 0° flexural specimens becomes equivalent to each other.

It appears from the flexural strength data that the 0° load-bearing plies in the 90° flexural specimens undergo thermal oxidative degradation very quickly after exposure to elevated temperatures. The degradation of these plies is probably one of the determining factors affecting the poorer percent flexural strength retention in the 90° laminates relative to the 0° laminates.

In the 90° specimens, there exists two 0° plies that are located immediately adjacent to the front and back surface plies of the laminate, with a 90° ply positioned in the middle of the laminate. In the 0° specimens, however, the two 90° plies are located immediately adjacent to the outer surface plies, and the middle ply is now a 0° ply. During temperature exposure, oxygen is assumed to diffuse principally through the outer surfaces of the laminate toward the interior of resin matrix, and an increased level of thermal oxidative degradation on the outer plies and less extensive degradation in the middle or interior plies would be expected to be observed.

Flexural testing embodies tension, compression, and shear components and therefore serves as a general indicator of laminate performance. During flexural testing, the middle of the laminate is ideally under no strain, whereas the upper, loaded surfaces and the lower surfaces are under compression and tension, respectively. Therefore, if the resin in the 0° outer plies of the 90° specimens becomes degraded, then the resin is less able to distribute the load among the reinforcing fibers. As a consequence of this degradation, the flexural strength is diminished to an extent dependent on the degree of heat damge. Further

spectroscopic and mechanical property testing with laminates having different ply lay-ups incorporating additional 0° and 90° plies would be needed to substantiate this level of reasoning.

In SBS testing, however, the middle of the laminate is ideally under maximum strain. It is unclear why the 0° and 90° SBS specimens are initially so different in strength, or, for that matter, why the addition of heat damage to the different lay-ups causes a similar pattern of strength-loss behavior experienced by the flexural specimens. Apparently, there are complex shear-stress distributions operating through the thickness of the laminates which are influencing the strength of the material. Work in finite element analysis would probably shed additional information concerning the complex stress distributions that are experienced by these different lay-ups during shear testing.

Other reasons for explaining why the 0° and 90° lay-ups experience different shear strengths at lower exposure temperatures may be because the ASTM D2344 SBS test was specifically intended for unidirectional laminates, and any deviations from fiber parallelism would probably invalidate the shear strength calculations. Both the 0° and 90° laminates contain 86% by weight of ± 45° plies, and therefore the equations given in ASTM D2344 to calculate the interlaminar shear strength may not be accurate.

ASTM does not currently have an approved test method dealing with the shear testing of flat, nonunidirectional laminates (except for ASTM D3518 which only concerns the in-plane shear stress-strain responses of ± 45° laminates) that have various combinations of 0°, 90°, and ± 45° plies. ASTM does stipulate, however, that the shear strength obtained in D2344 cannot be used as a design criteria but can be utilized for comparative testing of composite materials if all failures are in horizontal shear.

VISUAL/MICROSCOPIC/THICKNESS

No visual or microscopic damage or increase in thickness of the IM6/3501-6 3-by 1-in.-sized specimens was apparent at exposure temperatures of 550°F and below. Delamination, translaminar cracking, and an increase in specimen thickness were first visually observed at exposure temperatures of 650°F. At an exposure temperature of 650°F for 60 min, the thickness of the 3- by 1-in. specimens almost doubled compared with specimens exposed to 550°F and below. The cause of this tremendous change in laminate thickness can probably be attributed to the rapid expansion of gaseous by-products generated within the laminate during resin degradation. These undesirable geometric changes serve to produce areas of high stress concentration and are probably one of the major factors contributing to strength loss above 550°F.

PERCENT WEIGHT LOSS

Large weight losses also occur with these materials. These losses initiate around 450°F and account for 0 to 11% of the original dry weight of the laminate. Water, propenal, and other resin-degraded organic gaseous compounds are probably the major by-products generated as a result of this thermal exposure.[20,21]

USE OF COATINGS ON POLYMER-MATRIX COMPOSITES

It appears that the rate and the extent with which the TGDDM-DDS resin system experiences thermal oxidative degradation is quite rapid and extensive, especially in the presence of oxygen and elevated temperatures. The temperature dependance on the oxidation reaction rates and oxygen diffusion rates can be explained by Arrhenius's law—a rate law that has been demonstrated to have great generality.[9] Arrhenius's law states that the rate of oxidation and the rate of diffusion increases exponentially with temperature. To more fully characterize the problem of heat damage in IM6/3501-6 laminates as it relates to mechanical strength loss, the various factors affecting the rate and the extent with which the epoxy resin undergoes these complex degradation reactions should be addressed.

It is believed that one of the more important factors affecting the rate and the extent of the chemical-degradation reactions sustained with heat-damaged IM6/3501-6 laminates involves the mechanism of oxygen diffusion. The rate and the amount of oxygen diffusion occurring with the IM6/3501-6 laminates at elevated temperatures and at various partial pressures of oxygen are unknown. However, if oxygen diffusion occurs via a similar mechanism to that of the moisture-diffusion process that occurs in epoxy laminates (described by Fick's diffusion laws),[2,7,10,12] then the rate of oxygen diffusion occurring through the laminate would be primarily dependent on the temperature at which the laminate is exposed.[9] Moisture-absorption diffusion coefficients for epoxy resins increase substantially above 120 to 140°F.[19] Because water contains a large degree of hydrogen bonding, albeit there is less association in the vapor state, and oxygen is diatomic with no intermolecular bonding, then the oxygen-diffusion coefficient would generally be expected to be significantly higher than the moisture-diffusion coefficient.

On the other hand, the equilibrium-moisture content in epoxy resins is very much dependent on relative humidity but only slightly dependent on the temperature of exposure.[2,7,10,12,19] Therefore, it would be expected that the amount of oxygen that can diffuse through the laminate should be principally dependent on the concentration of oxygen located in the immediate vicinity of the outer surfaces of the laminate. This concentration gradient behavior is described by Fick's first law of diffusion,[9] which states that molecules move from areas where they are highly concentrated to areas where they are less concentrated.

Additionally, there would probably be some minor reactions involving the oxygen that is originally present in the TGDDM-DDS resin system, especially after significant degradation has resulted. The interaction from this oxygen would probably be fairly minimal because its concentration is so small. It has been shown by isothermal DRIFT experiments that if thermal heating is performed on IM6/3501-6 laminates in an inert atmosphere, there is less thermal oxidative degradation appearing on the surface of the material.

Previous work by Haskins and Chase demonstrated a direct correlation of thermal aging and oxygen pressure on the loss of residual strength on polymer matrix composites.[15,24] Haskins' study dealt with various thermal aging experiments on unidirectional and crossplied laminates of boron/epoxy, graphite/epoxy, and graphite/polyimide.[15] These laminates were aged at elevated temperatures for 10,000 h (1.14 years) and 50,000 h (5.7 years) under either ambient pressure (14.7 psi) or reduced pressure (2 psi). After aging, the laminates were tested in tension at elevated temperatures.

The results on the six-ply unidirectional graphite/epoxy (Hercules A-S/3501-5) laminates that were aged at 350°F and reduced pressure showed a 19 and 16% increase in tensile strength retention, compared with identical laminates aged at the same temperature at ambient pressure after 10,000 and 50,000 h, respectively.[15] Even better results were realized with the six-ply crossplied graphite/epoxy (Hercules A-S/3501-5) laminates ($[0 \pm 45]_s$) that were aged at 350°F and reduced pressure. These laminates yielded a 62 and 19% increase in tensile strength retention, compared with identical laminates that were aged at 350°F and ambient pressure after aging 10,000 and 50,000 h, respectively. Note that all tensile testing was performed at 350°F.

The results on the boron/epoxy and graphite/polyimide laminates showed a similar type of correlation between the tensile-strength retention and the oxygen-partial pressure. Another interesting finding from Haskins' study showed that at reduced pressure after elevated temperature aging, there appeared to be a significant increase in the T_g of the graphite/epoxy material.[15]

Systematic differential scanning calorimetry studies, conducted in the absence of oxygen, suggest that the TGDDM-DDS resin system undergoes thermal decomposition, principally by scission of bonds in the DDS portion of the matrix.[25]

If there is, indeed, a correlation between thermal heating and oxygen partial pressure on the residual strength of PMCs, then various measures could be implemented to decrease the level of oxygen coming into contact with the surface of the laminate, thereby slowing down the resin oxidation-degradation reactions. For instance, by applying specially formulated oxygen-barrier-resistant or oxygen-diffusion-resistant coatings to the surface of the laminates, the amount of heat damage and strength loss that is sustained at elevated temperatures could be reduced, thereby enabling these materials to be used at higher temperatures for longer periods of time.

These coatings could also act as moisture vapor barriers. Coatings have been successful at significantly reducing the moisture content in PMCs.[19] Although moisture absorption in composite laminates is usually regarded as being almost totally reversible, via drying out the moisture, it has been blamed for effectively plasticizing the epoxy resin, lowering the T_g, and serving to lower the elevated temperature properties of the composite.[2,7,10,12,19]

PART 2. LASER-PUMPED FLUORESCENCE

SUMMARY

This section of the report concerns the work conducted by the ORNL/Health and Safety Research Division on the LPF spectroscopic properties of heat-damaged IM6/3501-6 laminates and those not damaged by heat. The results indicate that this technique might serve a useful role as a tool for noninvasive characterization of the extent of thermally induced degradation.

A review of the LPF results confirms that significant differences exist in the LPF spectral signatures for samples undergoing different thermal treatments. These results are summarized in Tables 6 through 10 and Figs. 16 through 22.

Tables 6 and 7 refer to the LPF intensities and their logarithmic transformations, respectively, for the 0° IM6/3501-6 flexural specimens, 482.5-nm krypton-ion laser excitation, 5.5-mW laser power, 5-mm-diam illumination, 45° backscattering geometry, 2-m excitation, and collection optical fibers. The average intensities were calculated over successive 5-nm-wide regions (i.e., 510 to 515 nm). The thermal-treatment column indicates temperature of treatment (°F), duration of treatment, and type of pretreatment (wet or dry). The 0° flexural strength is recorded in pounds per square inch. All samples were positioned and optimized individually.

Tables 8 and 9 refer to the LPF intensities and their logarithmic transformations, respectively, for the 0° IM6/3501-6 flexural specimens, 488.0-nm argon-ion laser excitation, 6.5-mW laser power, 5-mm-diam illumination, 45° backscattering geometry, 2-m excitation, and collection optical fibers. The average intensities were calculated over successive 5-nm-wide regions (i.e., 510 to 515 nm). The thermal-treatment column indicates temperature of treatment (°F), duration of treatment, and type of pretreatment (wet or dry). The 0° flexural strength is recorded in pounds per square inch. All samples were positioned and optimized individually.

Table 10 refers to a dual comparison study of LPF intensities for the 0° flexural IM6/3501-6 specimens with 488-nm excitation. The conditions were the same as those in Table 8, except in the positioning of the sample—the first entry is for the sample placed in a prepositioned sample holder without additional optimization; the second entry is for the different region of the same sample, with careful optimization.

Figure 16 is a plot of the log (LPF intensity) vs log (flexural strength) of the 0° IM6/3501-6 specimens using excitation at 482.5 nm. Fig. 17 is a plot of the log (LPF intensity) vs log (flexural strength) of the 0° IM6/3501-6 specimens using excitation at 482.5 nm, separated into dry and wet pretreatments.

Figure 18 is a plot of the log (LPF intensity) vs log (flexural strength) of the 0° IM6/3501-6 specimens using excitation at 488.0 nm. Figure 19 is a plot of the log (LPF

Table 6. Laser-pumped fluorescence test results using 482.5-nm excitation

Sample (panel-specimen)	Thermal (°F/min/ pretreatment)	RT, 0° flexural strength (psi)	Average intensity (510-515 nm)	Average intensity (515-520 nm)	Average intensity (520-525 nm)	Average intensity (525-530 nm)	Average intensity (530-535 nm)
05-46	RT/W	53297	637	679	693	669	680
08-41	RT/W	53297	725	790	809	778	785
05-07	350/60/D	52759	333	362	381	371	383
05-18	RT/D	51660	681	727	724	701	711
05-47	350/60/W	50797	1900	2100	2170	2090	2130
02-62	350/60/W	50797	1060	1170	1210	1180	1210
03-08	450/60/D	47400	241	270	286	302	323
05-60	450/60/W	46010	152	166	171	177	186
08-55	450/60/W	46010	277	317	346	365	398
05-73	550/05/W	42805	132	139	148	149	162
03-41	550/05/W	42805	127	133	139	142	151
03-21	550/05/D	42642	126	130	136	140	148
03-54	550/30/W	31726	112	115	117	119	124
08-68	550/30/W	31726	124	128	131	133	142
08-22	550/30/D	30822	114	116	120	120	126
05-51	550/60/W	23076	111	113	113	115	121
03-64	550/60/W	23076	107	109	111	112	116
08-11	550/60/D	19873	110	113	114	116	121
02-24	650/05/D	10975	106	109	110	111	117
08-59	650/05/W	6045	105	111	111	112	117
02-56	650/05/W	6045	114	116	118	118	124
05-68	750/30/W	3880	108	108	110	110	115
05-37	650/30/D	3355	103	107	107	106	112
08-26	650/60/D	2729	108	109	110	110	117
08-61	650/60/W	2465	105	106	107	108	113
03-58	650/60/W	2465	105	105	106	108	112
03-57	650/30/W	2350	105	106	106	108	112
02-57	650/30/W	2350	105	106	108	108	113
02-28	750/30/D	2117	104	105	107	108	113

Table 7. Laser-pumped fluorescence test results using 482.5-nm excitation with logarithmic intensity data

Sample (panel-specimen)	Thermal (°F/min/ pretreatment)	RT, 0° Flexural Strength (psi)	Average intensity (510-515 nm)	Average intensity (515-520 nm)	Average intensity (520-525 nm)	Average intensity (525-530 nm)	Average intensity (530-535 nm)
05-46	RT/W	4.727	2.804	2.832	2.841	2.825	2.833
08-41	RT/W	4.727	2.860	2.898	2.908	2.891	2.895
05-07	350/60/D	4.722	2.522	2.559	2.581	2.569	2.583
05-18	RT/D	4.713	2.833	2.862	2.860	2.846	2.852
05-47	350/60/W	4.706	3.279	3.322	3.336	3.320	3.328
02-62	350/60/W	4.706	3.025	3.068	3.083	3.072	3.083
03-08	450/60/D	4.676	2.382	2.431	2.456	2.480	2.509
05-60	450/60/W	4.663	2.182	2.220	2.233	2.248	2.270
08-55	450/60/W	4.663	2.442	2.501	2.539	2.562	2.600
05-73	550/05/W	4.631	2.121	2.143	2.170	2.173	2.210
03-41	550/05/W	4.631	2.104	2.124	2.143	2.152	2.179
03-21	550/05/D	4.630	2.100	2.114	2.134	2.146	2.170
03-54	550/30/W	4.501	2.049	2.061	2.068	2.076	2.093
08-68	550/30/W	4.501	2.093	2.107	2.117	2.124	2.152
08-22	550/30/D	4.489	2.057	2.064	2.079	2.079	2.100
05-51	550/60/W	4.363	2.045	2.053	2.053	2.061	2.083
03-64	550/60/W	4.363	2.029	2.037	2.045	2.049	2.064
08-11	550/60/D	4.298	2.041	2.053	2.057	2.064	2.083
02-24	650/05/D	4.040	2.025	2.037	2.041	2.045	2.068
08-59	650/05/W	3.781	2.021	2.045	2.045	2.049	2.068
02-56	650/05/W	3.781	2.057	2.064	2.072	2.072	2.093
05-68	750/30/W	3.589	2.033	2.033	2.041	2.041	2.061
05-37	650/30/D	3.526	2.013	2.029	2.029	2.025	2.049
08-26	650/60/D	3.436	2.033	2.037	2.041	2.041	2.068
08-61	650/60/W	3.392	2.021	2.025	2.029	2.033	2.053
03-58	650/60/W	3.392	2.021	2.021	2.025	2.033	2.049
03-57	650/30/W	3.371	2.021	2.025	2.025	2.033	2.049
02-57	650/30/W	3.371	2.021	2.025	2.033	2.033	2.053
02-28	750/30/D	3.326	2.017	2.021	2.029	2.033	2.053

Table 8. Laser-pumped fluorescence test results using 488.0-nm excitation

Sample (panel-specimen)	Thermal (°F/min/ pretreatment)	RT, 0° flexural strength (psi)	Average intensity (510-515 nm)	Average intensity (515-520 nm)	Average intensity (520-525 nm)	Average intensity (525-530 nm)	Average intensity (530-535 nm)
08-41	RT/W	53297	793	900	926	948	987
05-46	RT/W	53297	587	659	678	692	716
05-07	350/60/D	52759	299	342	348	359	374
05-18	RT/D	51660	695	784	805	824	844
05-47	350/60/W	50797	1600	1850	1920	1990	2060
02-62	350/60/W	50797	1070	1220	1260	1320	1380
03-08	450/60/D	47400	241	282	306	334	367
05-60	450/60/W	46010	197	221	238	256	276
08-55	450/60/W	46010	370	447	498	558	627
03-41	550/05/W	42805	139	149	156	164	173
05-73	550/05/W	42805	154	172	179	192	203
03-21	550/05/D	42642	139	149	154	162	170
08-68	550/30/W	31726	133	142	144	152	158
03-54	550/30/W	31726	118	121	123	126	127
08-22	550/30/D	30822	120	125	127	130	131
05-51	550/60/W	23076	121	125	125	129	128
03-64	550/60/W	23076	115	119	117	120	120
08-11	550/60/D	19873	120	120	124	126	126
02-24	650/05/D	10975	111	111	111	113	115
02-56	650/05/W	6045	112	115	116	118	119
08-59	650/05/W	6045	117	120	120	122	122
05-68	750/30/W	3880	106	109	108	109	108
05-37	650/30/D	3355	109	111	112	113	112
08-26	650/60/D	2729	109	110	110	109	111
03-58	650/60/W	2465	106	107	109	108	107
08-61	650/60/W	2465	108	107	108	108	108
02-57	650/30/W	2350	108	111	111	110	110
03-57	650/30/W	2350	110	111	109	112	112
02-28	750/30/D	2117	107	108	110	110	111

Table 9. Laser-pumped fluorescence test results - 488.0-nm excitation with logarithmic intensity data

Sample (panel-specimen)	Thermal (°F/min/ pretreatment)	RT, 0° flexural strength (psi)	Average intensity (510-515 nm)	Average intensity (515-520 nm)	Average intensity (520-525 nm)	Average intensity (525-530 nm)	Average intensity (530-535 nm)
08-41	RT/W	4.727	2.899	2.954	2.967	2.977	2.994
05-46	RT/W	4.727	2.769	2.819	2.831	2.840	2.855
05-07	350/60/D	4.722	2.476	2.534	2.542	2.555	2.573
05-18	RT/D	4.713	2.842	2.894	2.906	2.916	2.926
05-47	350/60/W	4.706	3.204	3.267	3.283	3.299	3.314
02-62	350/60/W	4.706	3.029	3.086	3.100	3.121	3.140
03-08	450/60/D	4.676	2.382	2.450	2.486	2.524	2.565
05-60	450/60/W	4.663	2.294	2.344	2.377	2.408	2.441
08-55	450/60/W	4.663	2.568	2.650	2.697	2.747	2.797
03-41	550/05/W	4.631	2.143	2.173	2.193	2.215	2.238
05-73	550/05/W	4.631	2.188	2.236	2.253	2.283	2.307
03-21	550/05/D	4.630	2.143	2.173	2.188	2.210	2.230
08-68	550/30/W	4.501	2.124	2.152	2.158	2.182	2.199
03-54	550/30/W	4.501	2.072	2.083	2.090	2.100	2.104
08-22	550/30/D	4.489	2.079	2.097	2.104	2.114	2.117
05-51	550/60/W	4.363	2.083	2.097	2.097	2.111	2.107
03-64	550/60/W	4.363	2.061	2.076	2.068	2.079	2.079
08-11	550/60/D	4.298	2.079	2.079	2.093	2.100	2.100
02-24	650/05/D	4.040	2.045	2.045	2.045	2.053	2.061
02-56	650/05/W	3.781	2.049	2.061	2.064	2.072	2.076
08-59	650/05/W	3.781	2.068	2.079	2.079	2.086	2.086
05-68	750/30/W	3.589	2.025	2.037	2.033	2.037	2.033
05-37	650/30/D	3.526	2.037	2.045	2.049	2.053	2.049
08-26	650/60/D	3.436	2.037	2.041	2.041	2.037	2.045
03-58	650/60/W	3.392	2.025	2.029	2.037	2.033	2.029
08-61	650/60/W	3.392	2.033	2.029	2.033	2.033	2.033
02-57	650/30/W	3.371	2.033	2.045	2.045	2.041	2.041
03-57	650/30/W	3.371	2.041	2.045	2.037	2.049	2.049
02-28	750/30/D	3.326	2.029	2.033	2.041	2.041	2.045

Table 10. Dual Comparison Study - 488.0-nm excitation

Sample (panel specimen)	Thermal (°F/min/ pretreatment)	RT, 0° flexural strength (psi)	Average intensity (510-515 nm)	Average intensity (515-520 nm)	Average intensity (520-525 nm)	Average intensity (525-530 nm)	Average intensity (530-535 nm)
05-47	350/60/W	50797	1600	1850	1920	1990	2060
05-47	350/60/W	50797	1310	1500	1560	1610	1690
02-62	350/60/W	50797	1070	1220	1260	1320	1380
02-62	350/60/W	50797	1020	1180	1190	1240	1310
05-51	550/60/W	23076	121	125	125	129	128
05-51	550/60/W	23076	119	121	123	126	127
03-64	550/60/W	23076	115	119	117	120	120
03-64	550/60/W	23076	111	114	114	115	115
08-59	650/05/W	6045	117	120	120	122	122
08-59	650/05/W	6045	122	127	129	132	133
02-28	750/30/D	2117	107	108	110	110	111
02-28	750/30/D	2117	106	107	106	107	107

intensity) vs log (flexural strength) of the 0° IM6/3501-6 specimens using excitation at 488.0 nm, separated into dry and wet pretreatments. Figure 20 is a plot of log (LPF intensity) vs log (flexural strength) (close-up view from 4.2 to 4.8) of the 0° IM6/3501-6 specimens using excitation at 488.0 nm. Figure 21 is a plot of the log (LPF intensity) vs log (flexural strength) of the 0° IM6/3501-6 specimens using excitation at 488.0 nm, with the wet pretreated data circled. Figure 22 is a plot of the log (LPF intensity) (expanded intensity scale from 2 to 2.2) vs log (flexural strength) of the 0° IM6/3501-6 specimens using excitation at 488.0 nm.

From the data, it appears to be possible to determine the degree of thermal degradation, based on the LPF method, using laser excitation at 482.5 nm. More importantly, excitation at 488.0 nm appears to produce results that are comparable to those obtained with 482.5-nm excitation; use of the former wavelength is highly preferable because it is a strong argon-ion laser line, while the latter is a weak krypton-ion line. Some disparity appears to be present in an overall monotonic relationship between LPF intensity and sample strength, decreasing the apparent predictive power of the method, particularly at the high end of the strength curve. This analytical noise may be the result of microscopic or macroscopic variability in the amount of surface-exposed polymer and/or may be related to changes in the chemical composition of the polymer. Because of the highly inhomogeneous nature of the composite panels, further investigation is needed to elucidate the bases for spectroscopic measurement of thermally induced chemical and physical degradation.

EXPERIMENTAL

As far as practical, all experiments were performed in a blind manner, and samples were analyzed in random order. Twenty-nine 3- by 1-in.-sized 0° flexural samples were withdrawn singly from a bag and assigned a number from 1 to 29; this number was used throughout each experiment for internal identification of the samples so that knowledge of thermal history could not bias analyses or interpretation of data.

LPF experiments were performed with a research laser Raman spectroscopy system, using tunable krypton-ion (482.5 nm) and argon-ion lasers (488.0 nm) for excitation. Laser radiation was prefiltered using a 1-nm full width at half height (FWHH) dielectric laser line-pass filter and focused to a spot on the sample ~5 mm in diameter. Light was collected from the sample using a 2-m-long, 50-μm-diam optical fiber placed ~10 mm from the point of excitation; this fiber was oriented at an angle of ~45° relative to the excitation beam in a backscattering geometry. Light exiting the fiber was filtered through a 1-nm FWHH dielectric laser line-rejection filter and focused onto the slits of a 0.6-m single-grating Czerny-Turner spectrograph (slit width, 50 μm). Scattered and luminescent light was detected with a 700-channel intensified photodiode array detector, operated in the continuous-wave mode at approximately -9.4°F(-23°C).

For the 482.5-nm-excitation experiments, each sample was placed in a holder supported by a precision X-Y stage and its position optimized to provide the greatest average signal. The light collected in this manner was integrated for 15 s. Laser power delivered to the

sample was 5.5 mW. The 488.0-nm experiments were performed in a similar fashion; however, the samples were not individually optimized but rather were placed into a prealigned sample holder. This approach was much faster and provided a better estimate of the experimental approach that probably would be used in a field measurement. To gage the effects of nonoptimization, a second subset of the samples was retested under identical conditions, except that their position was carefully optimized. Laser power for this second set of experiments was ~6.5 mW. For all experiments in these studies, average intensities were calculated over 5-nm-wide regions of the spectrum, covering wavelengths from 510 to 535 nm.

RESULTS AND DISCUSSION

Linear and logarithmic versions of the results from these studies are compiled in Tables 6 to 10 and shown in Figs. 16 through 22. A general comparison of the results with those from an earlier ORNL study of LPF at 482.5 nm, indicates good qualitative agreement in terms of the relationship between flexural strength, thermal treatment, and LPF intensity. As before, the LPF intensity decreased rapidly as strength decreased, in a practically monotonic trend, especially for flexural strengths below 40,000 psi. Also as before, the LPF values for the high-strength samples showed significant increases at the outset of thermal treatment relative to the unheated samples, which may be due to additional curing of the epoxy resin during initial heating or changes in the quantity of exposed resin on the sample surface.

LPF is an exceedingly powerful means for probing localized changes in the electronic structure and environment of individual functional groups and for detecting small populations of molecules in a complex matrix. For opaque materials, such as the IM6/3501-6 laminates, LPF can be accurately modeled as a surface phenomenon. In the surface model, a monolayer of molecules on the planar surface is illuminated by the laser; those molecules that are resin based (nondegraded resin and resin degradation products) can be expected to fluoresce, while the IM6 graphite fibers are not expected to produce substantial fluorescence. Using this approach, LPF intensity (I_{LPF}, in counts/s) is determined by the following relationship:

$$I_{LPF,\lambda} = (k_{1,\lambda}\, \sigma_1 c_1 \;+\; k_{2,\lambda}\, \sigma_2 c_2 \;+\; \ldots)\, \gamma_\lambda \Phi_\lambda \,,$$

where

Φ_λ = photon flux at wavelength, λ, impinging on the sample (excitation-photons/area/s),

γ_λ = detection efficiency of the spectrometer system at wavelength, λ (counts/emission-photon),

c_n = concentration of species, n (molecules/area),

σ_n = exposed cross section of n,

$k_{n,\lambda}$ = fluorescence cross section of n at wavelength, λ (emission-photons/molecule/excitation-photon).

The value of σ_n varies between 1 and 0, depending on the fraction of component, n, exposed—for a hypothetical surface that is 50% resin, $\sigma = 0.5$.

Using this model, it is clear that factors that affect the fraction of exposed resin will have a proportional effect on the observed LPF signal. For many of the panels, visual inspection indicates that the amount of surface resin differs on a millimeter-to-centimeter scale, apparently due to thermally induced migration of resin while in the heated, glassy state; furthermore, such migration clearly affects the ratio of resin to fiber on the surface and so may also result in differences in LPF intensity on a submillimeter scale.

LPF response for the low-strength samples is quite low and shows little variation for samples with flexural strengths between 2,000 and 30,000 psi; this is in marked contrast with the results from the earlier study, which showed substantial changes in LPF intensity in this strength regime. This insensitivity is probably an artifact of the optical geometry used for these experiments, which is much less efficient than that used in the former studies (Fig. 23). Hence, the signal from the low-strength samples is barely detectable above the baseline, making quantitation difficult. The optical collection efficiency of the experiment could be improved dramatically with suitable engineering; this factor should be examined more carefully in subsequent studies.

To gage the role of sample positioning LPF response, a subset of six samples was examined twice using 488-nm excitation (Table 10). In the first experiment, samples were placed in a prepositioned sample holder that was kept in the same position for all six samples. Then the samples were retested, this time carefully optimizing the position of each panel. With the exception of sample 05-47, differences in response were in the range of 1 to 5%; sample 05-47 (350°F/60 min) had a difference of 22% between the two experiments. This large difference is probably due to greater inhomogeneity of exposed resin in the sample. Note that the three samples with this particular thermal treatment (05-47, 05-07, and 02-62) had LPF responses which varied from 333 to 1900 counts/s at 482.5 nm (Table 6) and proportional differences from 299 to 1600 counts/s at 488.0 nm (Table 8). Further study of this low-thermal-degradation regime will be necessary to determine the cause of these differences.

CONCLUSIONS

The results obtained with LPF confirm that clear differences exist between composite samples that exhibit varying degrees of thermal degradation. It was found that the LPF intensity measurements in the 510- to 535-nm region exhibited general decreases in intensity as strength decreases (or heat damage increases). These intensity decreases were fairly significant at the early to middle stages of heat damage, and tended to level off at the advanced stages of heat damage. Furthermore, the results obtained using laser excitation at 482.5 and 488.0 nm seem to provide equivalent results. Hence, the strong 488-nm argon-ion-laser line can be used in place of the much weaker 482-nm krypton-ion-laser line.

Instrumentation dedicated to an LPF composite heat-damage-detection device could be developed from a simple, portable, laser Raman spectrometer system being developed at ORNL. The initial prototype, based on an air-cooled argon-ion laser, uses a fiberoptic probe for remote Raman monitoring (Fig. 24). Modifications to the probe would allow this device to be utilized for LPF monitoring applications. The current 3-ft^3 instrument weighs ~40 lb and is designed for field operation; it is connected to the sampling probe via a duplex fiber-optic cable, which may be up to 100 m or more in length. An LPF probe would be designed for hand-held operation and could be scanned over exposed composite surfaces. Real-time data analysis could be implemented to facilitate interactive investigation of aircraft surfaces. As needed, smaller, self-contained instruments could be developed based on this system; these devices might be more applicable for field interrogation at forward-field locations (Fig. 25).

PART 3. DIFFUSE REFLECTANCE INFRARED FOURIER TRANSFORM

INTRODUCTION

DRIFT was evaluated as a means of analyzing IM6/3501-6 composite laminates for resin degradation as a possible technique for inspecting aircraft composite structures in service for heat damage and loss of mechanical properties. DRIFT is a method of scattering IR light from the surface of a material, collecting the diffusely scattered light, and reducing that to an infrared spectrum from which qualitative and quantitative chemical information can be obtained. Of particular use to composite materials is that the IR spectral information is specific to chemical functional groups such as ketones, esters, hydroxyls, hydrocarbons. Levy et al.,[18] Luoma and Rowland,[20] Lin et al.,[26] and Cole et al.[27] have demonstrated, in principal, that internal reflectance and, as demonstrated by Cole et al.,[27] diffuse reflectance, are applicable to the study of epoxy resins, including oxidation, and have discussed in detail spectral-band assignments and the general methods. Unlike internal-reflectance techniques for obtaining similar IR spectra, DRIFT does not require mechanical contact with the surface being studied and is, therefore, a more passive method of measurement.

EXPERIMENTAL

The available laboratory facilities for such analyses consisted of a BIO-RAD FTS-60 fourier transform infrared (FTIR) spectrometer with a praying-mantis diffuse-reflectance sample compartment accessory (Harrick Scientific Model DRA-3CQ), with evacuable cells for analyzing small specimens in a controlled environment and a barrel ellipsoid IR inspection accessory "SPECTROPUS" system. The use of evacuable cells with the praying-mantis optics was developed jointly by authors Powell and Smyrl with Harrick Scientific, Inc., for analyzing materials at elevated temperatures in controlled gaseous environments and is essentially described by Smyrl et al.[28] Fuller et al.[29,30] applied the technique to the *in situ* isothermal oxidation of coal that is very similar to studying the oxidation of graphite-epoxy composites. The evacuable cell with its gas inlet and exhaust system is shown in Fig. 26. Figure 27 shows the sample stage that is supported on a re-entrant heater, as seen through the zinc selenide (ZnSe) exit window, with the gas inlet tube and the thermocouple visible on the sample stage. Figure 28 shows the cell mounted in the praying-mantis optics with the sample stage visible through the ZnSe window in the inlet paraboloid. For these experiments, the specimen was 0.125 in. thick and 0.5 in. by 0.5 in. square with every diffuse reflectance spectrum obtained from the same 0.08-in.-(2-mm-) diam spot near the center of the square. The inlet gas was regulated by a precision-metering valve for which the supply gas could be either argon or compressed air at 19.6 psi (135 kPa). The sample was maintained at constant temperature, and oxidation was initiated by switching the supply gas from argon to compressed air using valves. The exit gas was connected to a hood exhaust. The barrel ellipsoid IR inspection accessory "SPECTROPUS" system is the prototype

system developed jointly by author Powell and Harrick Scientific, Inc.,[31] to extend diffuse reflectance measurements beyond the spectrometer sample compartment to analyze large surfaces. This accessory allows for diffuse reflectance spectra to be obtained from almost any convex or flat surface, with no purge-time delays and with spectral quality comparable to the best capabilities of FTIR instruments. The system is being offered commercially by Harrick Scientific, Inc., but currently these are the only accessories of their type in existence. The barrel ellipsoid accessory is a true inspection machine, and an artist's concept of the accessory is given in Fig. 29. This accessory was used to obtain DRIFT spectra from 0° IM6/3501-6 flexural specimens. With no particular emphasis on speed, the 130 analyses on the 1- by 3-in. flexural specimens presented here were carried out in two working days. The system is capable of obtaining several hundred spectra per day. Both the evacuable-cell/praying-mantis system and the barrel-ellipsoid system have excellent rejection of specularly reflected light, which was the main problem encountered by Cole et al.[27] with the diffuse-reflectance method.

The IR spectra were obtained using an open aperture with 4-wave number resolution and 4 × 0 filling. The working background spectra for both accessories was obtained using sandblasted 304L stainless steel. The spectra obtained from the IM6/3501-6 specimens were ratioed to this background and converted to absorbance units, a simple logarithmic relationship. At the end of the oxidation experiment that will be presented later in this report, the underside of that specimen that had been in contact with the heater yielded, when analyzed with the barrel ellipsoid, a spectrum that was featureless with respect to IR bands. This specimen was assumed to be representative of resin-free IM6 graphite fiber, and a spectrum obtained from a typical specimen using this background is shown in Fig. 30. The spectra obtained using the stainless-steel reference was very similar, except the baseline sloped from 0.7 absorbance units at 4000 wave numbers to 0.56 absorbance units at 500 wave numbers. The spectra were not converted to Kubelka-Munk units[27] because this requires near-perfect confidence in the background correction. If Fig. 30 represents the appropriate background correction, then the Kubelka-Munk algorithm would result in only a minor change because Kubelka-Munk and absorbance units have the same values near 0.3 but would exaggerate larger values for absorbance. The main features in the spectrum shown in Fig. 30 are the O-H (hydroxyl) stretching band at 3500 wave numbers, the C-H stretching bands near 3000 wave numbers (aromatic hydrocarbons above 3000 wave numbers, aliphatic hydrocarbons below 3000 wave numbers), the aliphatic ketone or aldehyde near 1730 wave numbers, and aromatic ring bands at 1600 and 1520 wave numbers. Spectral data were reduced to a few simple numbers using quantitative analysis software provided with the BIO-RAD spectrometer, in particular the program class from the Quant32 software package. Spectra obtained using the stainless-steel reference were linearly baseline corrected using an average value over 20 wave numbers, ~3800 wave numbers, and ~2000 wave numbers, followed by the measurement of peak heights and band areas using the program CLASS. These reduced spectra were written into a data file, along with other data such as the time the spectra was obtained and comments on individual analyses. This data file was transferred to an IBM-compatible personal computer and further processed or merged with flexural strength property data using a spread-sheet program. The temperature of the sample stage was monitored using a digital pyrometer having an analogue output monitored at 5-s intervals using a Nicolet 4094 digital oscilloscope with a calendar clock that was synchronized with that of the IR spectrometer.

EVACUABLE CELL RESULTS ON A SINGLE IM6/3501-6 SAMPLE

A specimen loaded into an evacuable cell was given a temperature cycle with an argon flow to check out the temperature control system and to evaluate spectral changes related to thermal effects rather than oxidation. The temperature cycle consisted of stepwise heating to 290°F, 360°F, 470°F, and 540°F with 1.2-ks hold times at each step, and, finally, the temperature was raised to 608°F for 3.2 ks before turning the power off. These thermally induced changes were minor, and the most significant was a 15% decrease in absorbance units for the hydroxyl band and a comparable decrease in the 1730-wave number carbonyl band that was accompanied by some line broadening. The specimen was isothermed at 553°F under an argon flow and, at time = 0 s, the gas was switched to compressed air. The specimen was maintained at 553°F for 172 ks, after which the temperature was raised to 650°F for an additional 20 ks. Spectra were obtained as rapidly as possible (140 s per spectrum) for the first 4 ks, after which a delay between spectra was used to monitor the slower changes at longer times. Figure 31 shows baseline-corrected spectra in the carbonyl region indicating oxygen addition reactions. During the first kilosecond, the specimen experienced the rapid addition of a phenone (1650 wave numbers) and the assimilation of the 1730-wave number aliphatic ketone/aldehyde band into a broad structure, including the ketone-phenone spectral region. At longer times, the carbonyl region expanded below 1800 wave numbers, indicating a general increase in the degree of oxidation with the formation of acids, esters, acid anhydrides, and carbonate esters. A decrease in the aromatic-ring character was also apparent from the 1600 and 1520 wave number bands. Figure 32 shows baseline corrected spectra in the C-H, O-H, N-H region, where the loss of aliphatic hydrocarbons (2900 wave numbers) occured in preference to aromatic hydrocarbon (3050 wave numbers) as observed for coal,[29-30] a similar loss was observed for aliphatic hydroxyls (3550 wave numbers), and a new band appeared (perhaps an amine) at 3470 wave numbers.

Figures 33 through 35 show the time dependence of the oxidation processes using reduced-spectral data as relative absorbance obtained as follows. The term "band" refers to the factor multiplying the last unoxidized spectra that would subtract that feature from a particular oxidized spectrum, i.e. a normalized peak height. The term "band edge" is the value of the baseline-corrected spectrum at the indicated wave number divided by some feature in the spectrum, i.e., the maximum value between 1720 and 1750 wave numbers for the carbonyl region (1600 to 2000 wave numbers) and the maximum value between 3350 and 3425 wave numbers for the hydroxyl region (3000 to 4000 wave numbers). The "band area" is an integral over some region of the baseline-corrected spectrum divided by the integral between 1320 and 1380 wave numbers, a region of the spectrum that is not strongly affected by oxidation. For the carbonyl region, the integration range was 1600 to 2000 wave numbers. For the hydrocarbon region the integration range was from 2670 to 3130 wave numbers with the baseline corrected for a 20-wave-number average over the integration limits. For Figs. 35 through 37, the band edge and band area determinations were further normalized by a factor that made the value for the last unoxidized spectrum unity. These spectral-reduction calculations are probably not the most optimal spectral-reduction procedures, but they do yield a useful means of monitoring oxidative changes. The division of band edges and band areas by other features in the spectrum are not essential to the analysis of the evacuable cell data where the spectrum was obtained from one spot on one

specimen. They were essential for the analysis of flexural-test specimens where sample-to-sample variations in resin content, generally taken as the variation in the spectrum at 1350 wave numbers, were very significant.

The 1730-wave-number carbonyl band present in the specimen that was not heat damaged was assimilated into the ketone-phenone region of the spectrum as the phenone band appeared, i.e., in the first kilosecond of oxidation. During the first 10 ks of oxidation, half the aliphatic hydrocarbon and hydroxyls were burned away and the apparent resin thickness (1350 wave numbers) decreased by ~20%. Eventually, all of the aliphatic hydrocarbons and hydroxyls were removed by oxidation at approximately the same rate. The hydroxyl-band-edge measurement does not go to zero because of the formation of another band, probably an amine, with a maximum value at 3470 wave numbers. A comparison of the carbonyl-band edge and area measurements shows that the band area responds most rapidly at early times because it includes the phenone region. The carbonyl-band area best monitors the total oxidation. The 1775-wave-number band edge responds more slowly and may be interpreted, in an over simplified manner, as the formation of organic acids. The 1800-wave-number band edge even grows more slowly and probably indicates the formation of acid anhydrides or carbonate esters.[29-30] Heating the specimen to 650°F had little effect on the reduced spectra; however, the baseline gradually shifted from 0.7 absorbance units to >2 absorbance units, with a marked decrease in signal-to-noise ratio indicating that the specimen was deteriorating and probably moving outside the focal plane of the optics. A notable bulge on the top surface of the specimen was observed when the evacuation cell was dismantled.

BARREL ELLIPSOID RESULTS ON 0° IM6/3501-6 FLEXURAL SPECIMENS

The 1 × 3 × 0.125-in.-thick 0° IM6/3501-6 flexural specimens had been tested to failure by bending about their midpoint, leaving a 1- by 1-in. area on each end that had no cracks. This region was analyzed using the barrel ellipsoid operated in an inverted mode so that the specimen was simply placed on the opening containing the sample position focal point. Two analyses were obtained for each specimen, one from each end of the specimen. These specimens typically consisted of lots of four to nine (from four different panels), each having the same time-temperature exposure to an air environment heated by radiant quartz lamps (described in Part 1), including as-cured (room temperature specimens), 350°F for 60 min, 450°F for 60 min, 550°F for 5 min, 550°F for 30 min, 550°F for 60 min, 650° for 5 min, 650°F for 30 min, 650°F for 60 min, and 750°F for 30 min. These specimens yielded excellent spectra; however, the amount of resin on each, as indicated by the 1350- wave-number absorbance varied from specimen to specimen by as much as a factor of 2. Approximately 7% of the specimens had little or no resin as detected by the IR spectrum, and a notable change in the surface reflectivity as observed visually. These highly resin deficient specimens were discarded. Figures 36 through 39 give the results of these analyses in terms of the flexural strength plotted as a function of reduced-spectral parameters. The data correlated well with the exception of the 650 and 750°F data. Specimens given these extreme conditions did not show as much evidence of carbonyl addition or hydrocarbon loss as did the specimens oxidized at lower temperatures. The hydroxyl band edge, however, did correlate well with flexural-strength data for all heat treatments (Fig. 39). This indicates

that the oxidation process probably involves a number of different reactions involving the addition of oxygen as various carbonyl species that generally increase in oxygen content as oxidation progresses and the removal of hydrocarbons by water formation. The early addition of oxygen as phenones and ketones or aldehydes does not appear to have a marked effect on the mechanical strength properties but makes an excellent indicator that the specimen has experienced an oxidizing environment. That the loss of hydroxyl species best correlates with the loss of strength is best explained by the fact that the hydroxyl species is the residual oxygen from the epoxide ring, and its loss may be directly associated with the breaking of the resin cross-links that were formed during the curing reactions. The loss of hydroxyls and the formation of amines, along with the observation in the literature of the formation of propenal in the gas phase,[32] is consistent with the expulsion of the three-carbon chain that had contained the original epoxide ring being the main reason for loss of strength.

CONCLUSIONS

Diffuse reflectance DRIFT is an excellent method for monitoring the oxidation of the TGDDM-DDS polymer matrix resin in the laboratory using evacuable cells and for inspecting large polymer matrix composite parts in the field. Flexural-strength measurements correlate well with reduced-spectral parameters. The formation of phenones and ketones signal that a surface has seen some oxidizing environment before loss of strength and the hydroxyl band edge can be calibrated to directly indicate mechanical strength.

RECOMMENDATIONS FOR FUTURE WORK

The results from this study have demonstrated that LPF and DRIFT can detect and quantify heat damage in PMCs and correlate this damage to the residual mechanical strength properties. In addition, preliminary results indicate that by retarding the amount of oxygen coming into contact with the composite, the heat damage that is sustained at elevated temperatures may be diminished, thereby extending the useful service life of the material.

The present work suggests many areas of research and development for the LPF and DRIFT techniques, including building a lightweight and rapid-scanning, field-portable inspection device that directly estimates the extent of heat damage on IM6/3501-6 (and/or other fiber/resin combinations) panels located on aircraft and/or on other composite structures susceptible to this type of damage.

The optimization of the peculiar design and utility considerations of the device, including weight, size, scan speed, environmental durability, type of data output, and cost needs to be evaluated.

The evaluation of the composite structure in its service environment, including the effects of superficial contaminantion (i.e. paints, moisture, and engine exhaust) and variable surface resin content on the LPF and DRIFT spectral features of simulated and/or actual heat-damaged panels needs to be addressed.

Other areas needing additional study include the development of new and better statistically valid algorithms for obtaining reduced-spectral data to improve the correlation of mechanical properties and the speed of analyses.

Various evacuable cell experiments with DRIFT and mass-spectrometric gas analysis that would better define the mechanisms and rates of reactions and oxygen transport through a material should be evaluated. These experiments would be used to further optimize the inspection device and determine the dependance of oxygen at elevated temperatures on the mechanical properties of heat damaged laminates. From the results of this study, a development effort could be initiated to study various protective coatings capable of retarding composite-heat damage.

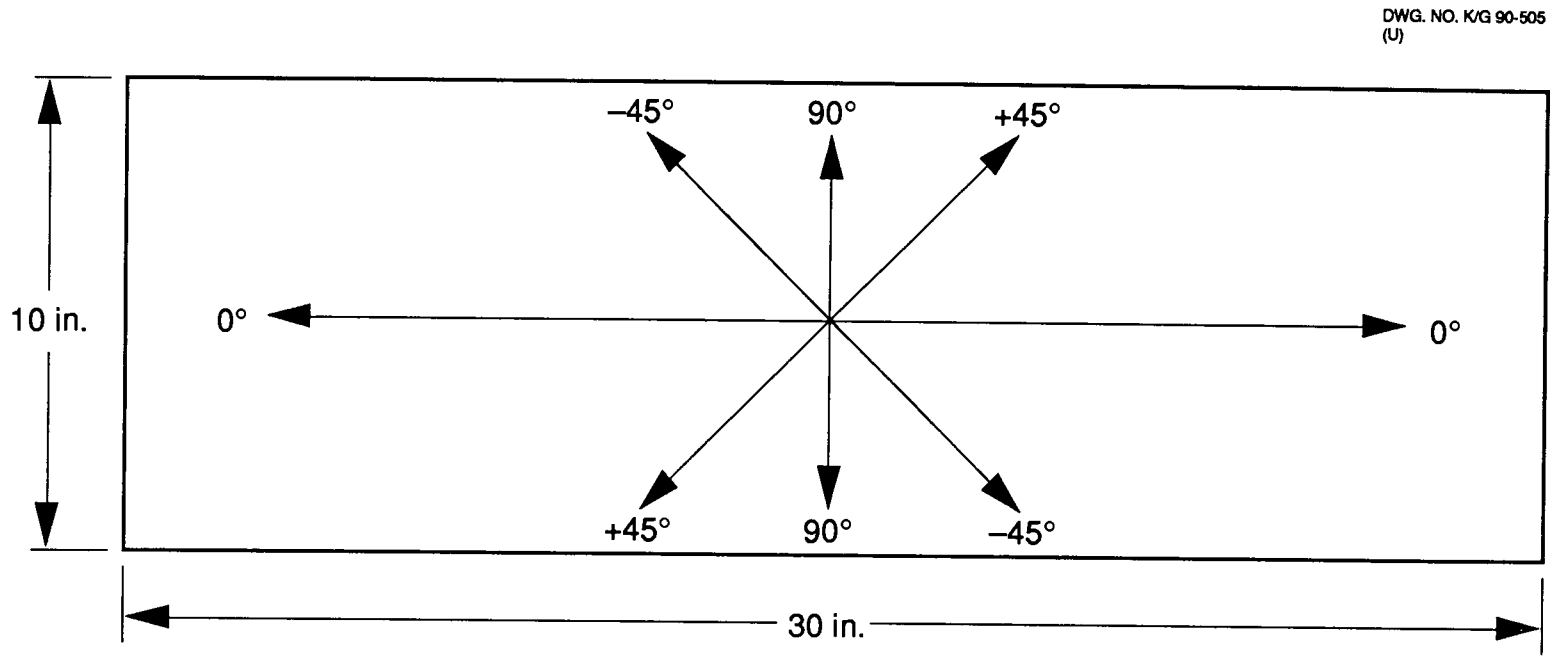

Fig. 1. Panel fiber orientation.

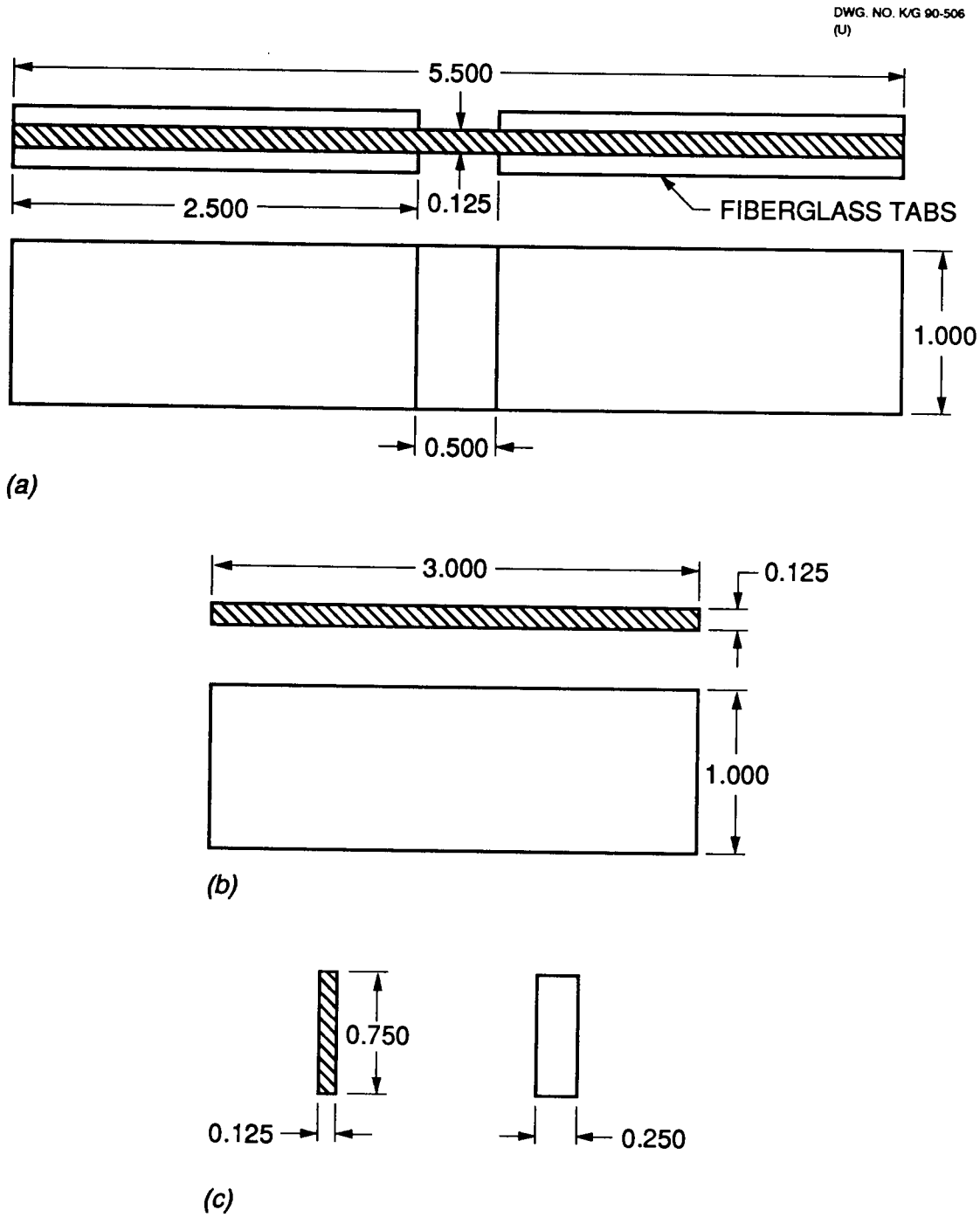

Fig. 2. Geometry of specimens for *(a)* compression, *(b)* flexure/shore-D, *(c)* short-beam-shear testing.

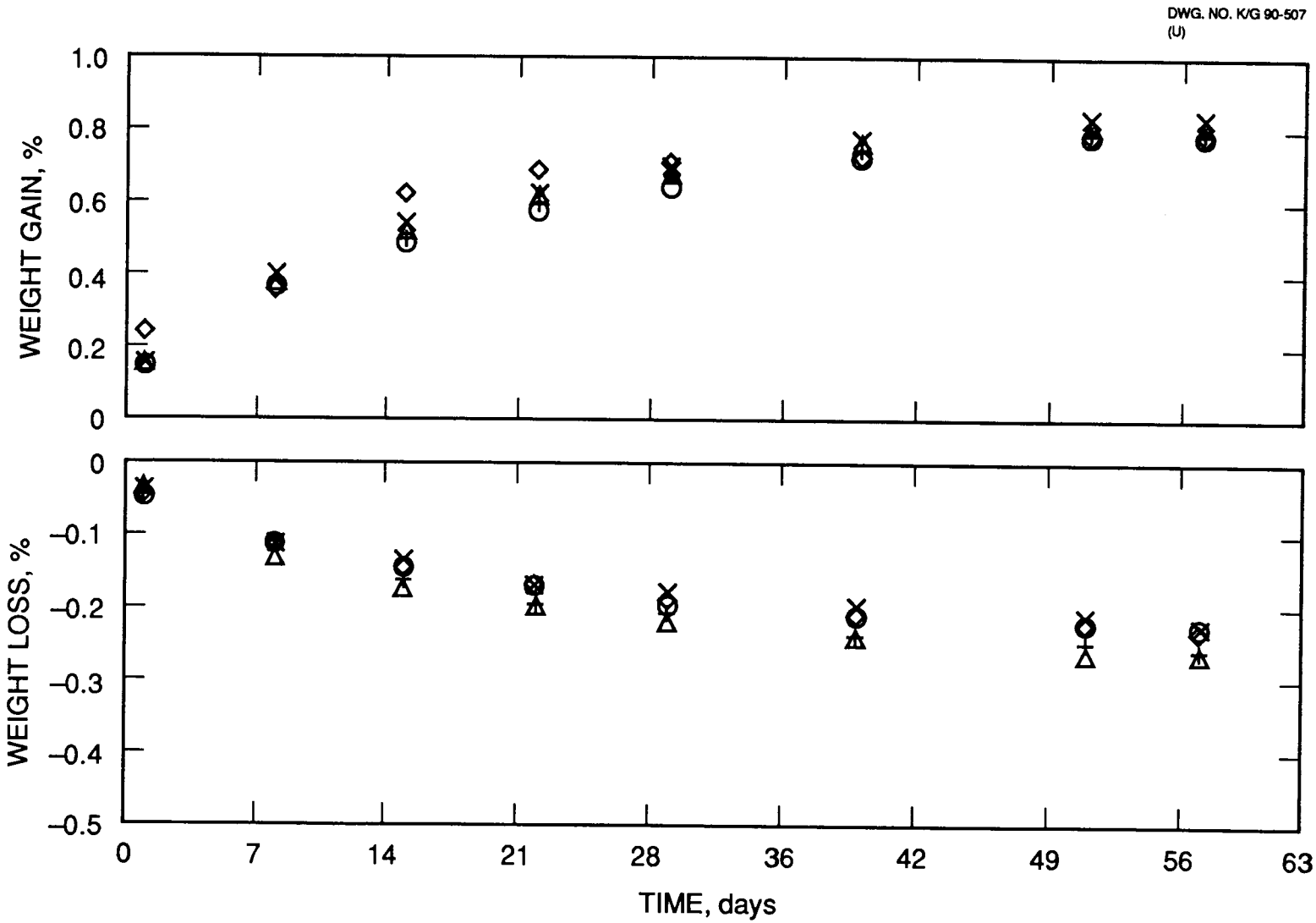

Fig. 3. Preconditioning profile of wet and dry IM6/3501-6 specimens, panel 5 data.

Fig. 4. Specimen heating chamber.

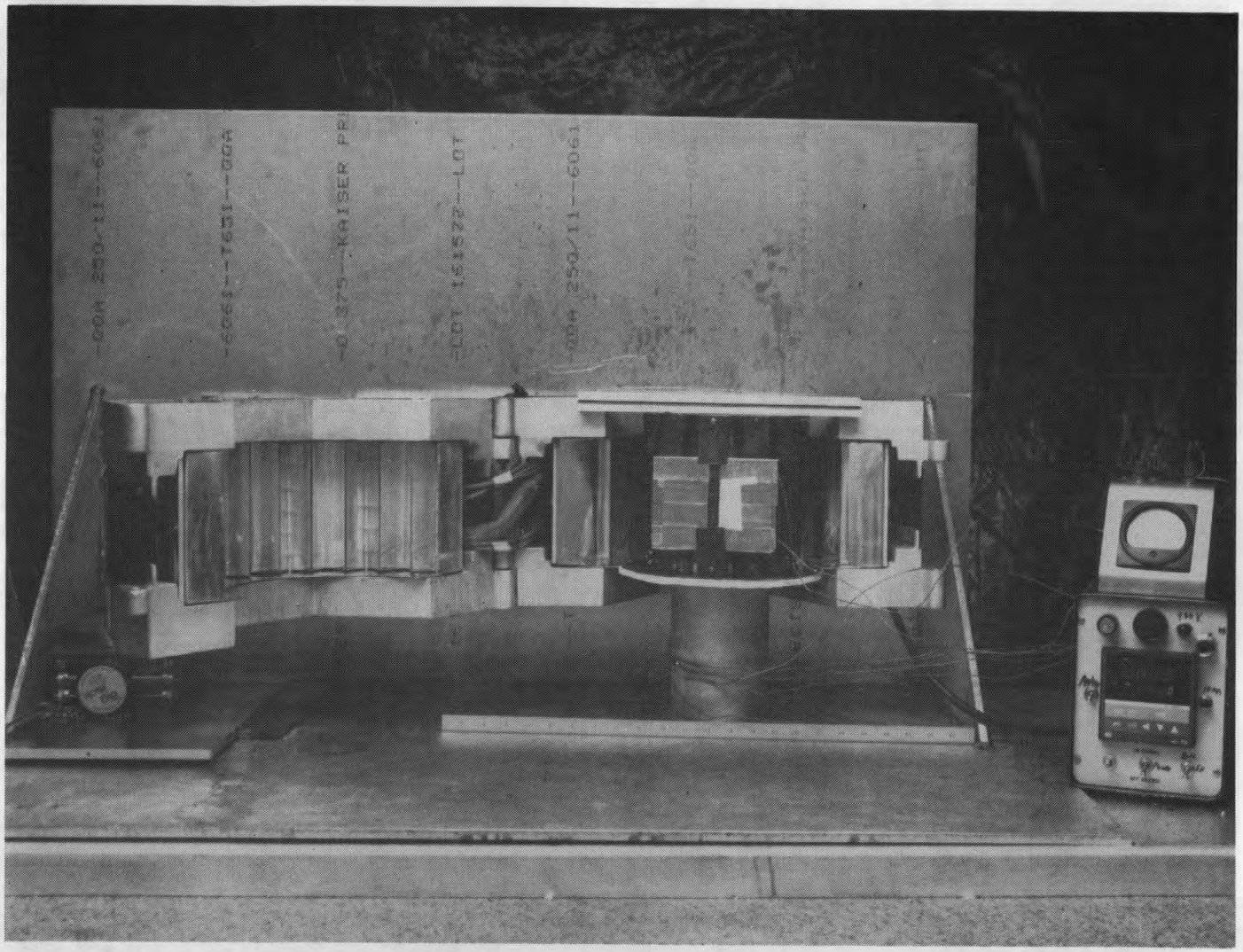

Fig. 5. Specimen heating chamber.

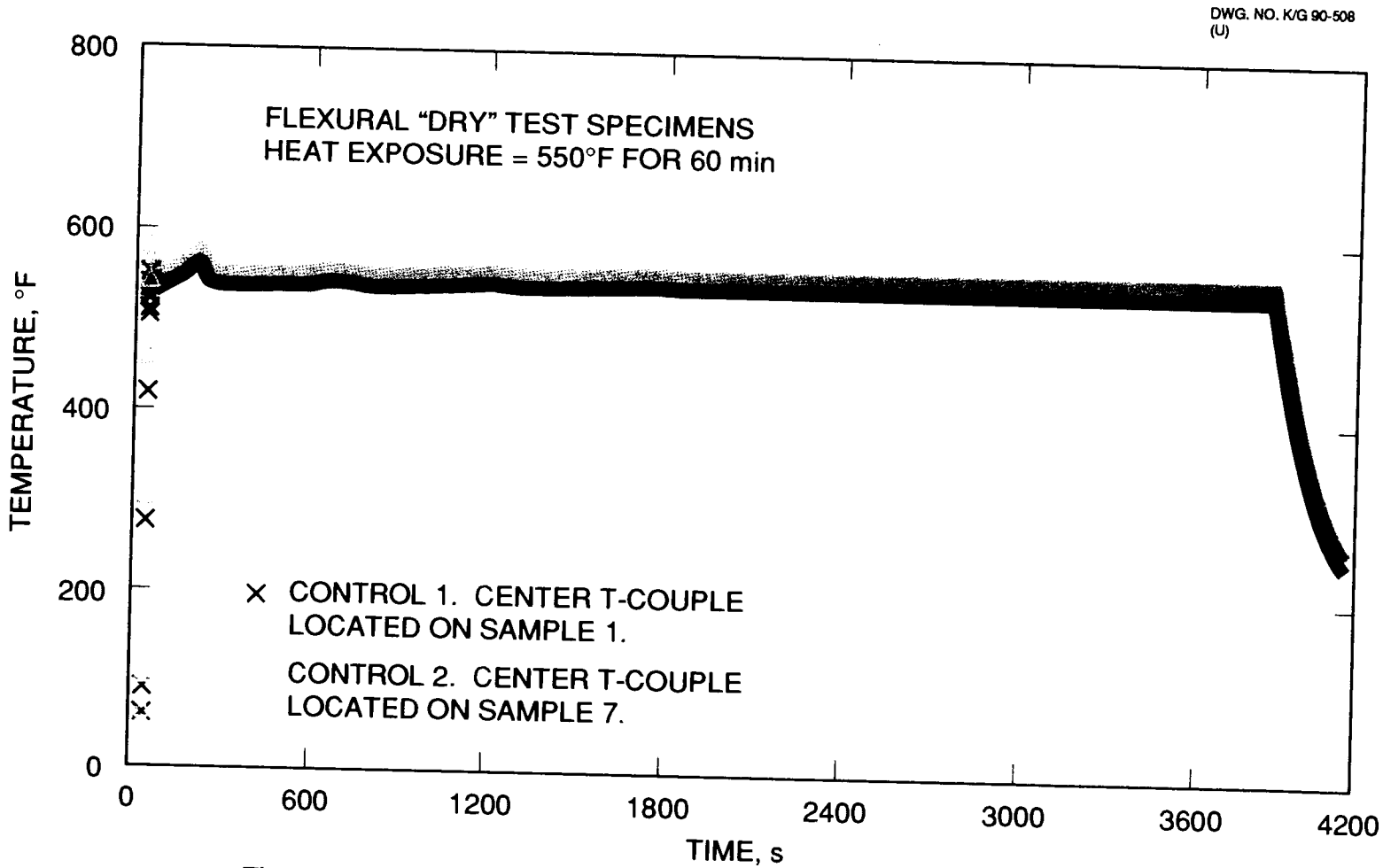

Fig. 6. Temperature monitoring of IM6/3501-6 specimens during heat exposure.

DWG. NO. K/G 90-960
(U)

COMPRESSION

Test method:	ASTM D3410-87
Specimen thickness, in.:	0.125
Specimen width, in.:	1
Specimen length, in.:	5.50
Gage length, in.:	0.50
Rate of test, in./min:	0.05

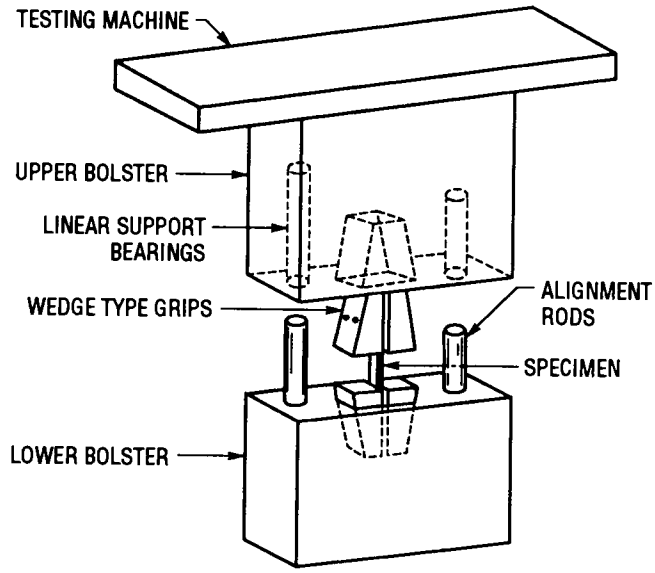

SHORT BEAM SHEAR

Test method:	ASTM D2344-84
Specimen thickness, in.:	0.125
Specimen width, in.:	0.25
Specimen length, in.:	0.75
Span, in.:	0.50
Rate of test, in./min:	0.05

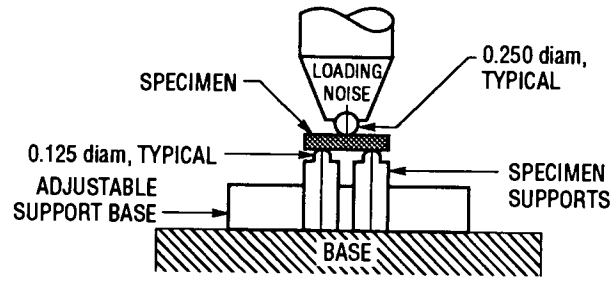

FLEXURE

Test method:	ASTM D790-87
Specimen thickness, in.:	0.125
Specimen width, in.:	1
Specimen length, in.:	3
Span, in.:	2
Rate of test, in./min:	0.05

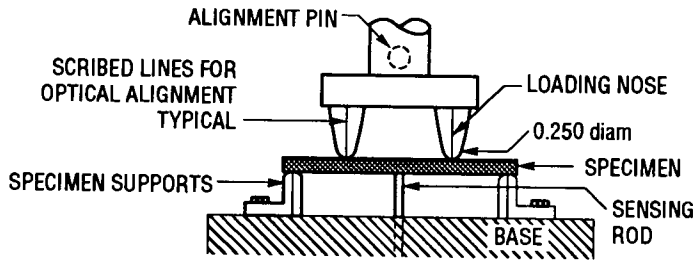

Fig. 7. Testing procedures for compression, short-beam-shear and flexure.

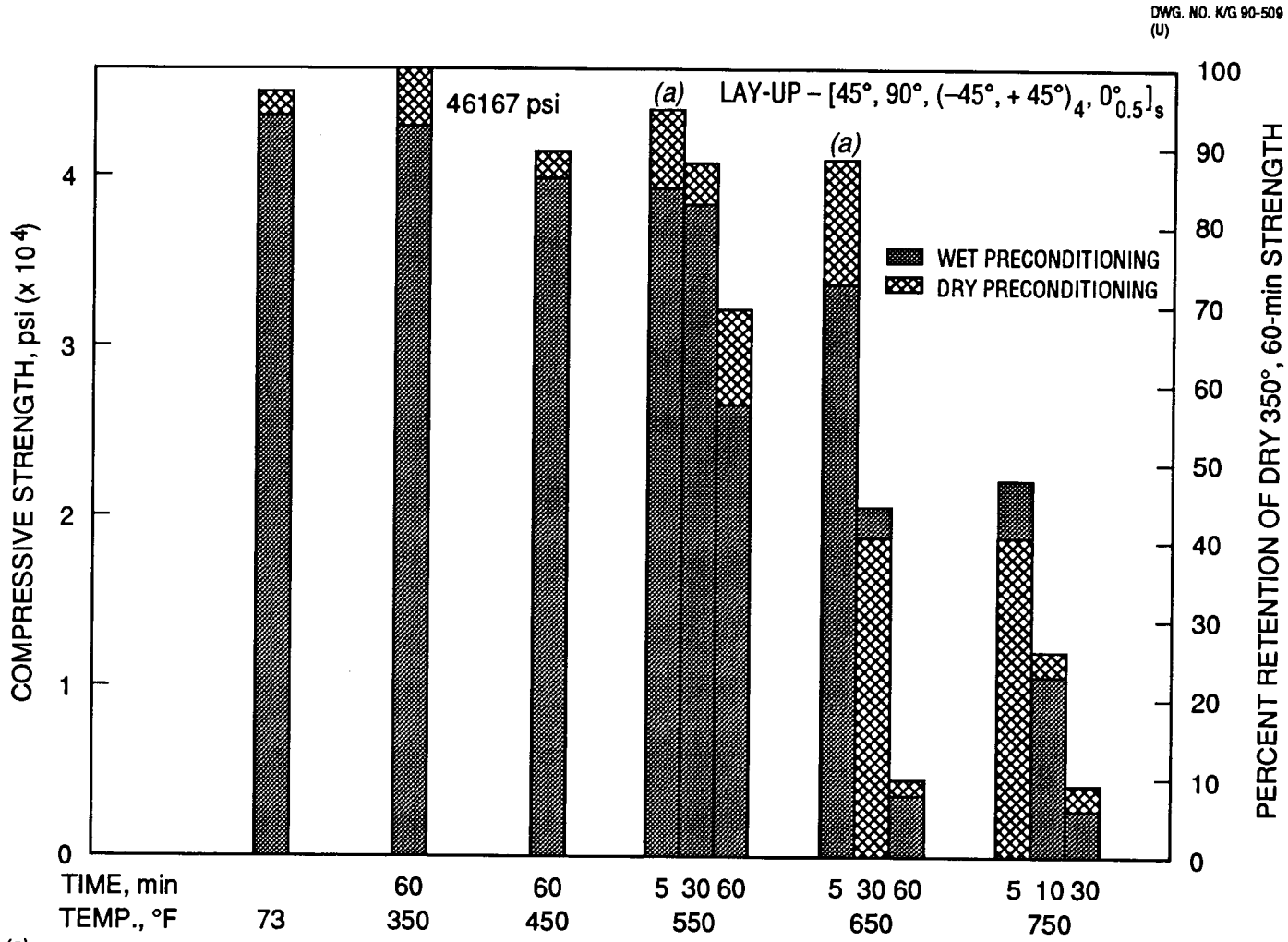

(a) WET AND DRY STRENGTH AVERAGES ARE STATISTICALLY SIGNIFICANTLY DIFFERENT AT THE 95% CONFIDENCE LEVEL.

Fig. 8. Test results for IM6/3501-6: ASTM D3410. Zero-degree compressive strength-vs-heat exposure temperature/time for wet and dry preconditioned specimens.

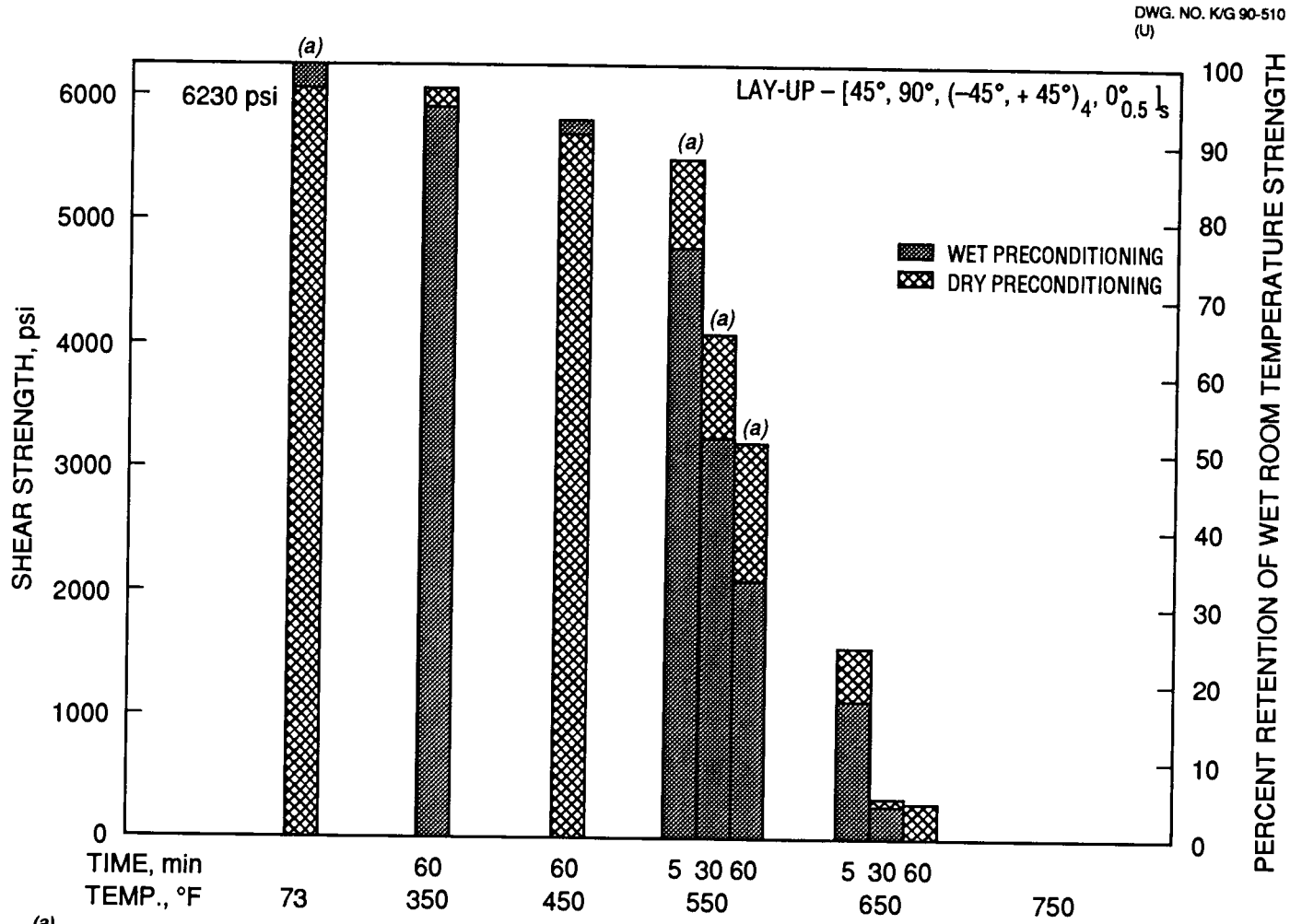

(a)WET AND DRY STRENGTH AVERAGES ARE STATISTICALLY SIGNIFICANTLY DIFFERENT AT THE 95% CONFIDENCE LEVEL.

Fig. 9. Test results for IM6/3501-6: ASTM D2344. Zero-degree short-beam-shear strength-vs-heat exposure temperature/time for wet and dry preconditioned specimens.

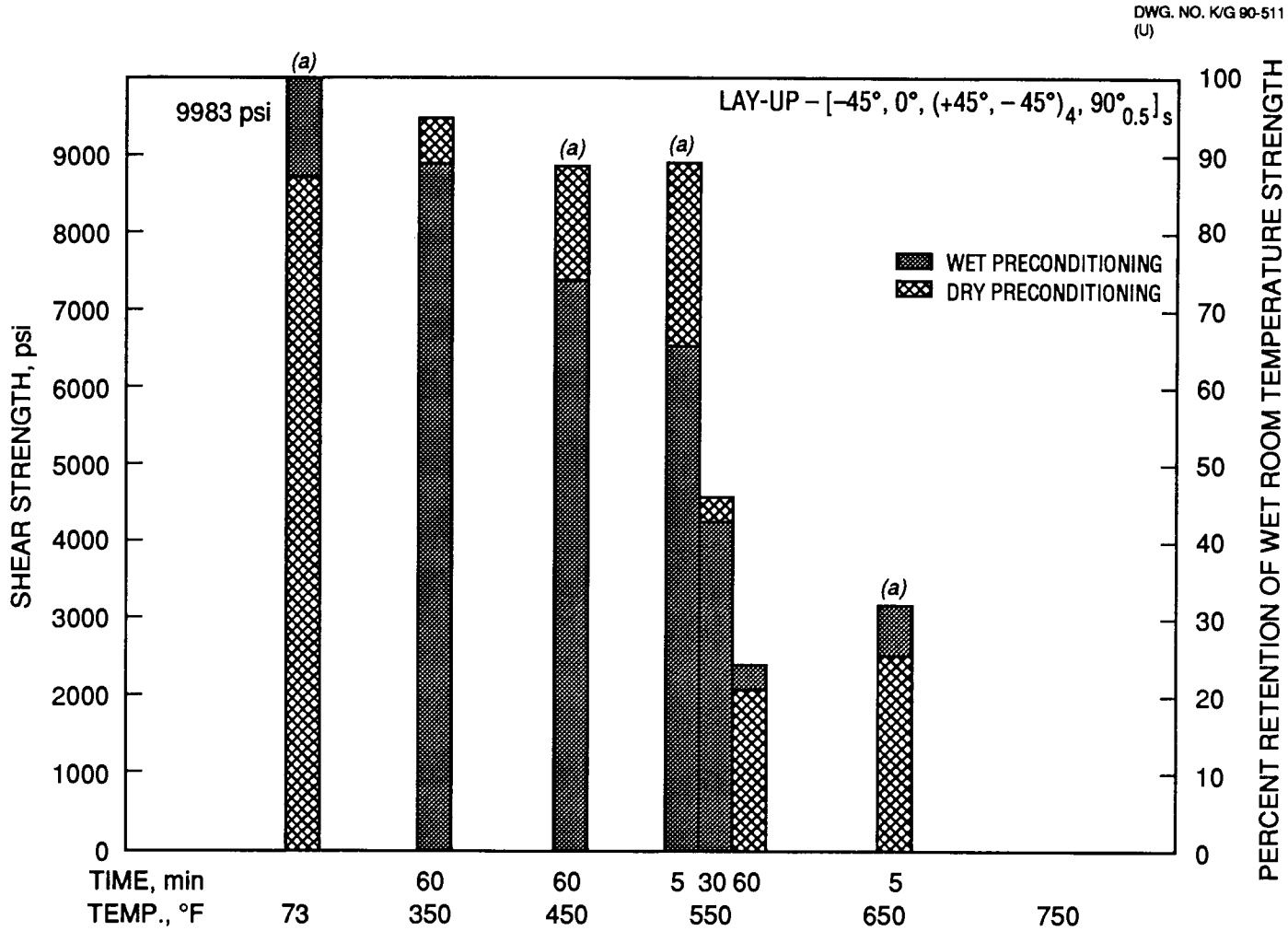

(a) WET AND DRY STRENGTH AVERAGES ARE STATISTICALLY SIGNIFICANTLY DIFFERENT AT THE 95% CONFIDENCE LEVEL.

Fig. 10. Test results for IM6/3501-6: ASTM D2344. Ninety-degree short-beam-shear strength-vs-heat exposure temperature/time for wet and dry preconditioned specimens.

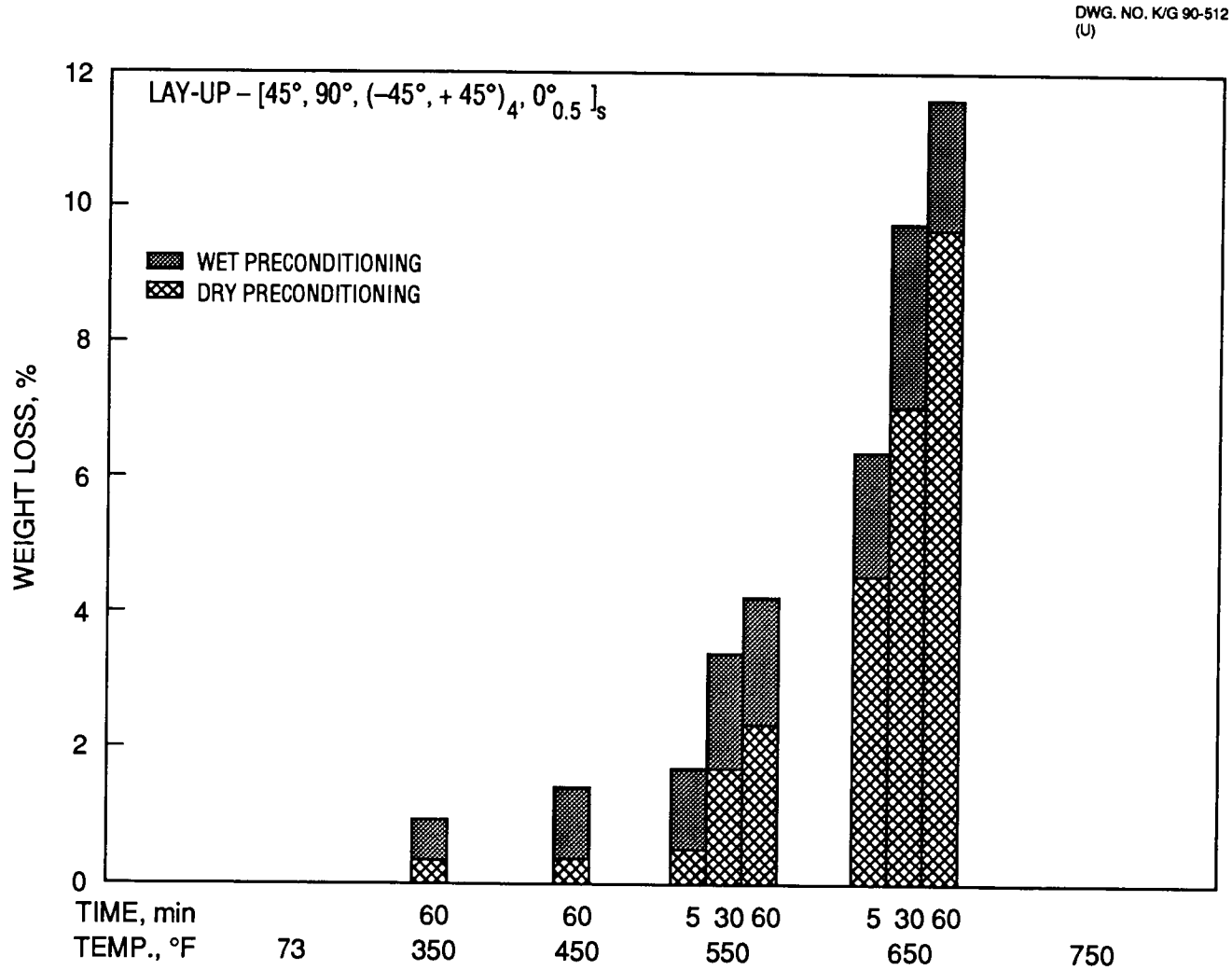

Fig. 11. Test results for IM6/3501-6. Percent weight loss-vs-heat exposure temperature/time for wet and dry preconditioned zero-degree short-beam-shear specimens.

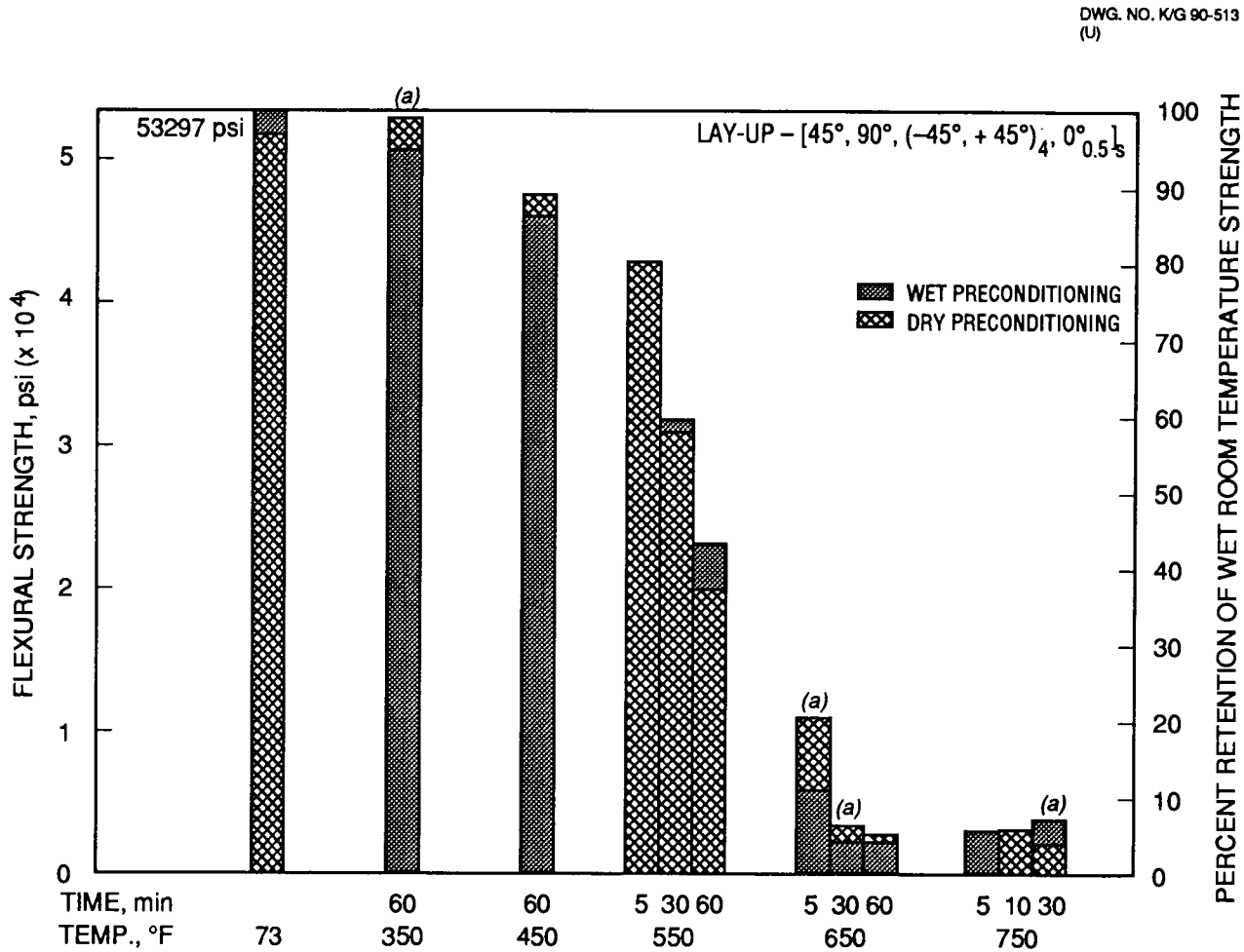

(a)WET AND DRY STRENGTH AVERAGES ARE STATISTICALLY SIGNIFICANTLY DIFFERENT AT THE 95% CONFIDENCE LEVEL.

Fig. 12. Test results for IM6/3501-6: ASTM D790. Zero-degree flexural strength-vs-heat exposure temperature/time for wet and dry preconditioned specimens.

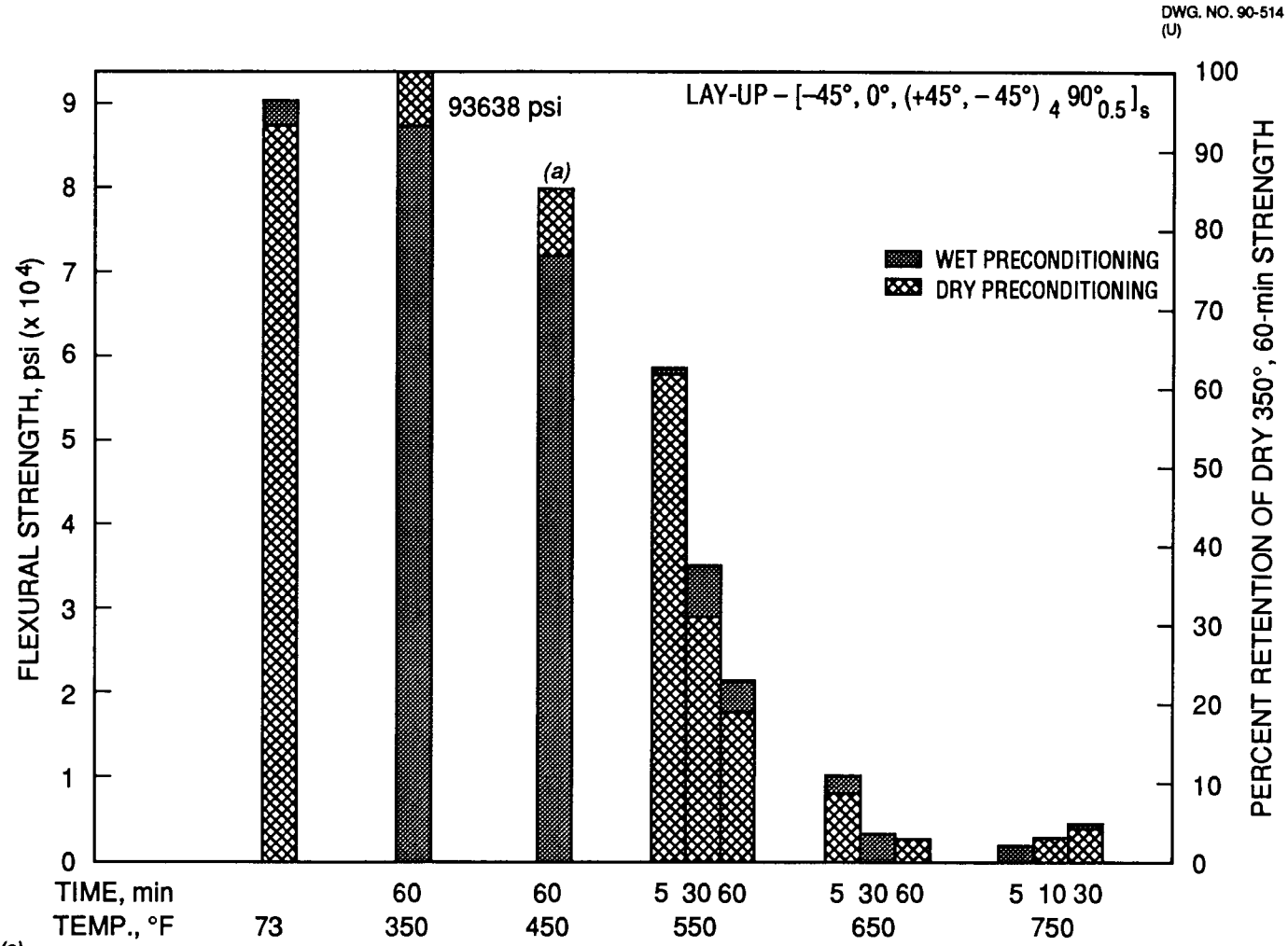

(a)WET AND DRY STRENGTH AVERAGES ARE STATISTICALLY SIGNIFICANTLY DIFFERENT AT THE 95% CONFIDENCE LEVEL.

Fig. 13. Test results for IM6/3501-6: ASTM D790. Ninety-degree flexural strength-vs-heat exposure temperature/time for wet and dry preconditioned specimens.

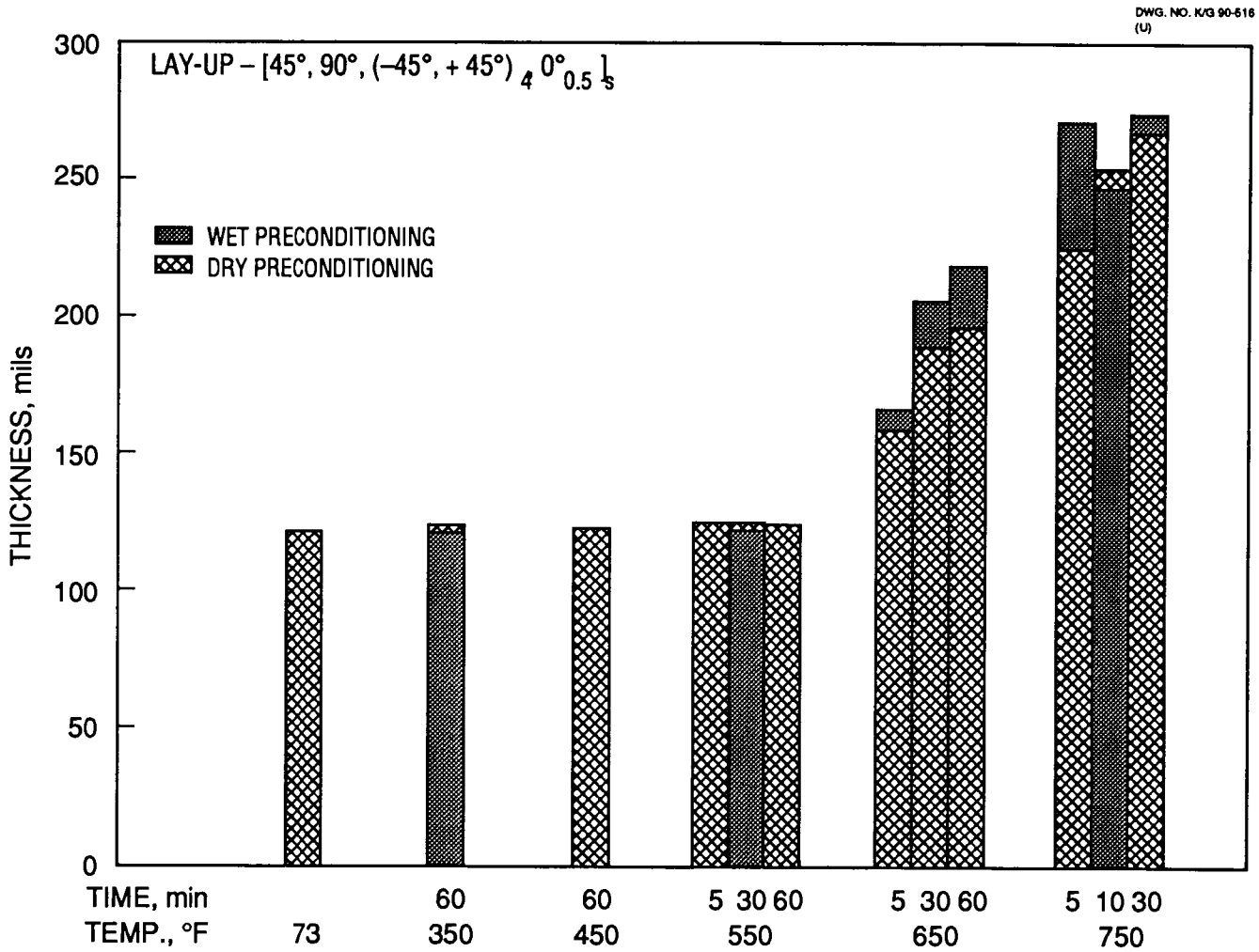

Fig. 14. Tests results for IM6/3501-6. Maximum thickness-vs-heat exposure temperature/time for wet and dry preconditioned specimens.

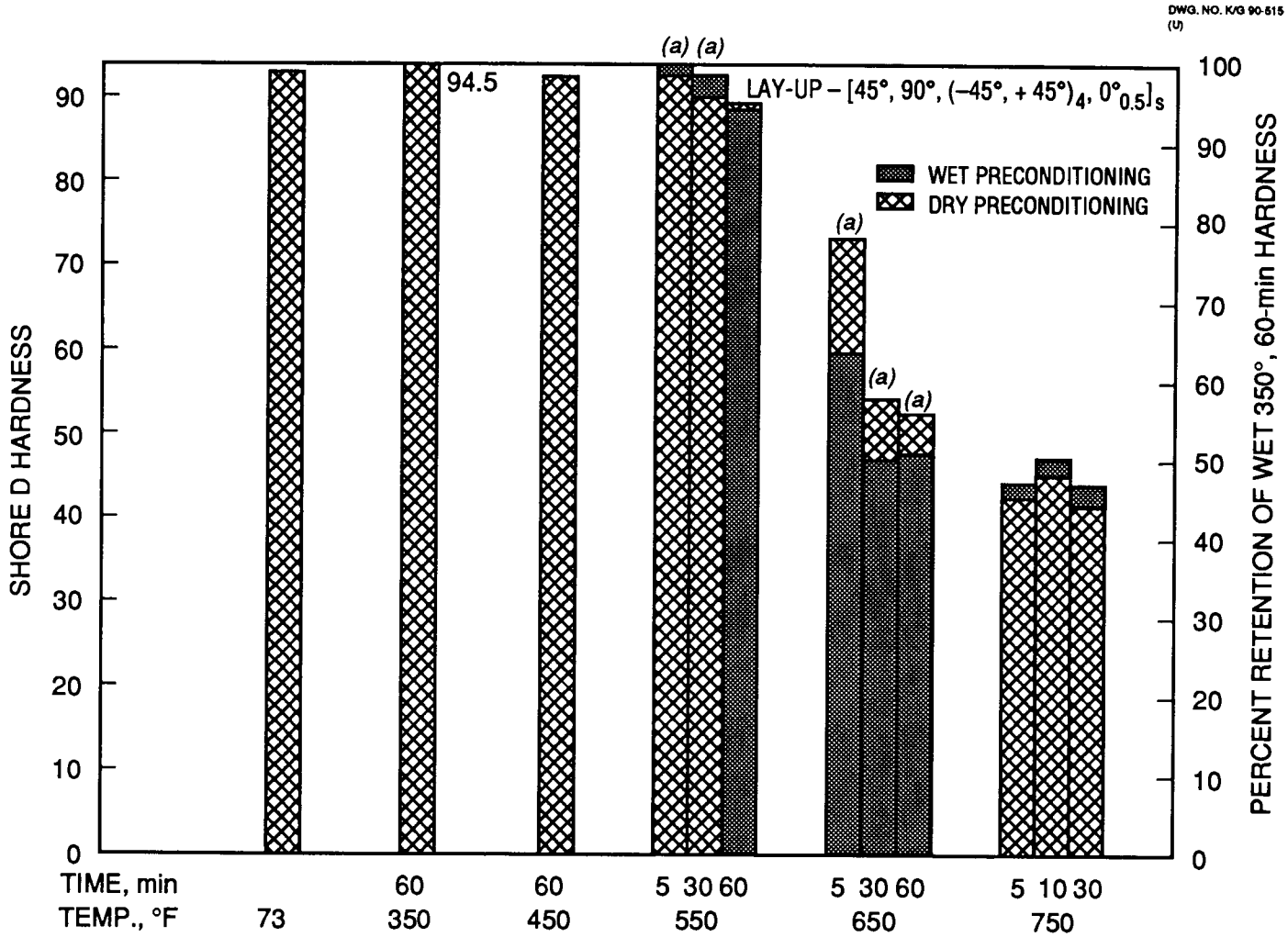

(a)WET AND DRY STRENGTH AVERAGES ARE STATISTICALLY SIGNIFICANTLY DIFFERENT AT THE 95% CONFIDENCE LEVEL.

Fig. 15. Test results for IM6/3501-6: ASTM D2440. Shore-D hardness-vs-heat exposure temperature/time for wet and dry preconditioned specimens.

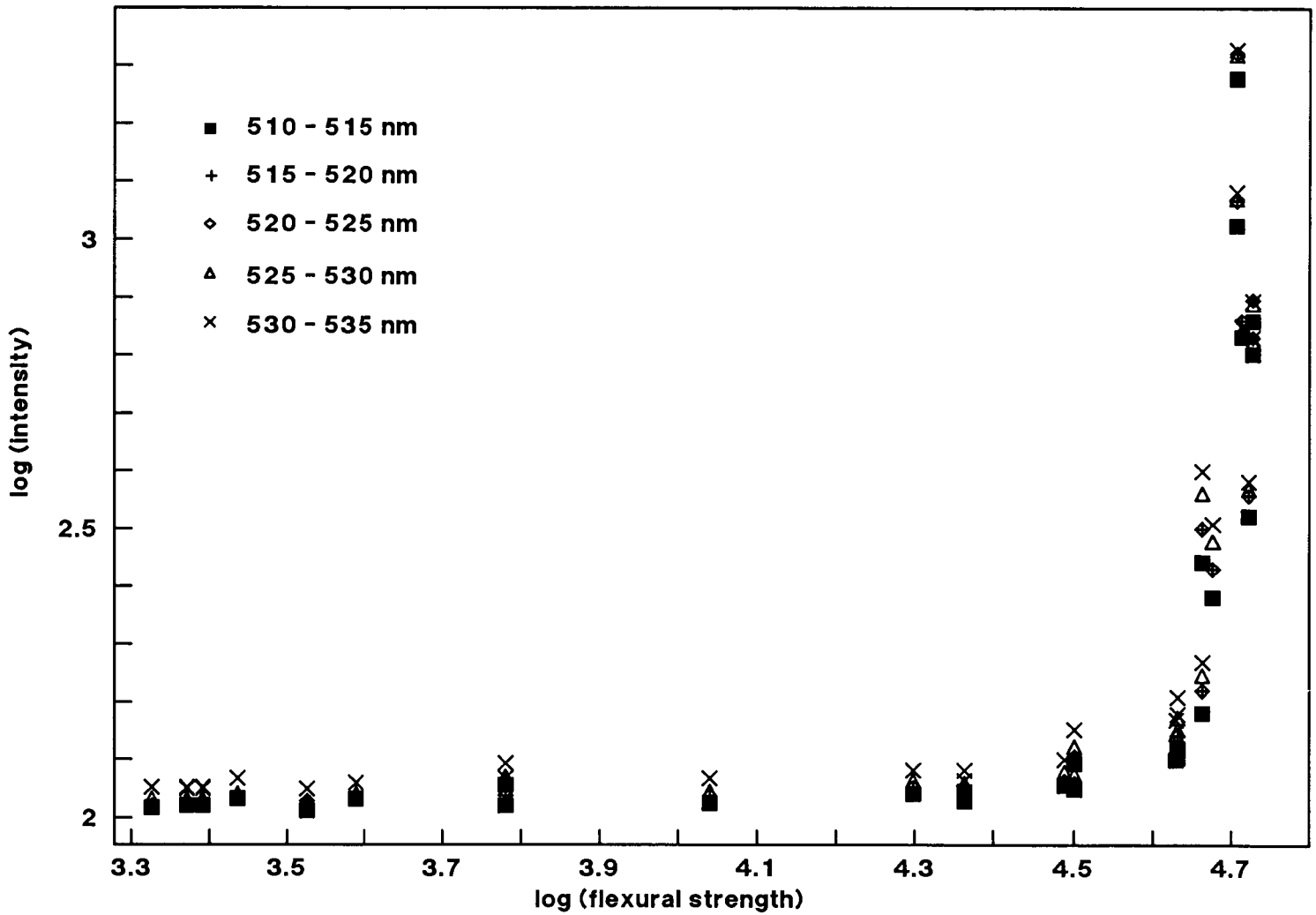

Fig. 16. Laser-pumped fluorescence using 482.5-nm excitation.

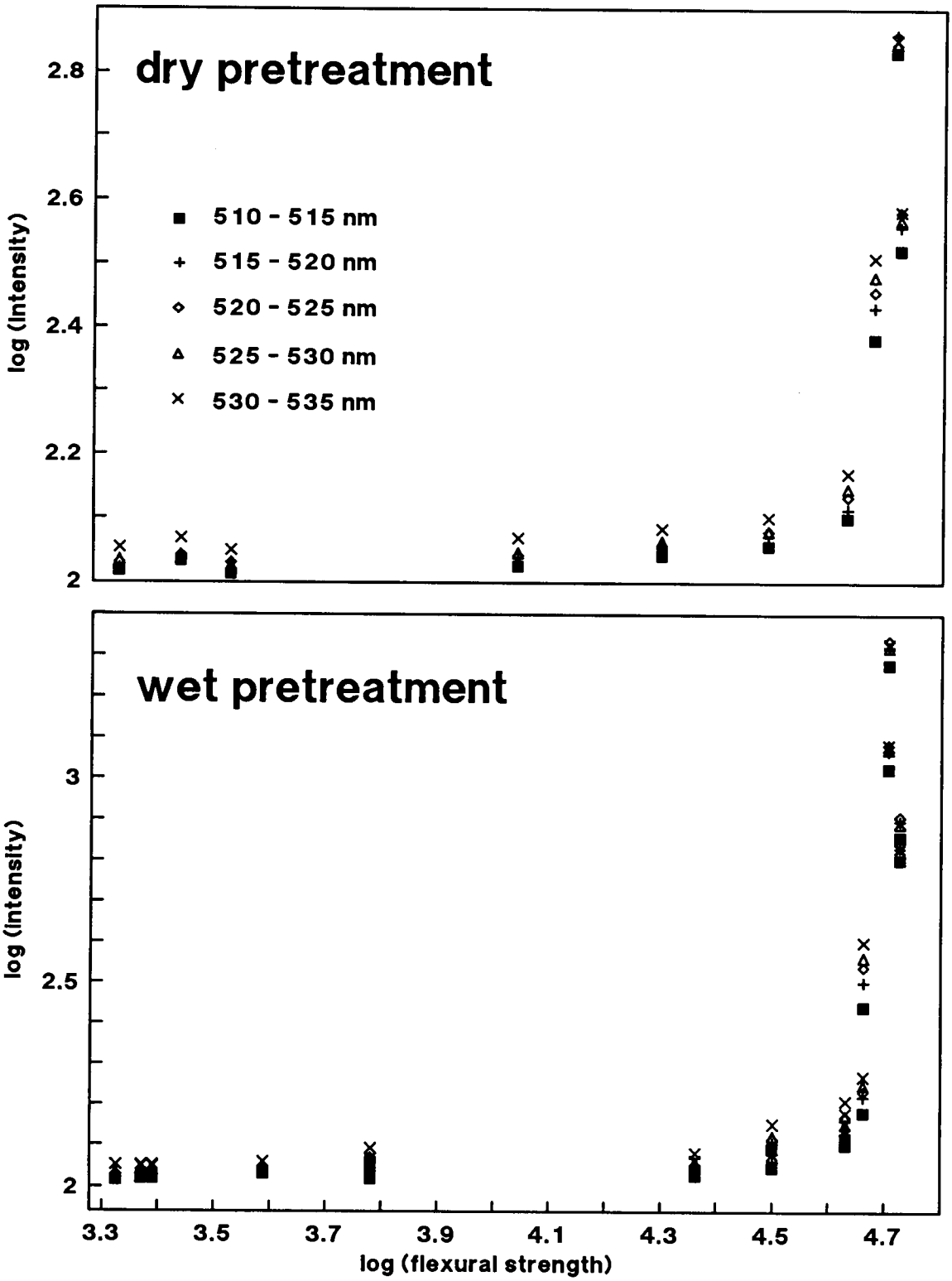

Fig. 17. Laser-pumped fluorescence using 482.5-nm excitation (separated by dry and wet pretreatment).

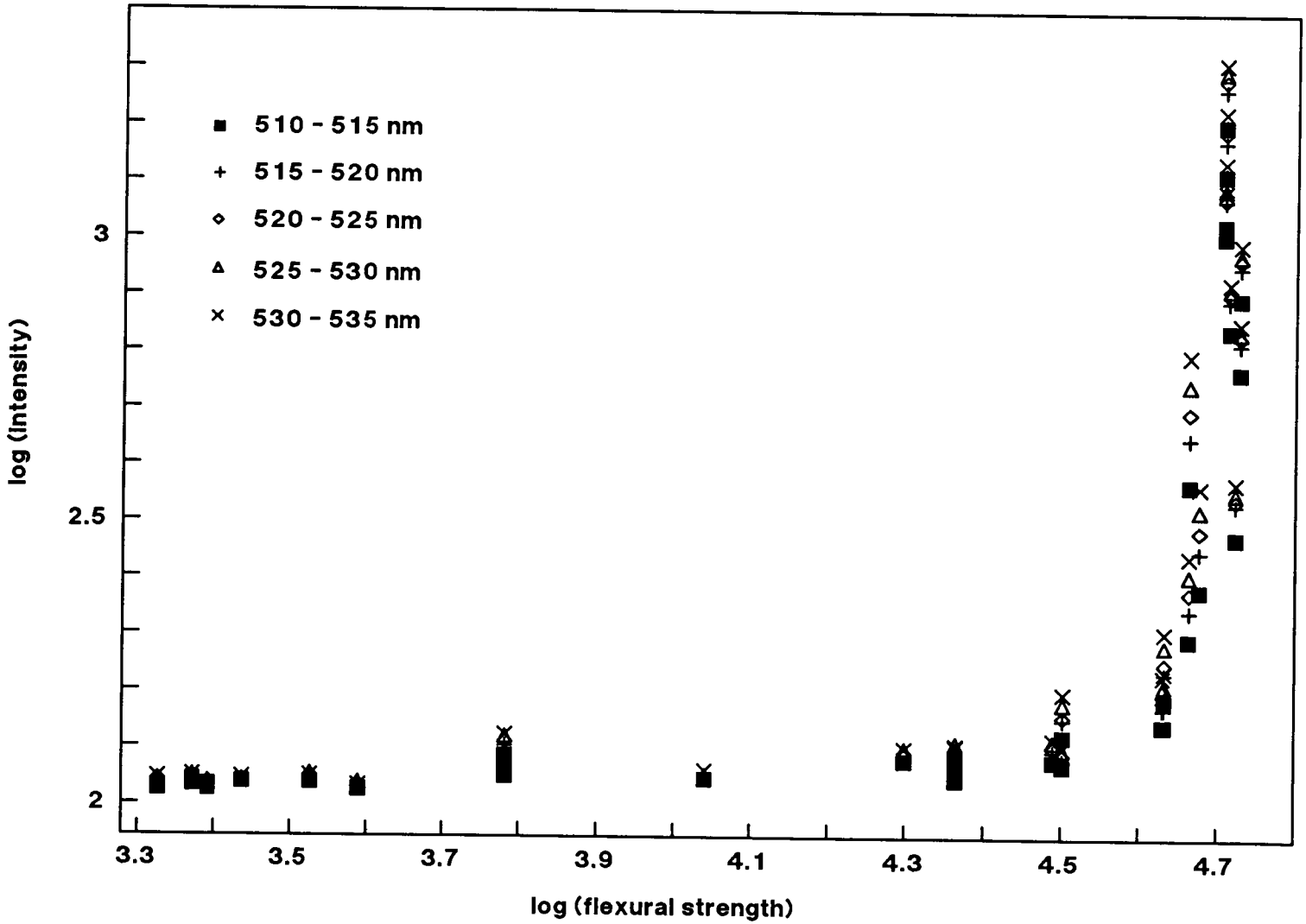

Fig. 18. Laser-pumped fluorescence using 488.0-nm excitation.

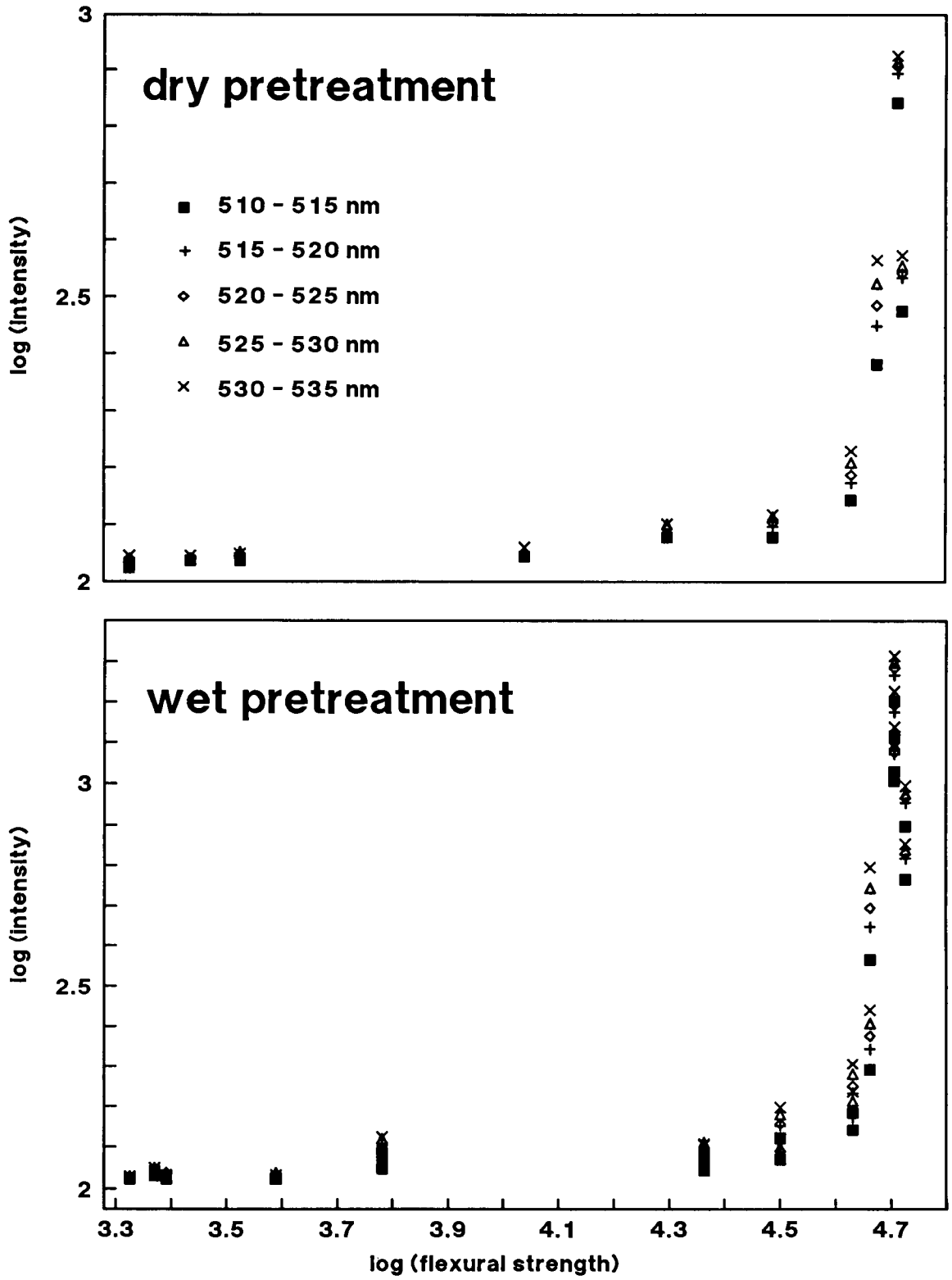

Fig. 19. Laser-pumped fluorescence using 488.0-nm excitation (separated by dry and wet pretreatment).

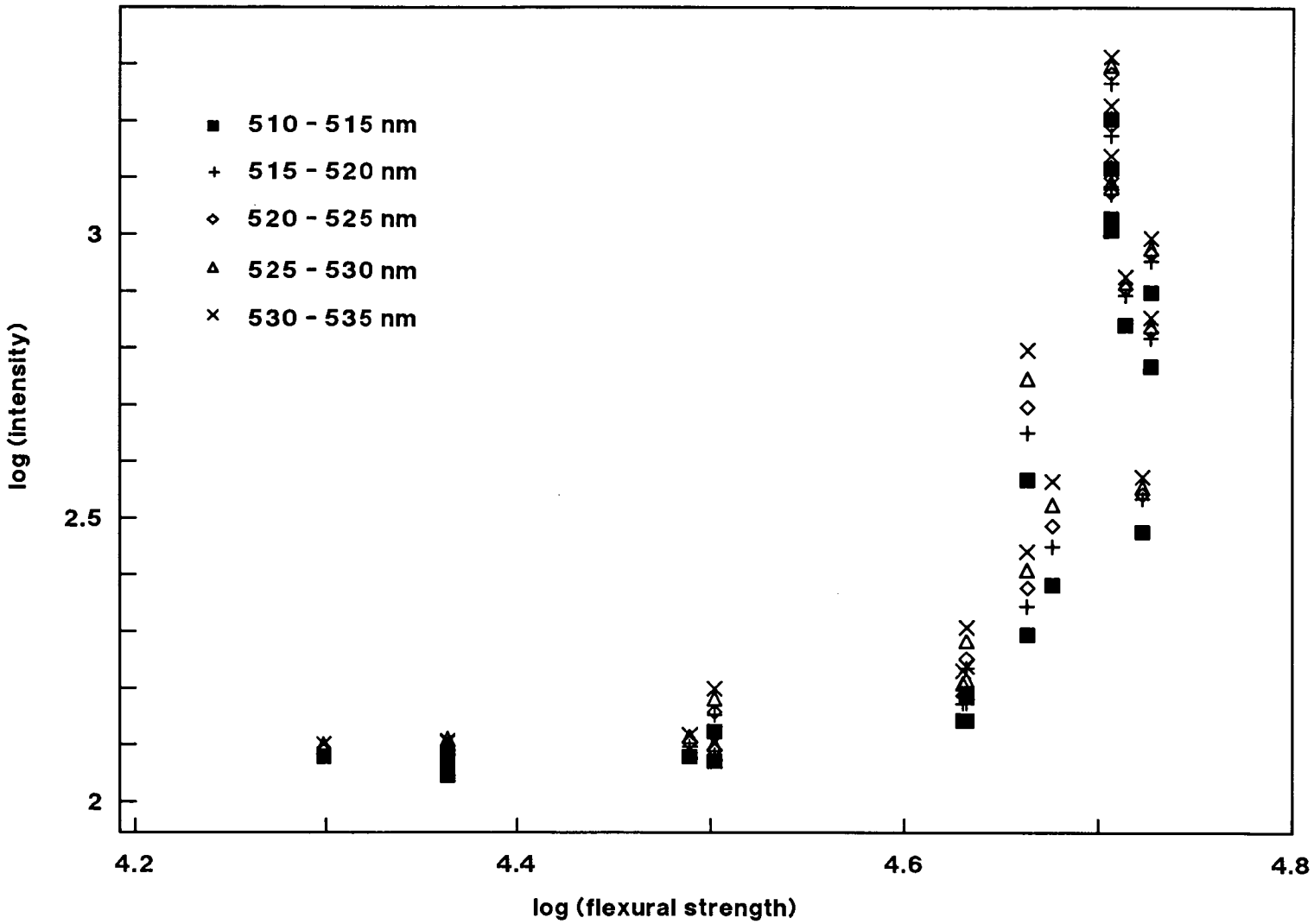

Fig. 20. Laser-pumped fluorescence using 488.0-nm excitation [(close-up view from 4.2 to 4.8 log (flexural strength)].

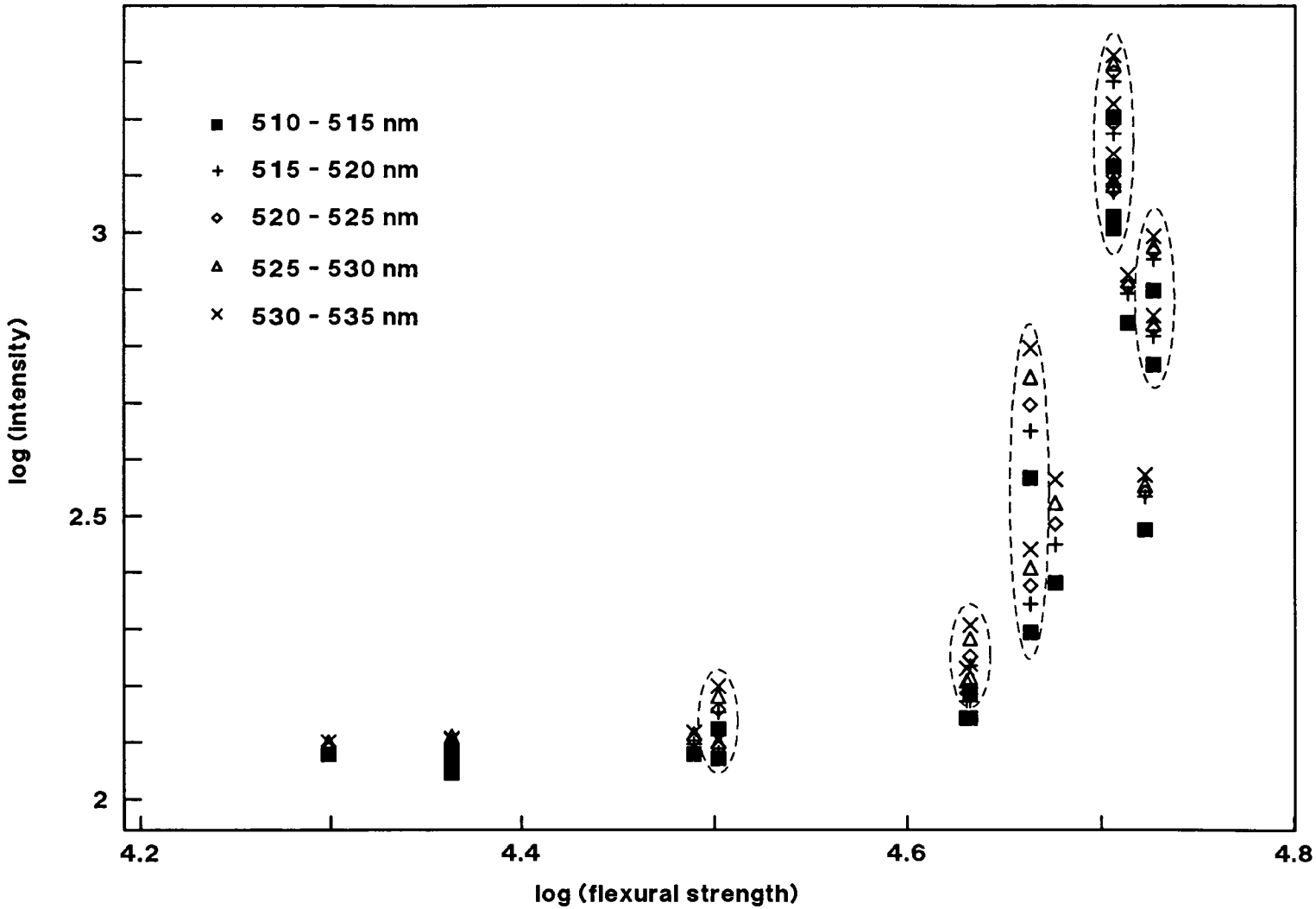

Fig. 21. Laser-pumped fluorescence using 488.0-nm excitation (with circled wet pretreatment).

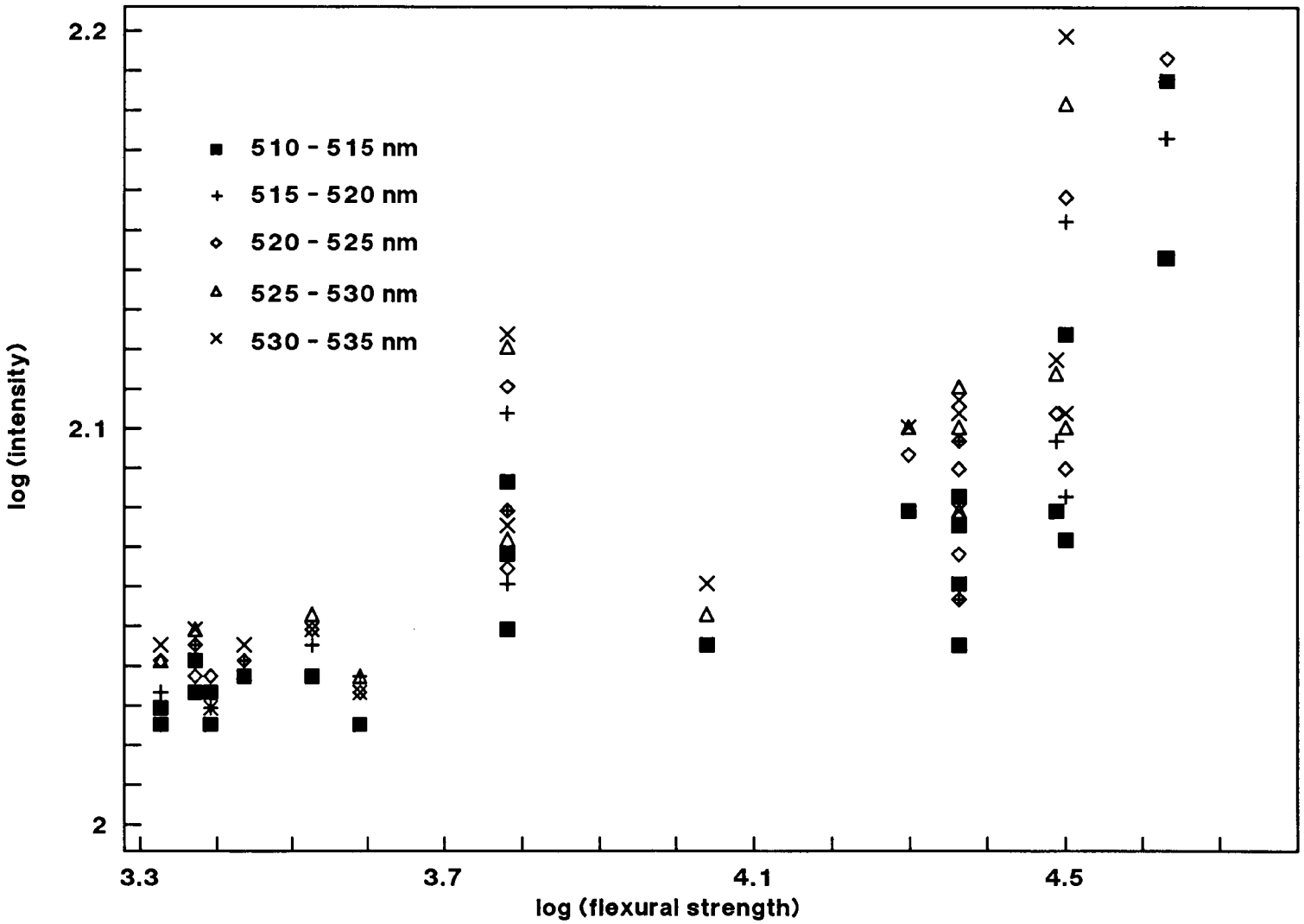

Fig. 22. Laser-pumped fluorescence using 488.0-nm excitation [with expanded log (intensity)].

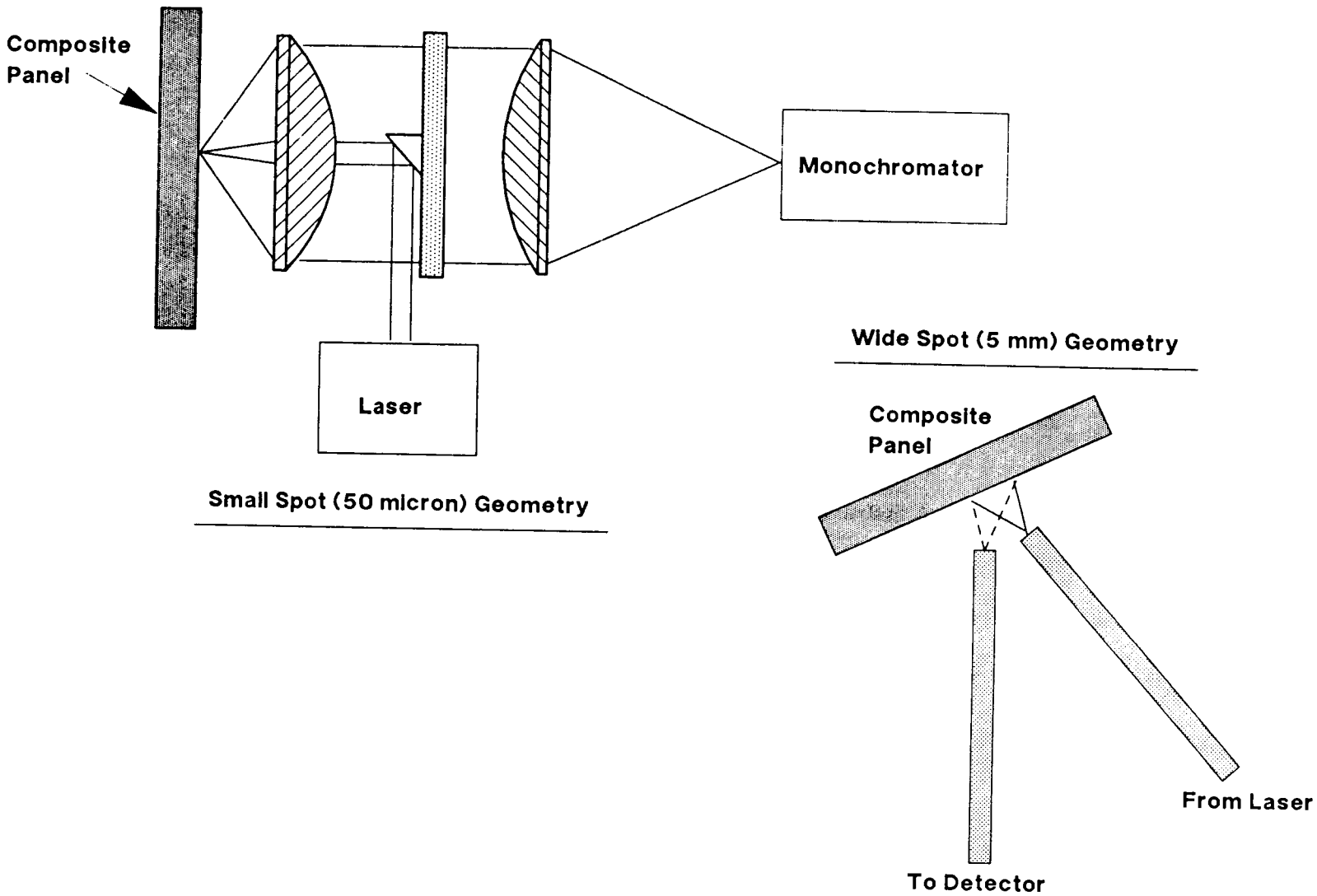

Fig. 23. Optical geometries used for LPF.

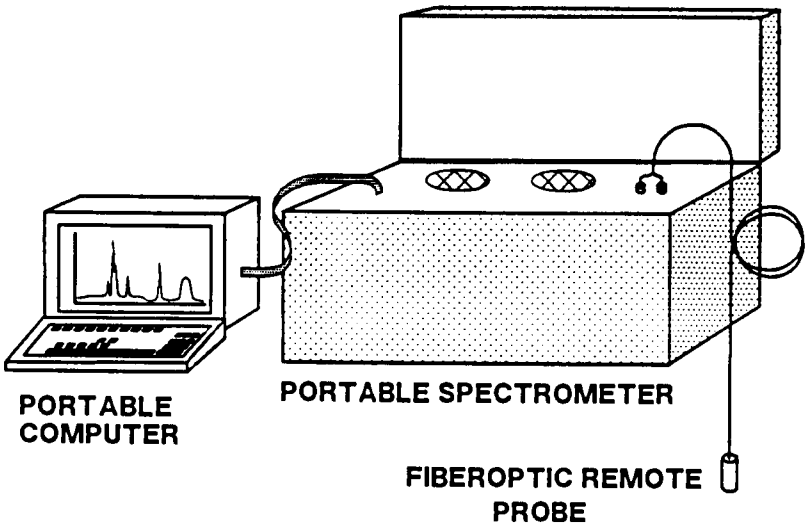

Fig. 24. ORNL field laser spectrometer system.

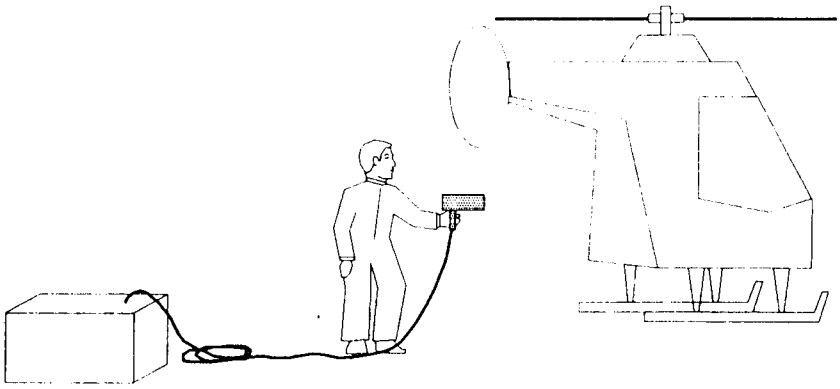

(a)

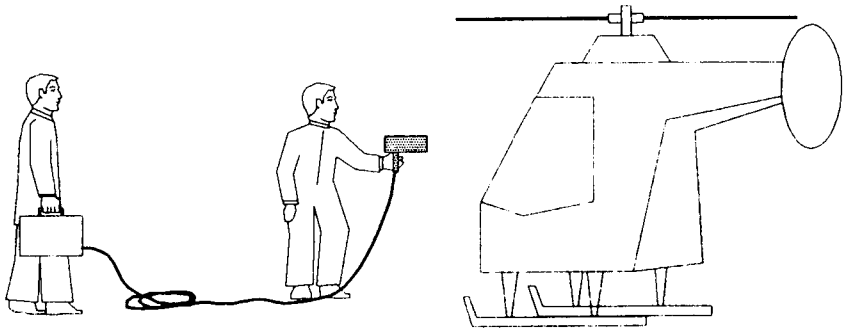

(b)

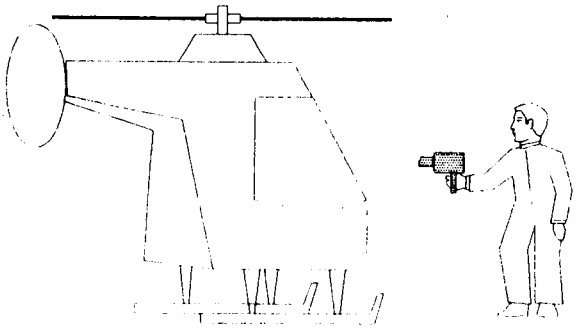

(c)

Fig. 25. Potential LPF instruments. *(a)* Mobile reader with fiber-optic probe, *(b)* portable reader with fiber optic probe, *(c)* self-contained reader.

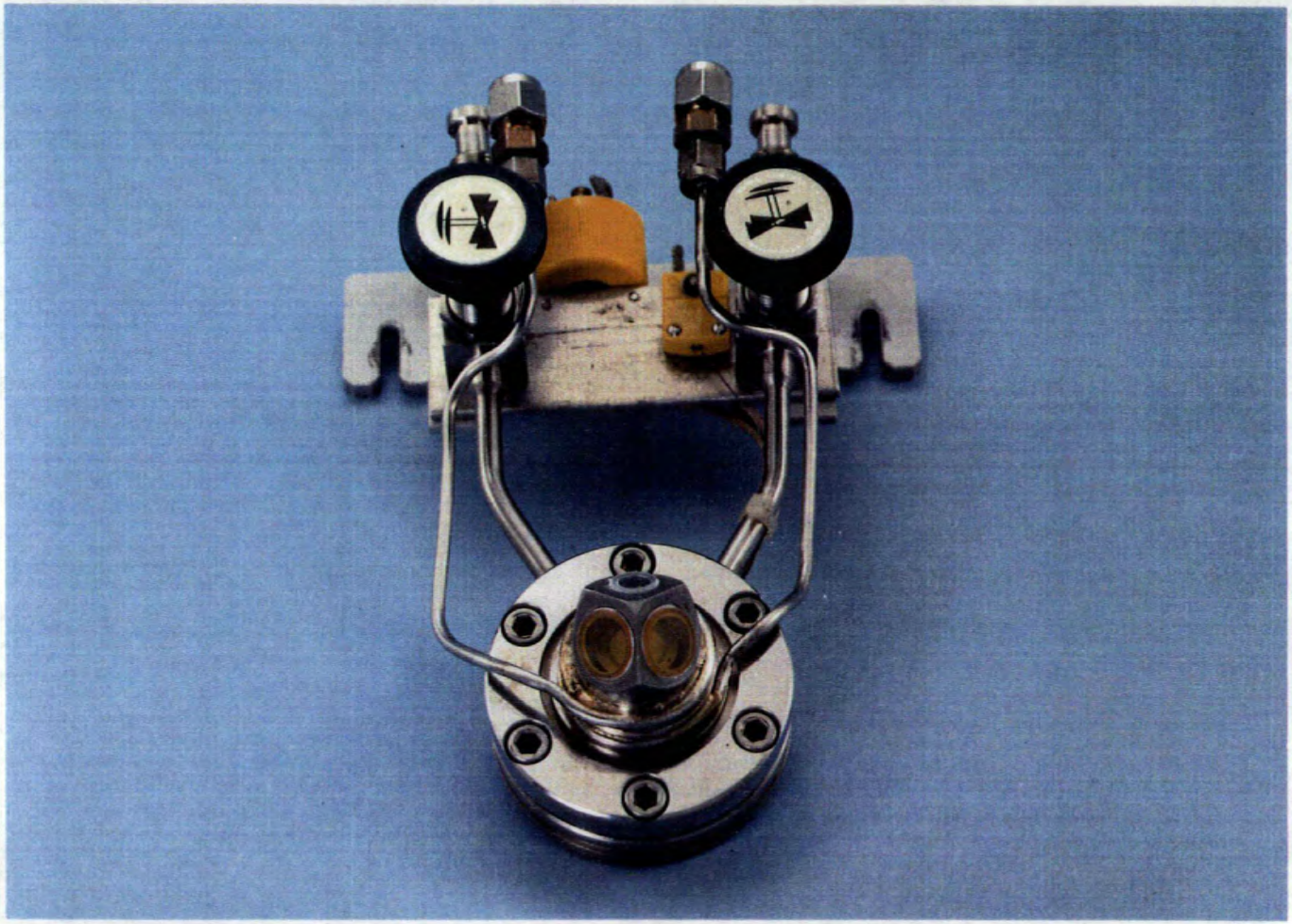

Fig. 26. An evacuable cell for use with a Harrick DRA-3CQ praying mantis diffuse reflectance cell. Note valves for gas inlet and exhaust lines and valves, ZnSe windows (right-beam entrance, left-beam exit), quartz window for viewing the sample, water cooling lines (small tubing), and 2-3/4-in. ultra-high-vacuum flange.

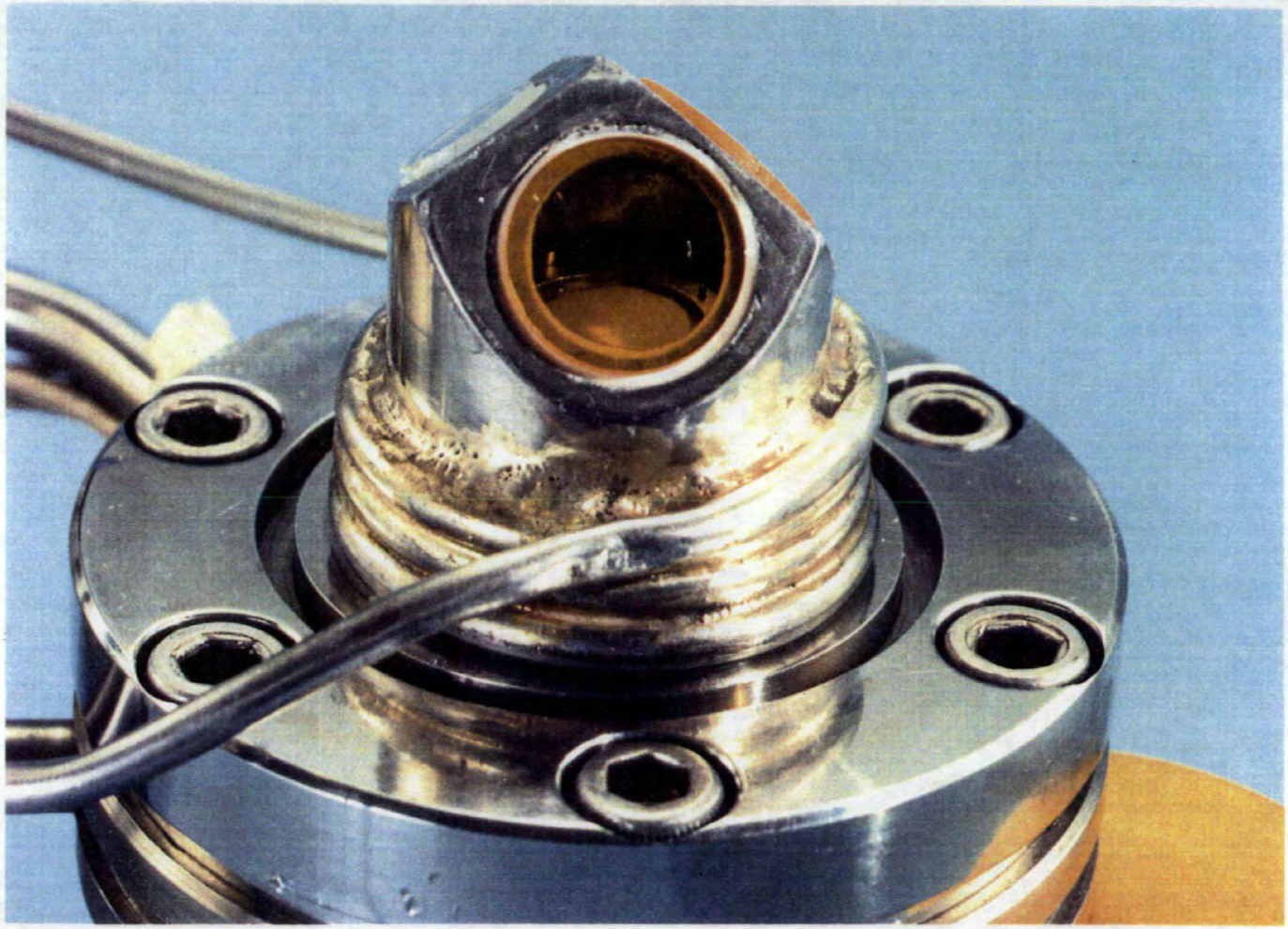

Fig. 27. An evacuable cell for use with a Harrick DRA-3CQ praying mantis diffuse reflectance cell showing the sample stage through the beam exit window. Note gas supply tube on the left of the stage, thermocouple on the right of the stage, and the sample position is indicated by the light colored disc.

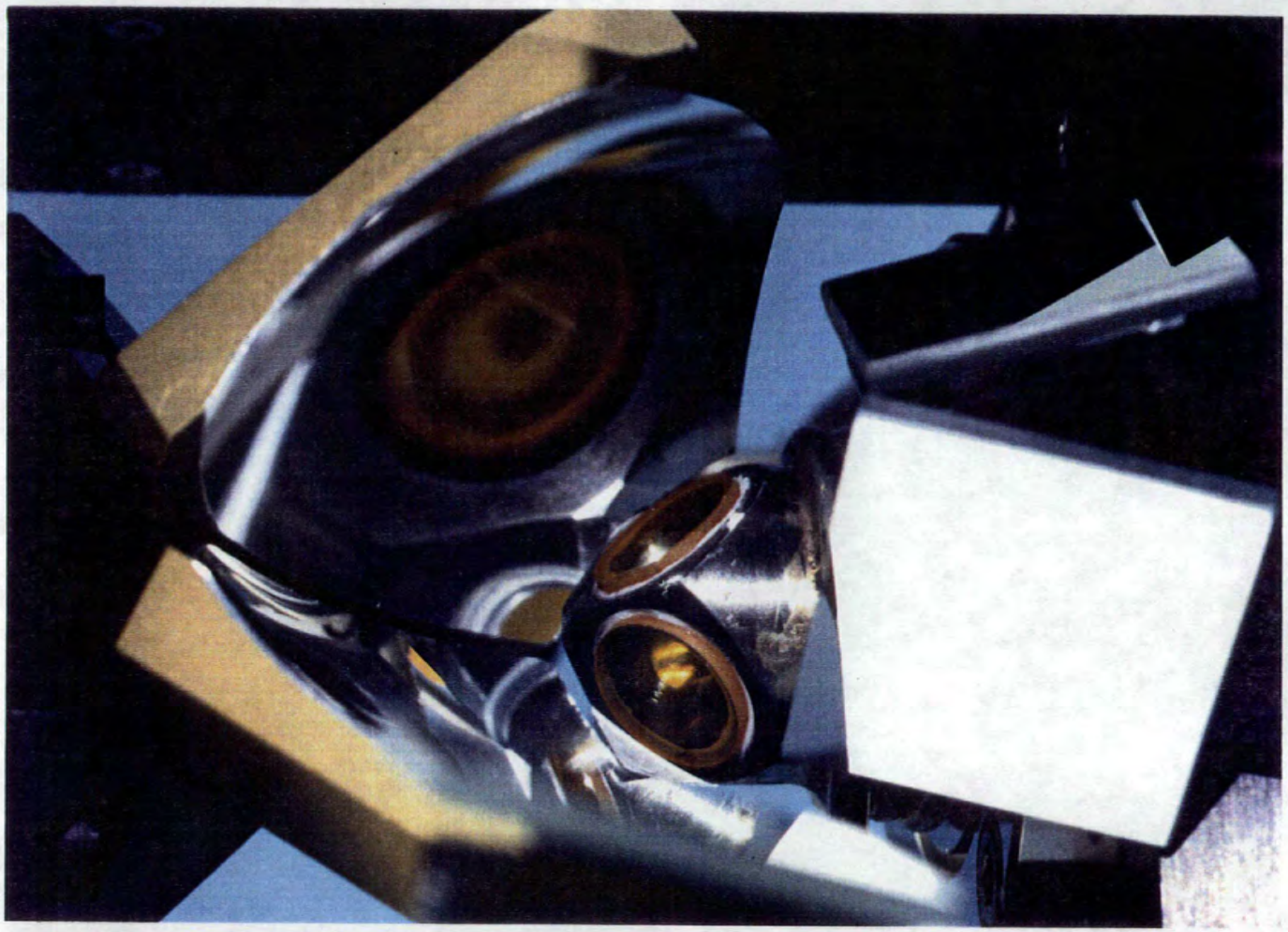

Fig. 28. An evacuable cell for use with a Harrick DRA-3CQ praying mantis diffuse reflectance cell mounted in the praying-mantis sample compartment optics. The spectrometer beam enters from the left striking the white mirror where it is deflected to the mirror in the left foreground (out of focus). The beam is then focused onto the sample stage by the entrance parabolic mirror (right side with the sample stage imaged in it). Diffusely scattered light is collected by the exit parabolic mirror (left side) and transferred out of the sample compartment by a flat mirror out of the picture to the right and the flat mirror on the lower right. The sample stage is imaged in the beam entrance paraboloid.

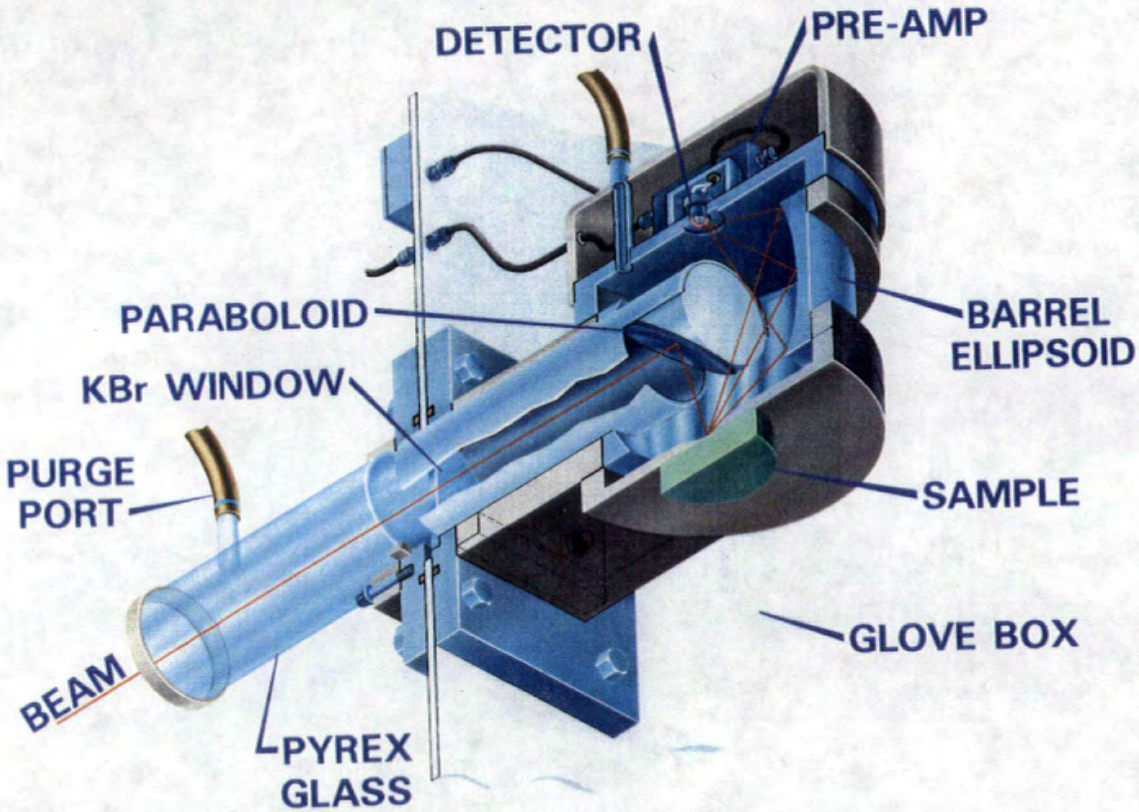

Fig. 29. An artist concept of the barrel-ellipsoid diffuse-reflectance inspection accessory. In the present application the accessory was attached to the external port of the FTS-60 spectrometer in an inverted position so that the sample lay on top of the accessory.

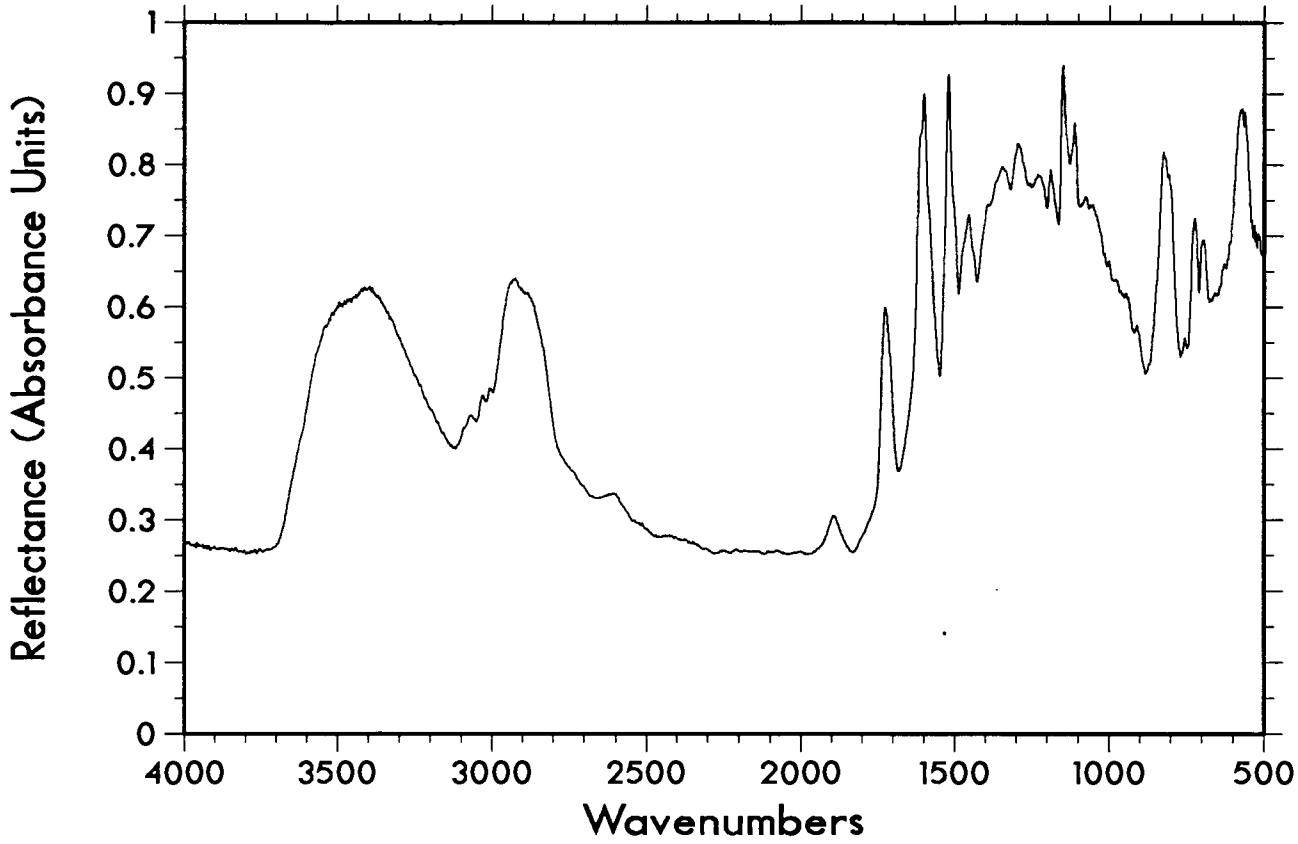

Fig. 30. A diffuse reflectance spectrum of a 0° IM6/3501-6 flexural specimen using the barrel ellipsoid inspection accessory using resin-free IM6 graphite fibers as a background spectrum.

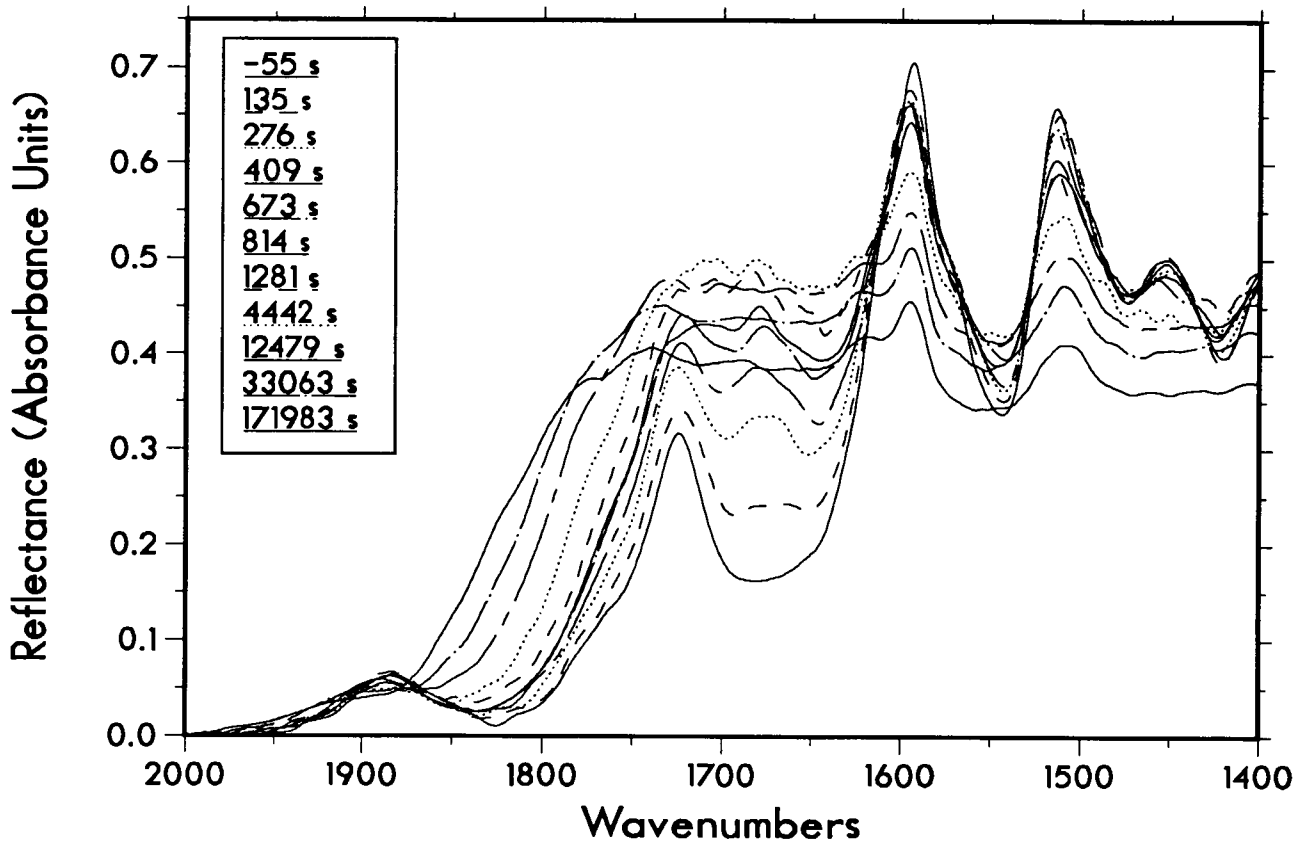

Fig. 31. Diffuse reflectance spectra showing the carbonyl region of the spectrum obtained from an IM6/3501-6 laminate specimen in the evacuable cell at the indicated time intervals in flowing air at 553°F. At t = 0 s an argon purge was switched to an air purge.

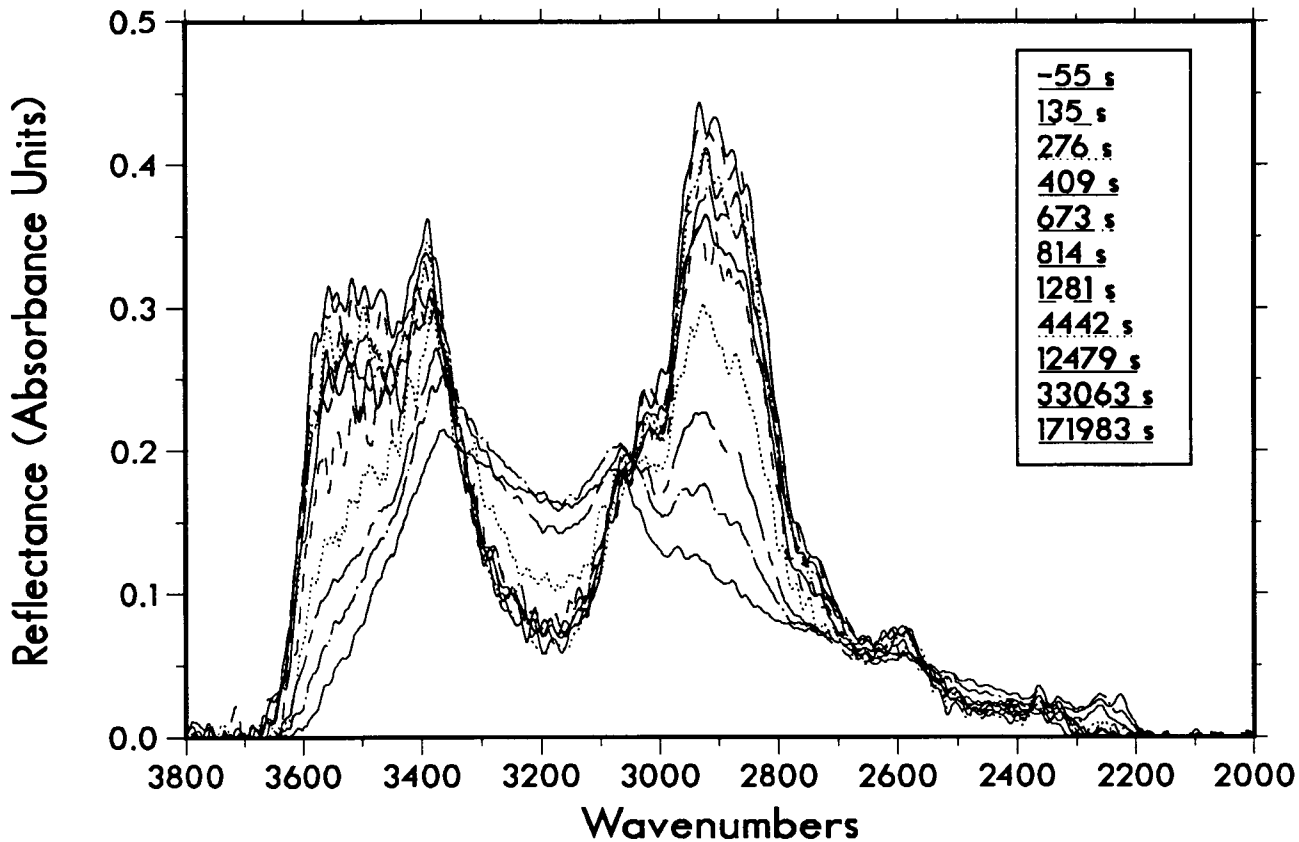

Fig. 32. Diffuse reflectance spectra showing the C-H, N-H, O-H region of the spectrum obtained from an IM6/3501-6 laminate specimen in the evacuable cell at the indicated time intervals in flowing air at 553°F. At t = 0 s an argon purge was switched to an air purge.

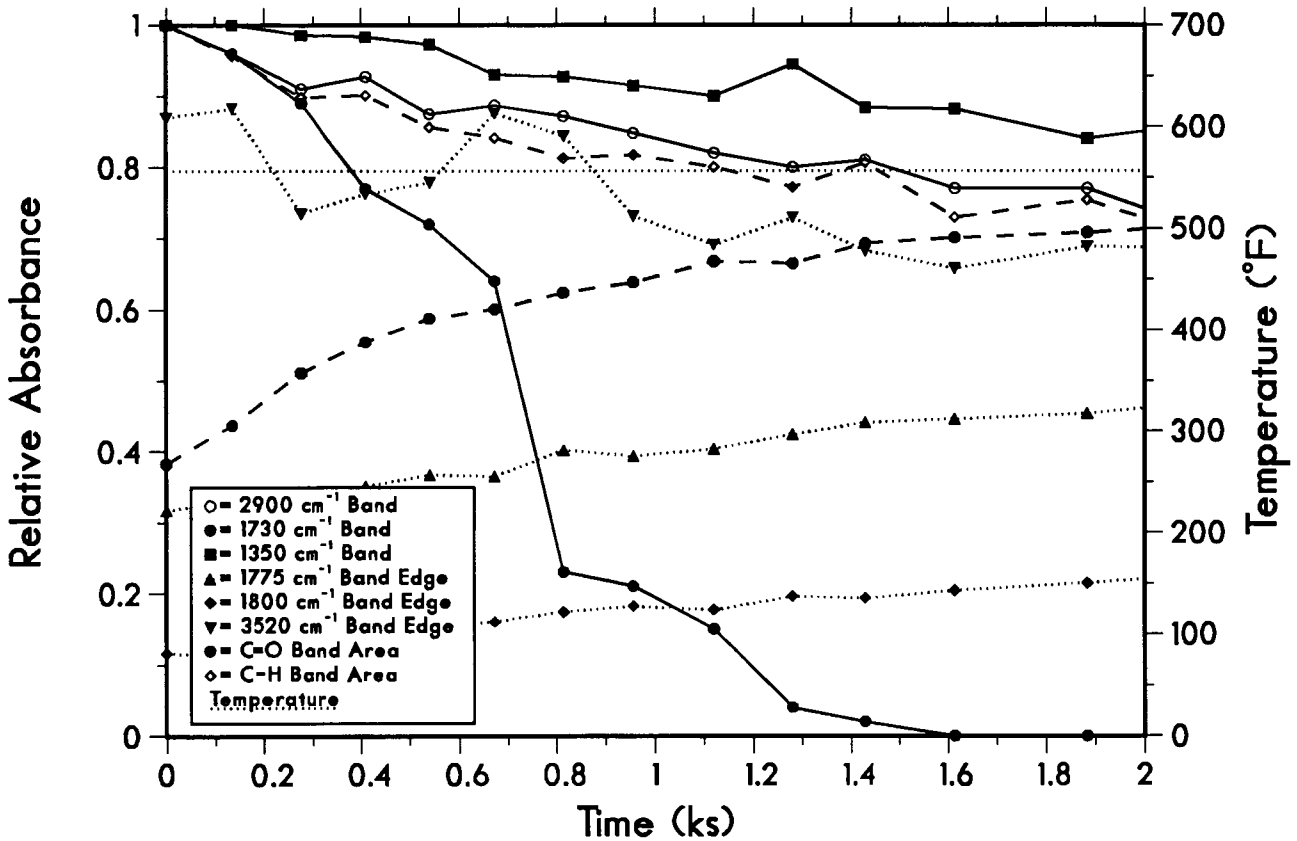

Fig. 33. Normalized reduced spectral data as a function of time for the oxidation of an IM6/3501-6 laminate specimen reacting with air at 553°F at early times.

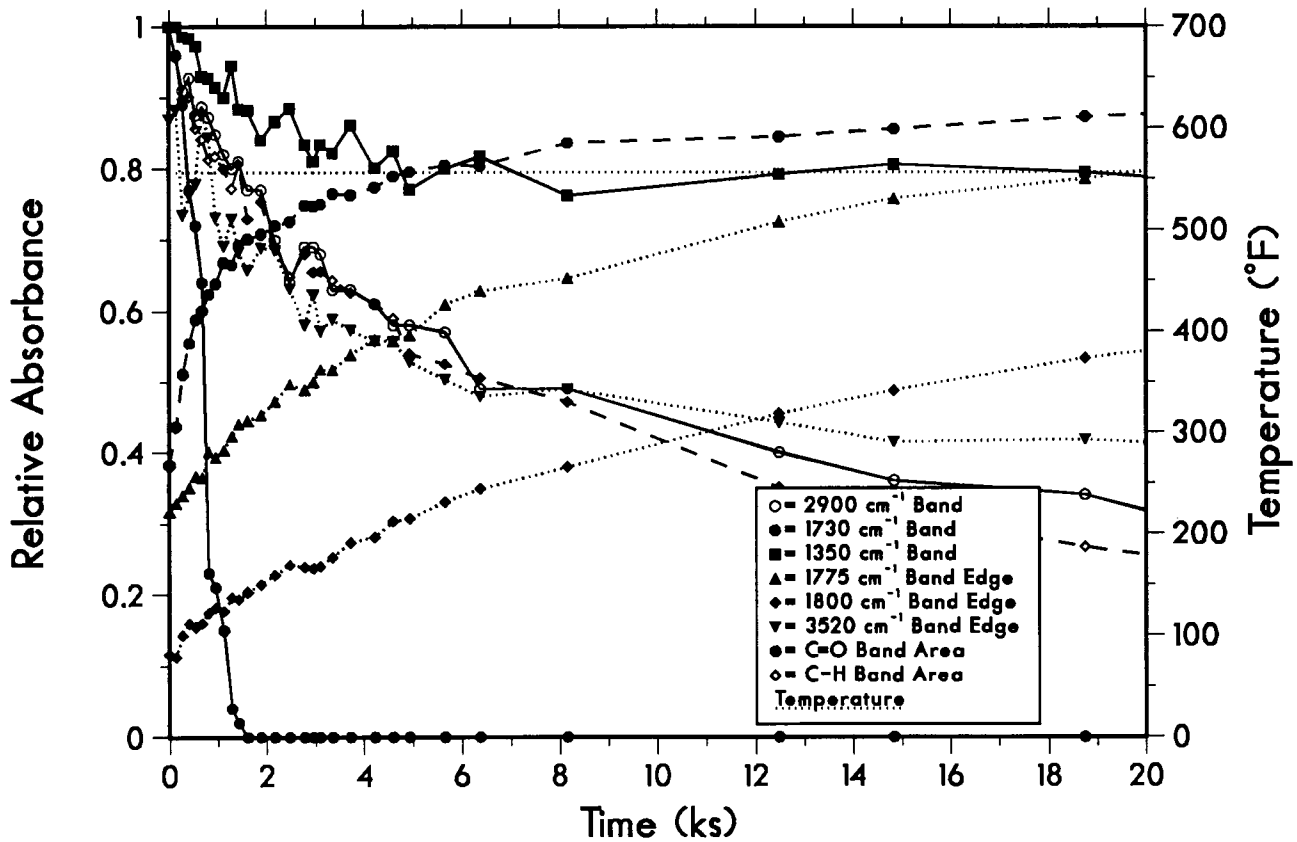

Fig. 34. Normalized reduced spectral data as a function of time for the oxidation of an IM6/3501-6 laminate specimen reacting with air at 553°F at medium times.

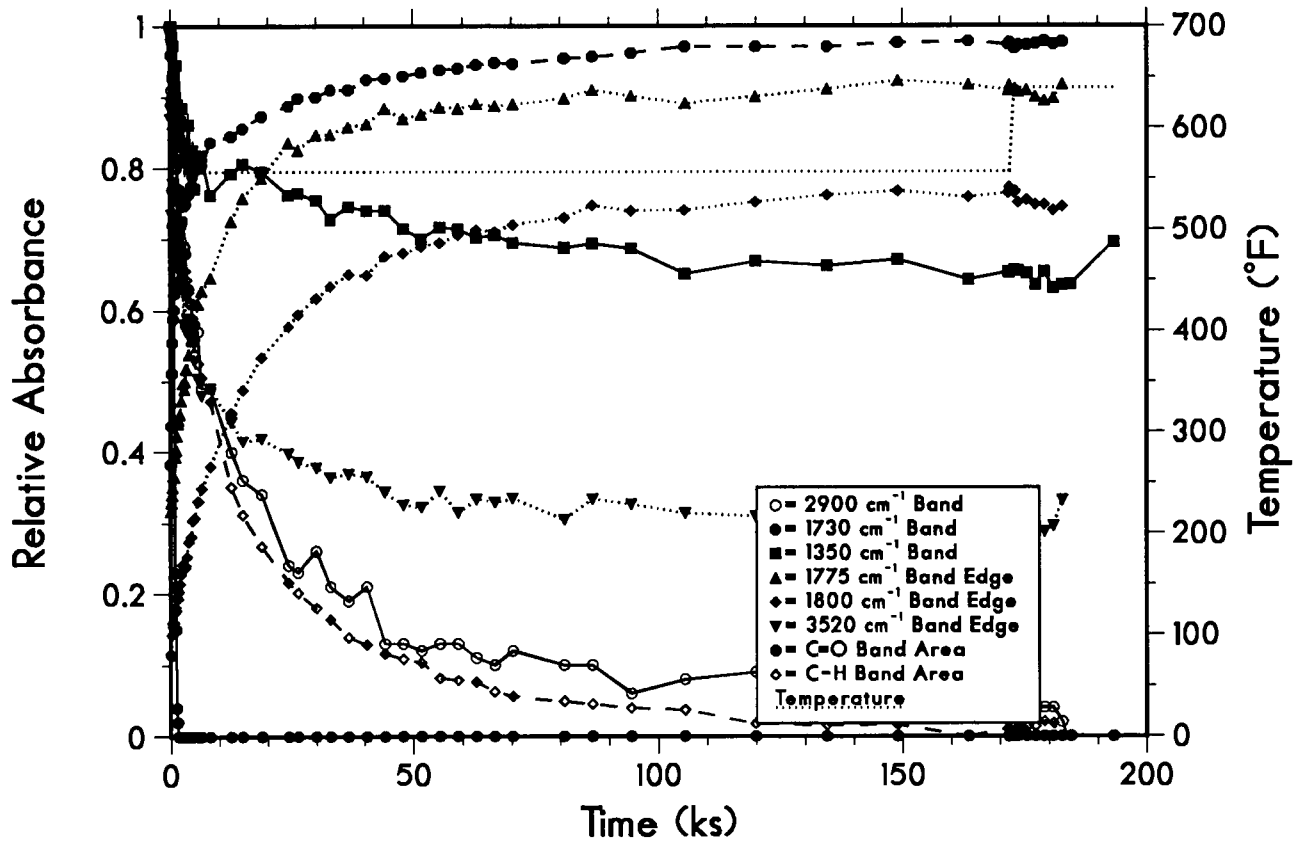

Fig. 35. Normalized reduced spectral data as a function of time for the oxidation of an IM6/3501-6 laminate specimen reacting with air at 553°F at long times.

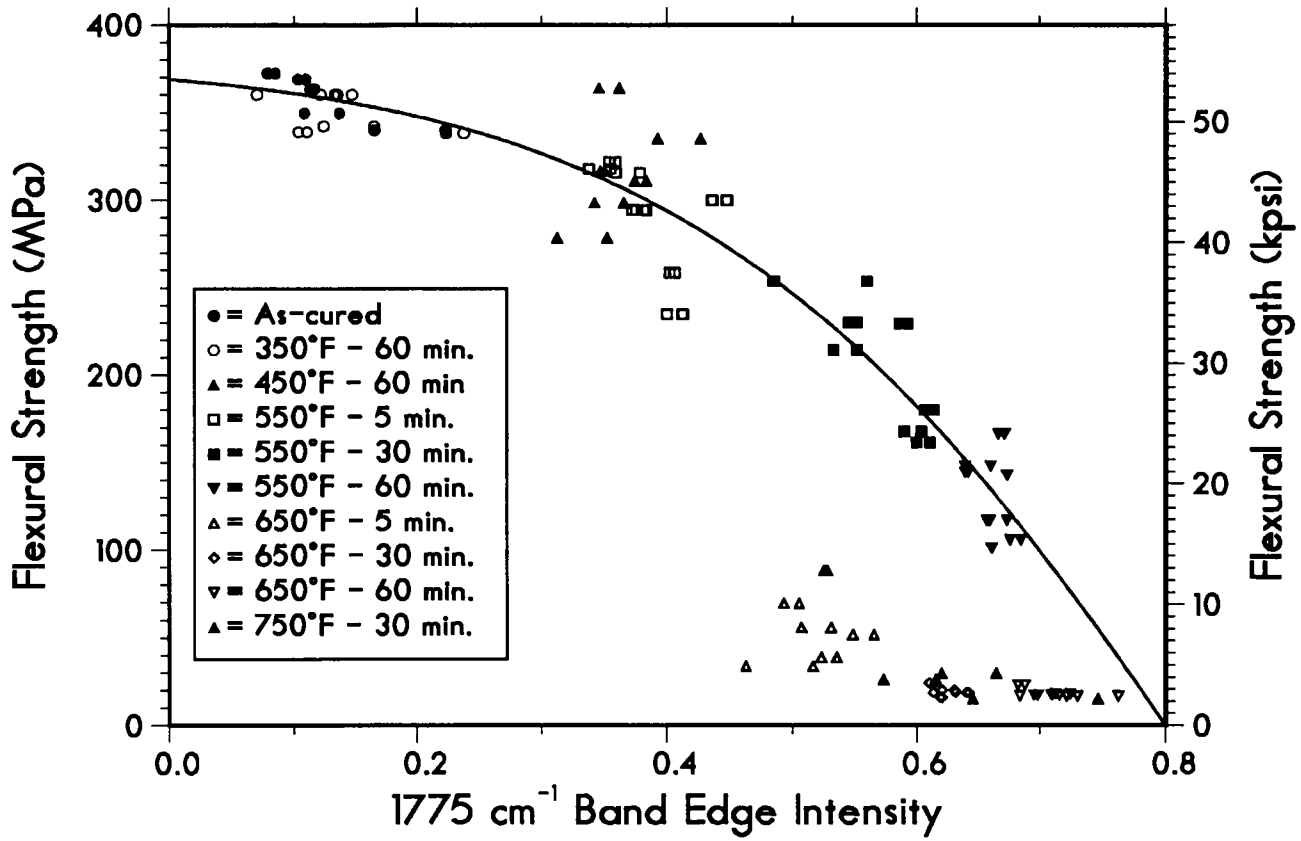

Fig. 36. Flexural strength data for 0° IM6/3501-6 laminate specimens as a function of the 1775 wavenumber band edge intensity.

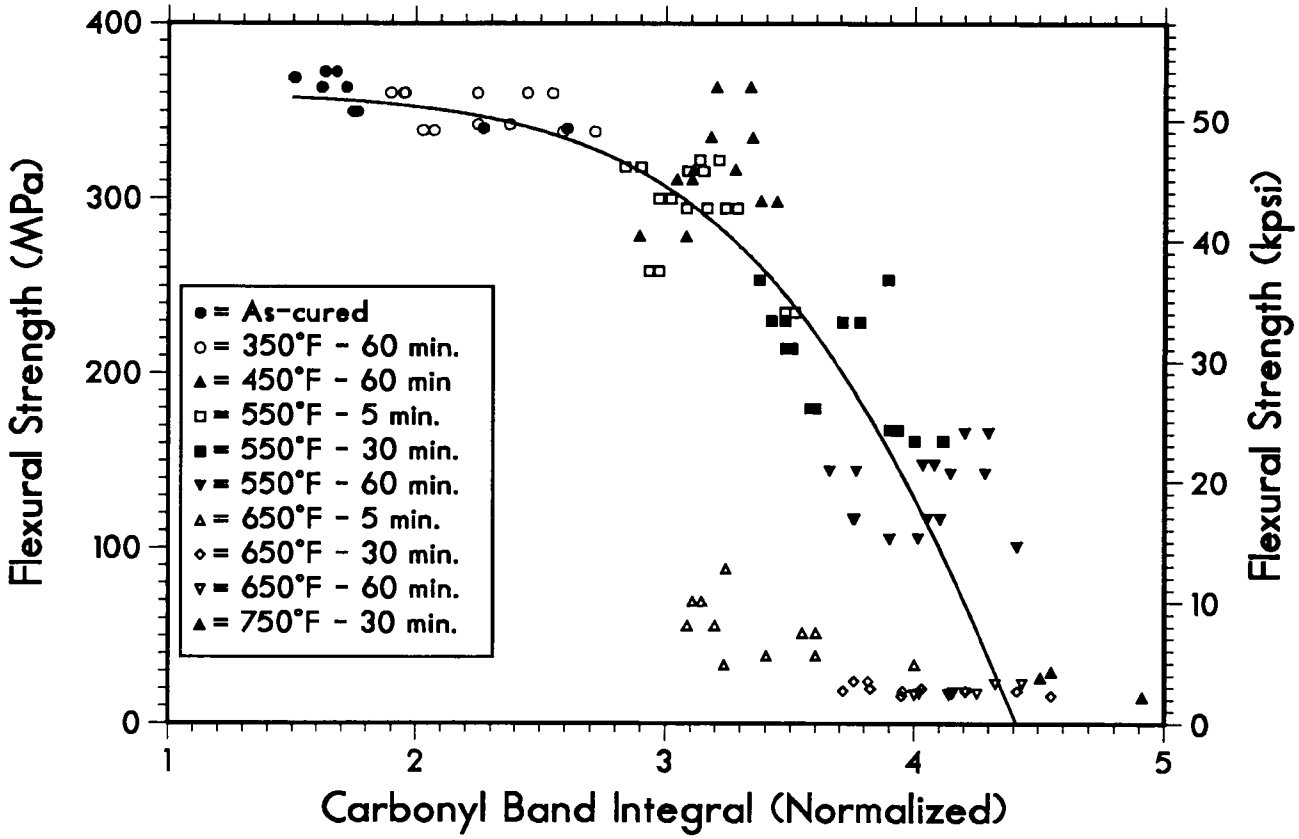

Fig. 37. Flexural strength data for 0° IM6/3501-6 laminate specimens as a function of the normalized carbonyl (C = 0) band integral.

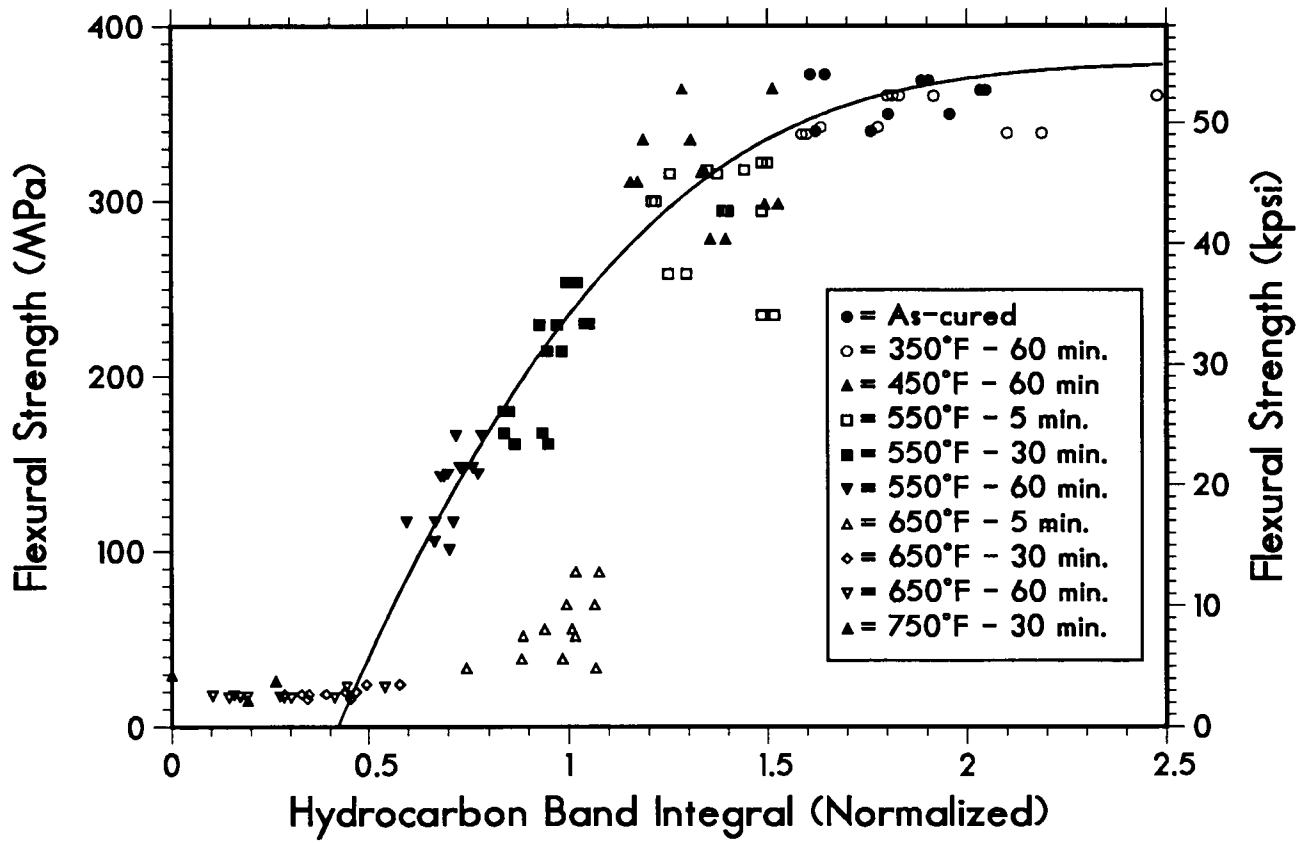

Fig. 38. Flexural strength data for 0° IM6/3501-6 laminate specimens as a function of the normalized hydrocarbon band integral.

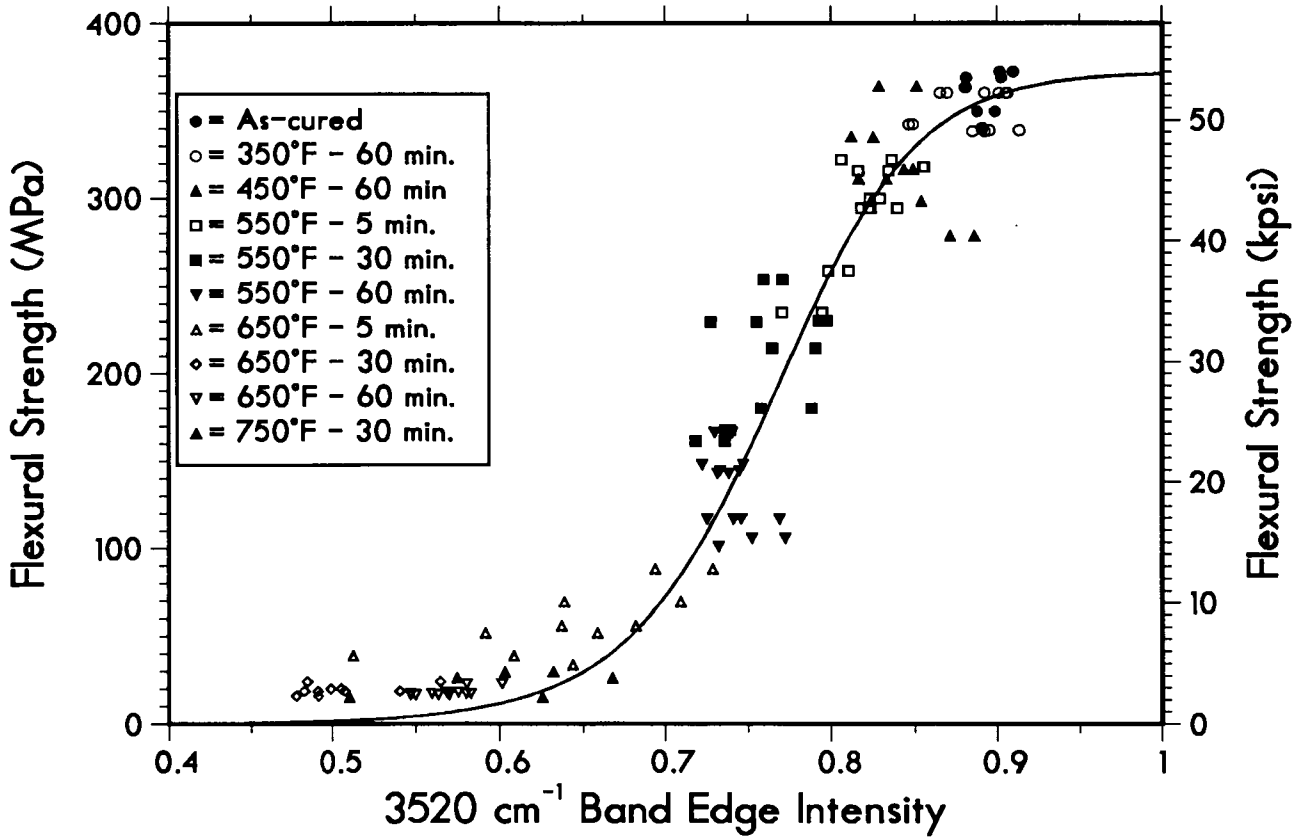

Fig. 39. Flexural strength data for 0° IM6/3501-6 laminate specimens as a function of the 3520 wavenumber (hydroxyl, O-H) band edge intensity.

REFERENCES

1. B. J. Frame, et al., *Composite Heat Damage, Part 1. Mechanical Testing Of IM6/3501-6 Laminates, Part 2. Nondestructive Evaluation Studies Of IM6/3501-6 Laminates,* ORNL/ATD-33, Martin Marietta Energy Systems, Inc., Oak Ridge Natl. Lab., May 1990.

2. T. A. Collings and D. L. Mead, "Effect of High Temperature Spikes on a Carbon Fibre-Reinforced Epoxy Laminate," *Composites* **19**(1), 61-66 (1988).

3. A. Ankara, D. Weisgerber and J. Vilsmeier, "Influence of Thermal Spiking on Properties of Carbon Fibre Reinforced Plastic," *Materials Science and Technology* **2**, 1081-1085 (1986).

4. A. C. Loos and G. S. Springer, "Effects of Thermal Spiking on Graphite-Epoxy Composites," *J. Composite Materials* **13**, 17-34 (1979).

5. C. A. Griffis et al., "Degradation in Strength of Laminated Composites Subjected to Intense Heating and Mechanical Loading," *J. Composite Materials* **20**, 216-235 (1986).

6. B. L. Burton, "The Effects of Moisture Absorption on a Variety of Cured Epoxy Resins," *18th International SAMPE Technical Conference Series* **18**, 124-134 (1986).

7. O. K. Joshi, "The Effect of Moisture on the Shear Properties of Carbon Fibre Composites," *Composites* **14**(3), 196-200 (1983).

8. R. E. Allred, "The Effect of Temperature and Moisture Content on the Flexural Response of Kevlar/Epoxy Laminates: Part I. [0/90] Filament Orientation and Part II. [‡45,0/90] Filament Orientation," *J. Composite Materials* **15**, 100-32 (1981).

9. M. F. Ashby and D. R. H. Jones, " Kinetic Theory of Diffusion and the Oxidation of Materials," pp. 165-172 and 193-201 in *Engineering Materials. An Introduction to their Properties and Applications*, A. Wheaton & Co. Ltd., Exeter, 1980.

10. H. M. Clancy and D. E. Lutfi, "Moisture in Composites-A Reminder," *18th International SAMPE Technical Conference Series* **18**, 135-141 (1986).

11. G. A. Pering, P. V. Farrell and G. S. Springer, "Degradation of Tensile and Shear Properties of Composites Exposed to Fire or High Temperature," *J. Composite Materials* **14**, 54-68 (1980).

12. R. J. Morgan and E. T. Mones, "The Effect of Thermal Environment and Sorbed Moisture on the Durability of Epoxies," *11th National SAMPE Technical Conference Series* **11**, 218-232 (1979).

13. L. W. Ashford, "Analysis and Test of Carbon/Bismaleimide Laminates Subjected to Internal Pressures Resulting from Trapped Moisture," *18th International SAMPE Technical Conference Series* **18**, 379-389 (1986).

14. C. A. Griffis, R. A. Masumura and C. I. Chang, "Thermal Response of Graphite Epoxy Composite Subjected to Rapid Heating," *J. Composite Materials* **15**, 427-442 (1981).

15. J. F. Haskins, "Thermal Aging," *SAMPE Journal* **25**(2), 29-33 (1989).

16. R. J. Morgan and J. E. O'Neal, "The Durability of Epoxies," *Polm.-Plast. Technol. Eng.,* **10**(1), 49-116 (1978).

17. T. A. Collings and D. E. W. Stone, "Hygrothermal Effects in CFC Laminates: Damaging Effects of Temperature, Moisture and Thermal Spiking," *Composite Structure* **3**, 341-378 (1985).

18. R. L. Levy, D. L. Fanter and C. J. Summers, "Spectroscopic Evidence for Mechanochemical Effects of Moisture in Epoxy Resins," *J. Appl. Polym. Sci.* **24**, 1643-1664 (1979).

19. W. W. Wright, "The Effect of Diffusion of Water into Epoxy Resins and their Carbon-Fibre Reinforced Composites," *Composites* 201-205 (1981).

20. G. A. Luoma and R. D. Rowland, "Environmental Degradation of an Epoxy Resin Matrix," *J. Appl. Polym. Sci.* **32**, 5777-5790 (1986).

21. R. J. Morgan and E. T. Mones, "The Cure Reactions, Network Structure, and Mechical Response of Diaminodiphenyl Sulfone-Cured Tetraglycidyl 4,4' Diaminodiphenyl Methane Epoxies," *J. Appl. Polym. Sci.* **33**, 999-1020 (1987).

22. "Magnamite[R] Graphite Prepreg Tape IM6/3501-6 Product Data Sheet, Number 865," Hercules Inc., (1986).

23. R. J. Morgan, J. E. O'Neal and D. L. Fanter, *J. Mater. Sci.* **15**, 751 (1980).

24. V. Chase and D. Beeler, *Manufacturing Methods for Large High Temperature Sandwich Structures*, AFML-TR-70-211, (1970).

25. R. J. Morgan, C. M. Walkup and T. H. Hoheisel, "Differential Scanning Calorimetry Studies of the Cure of Carbon Fiber-Epoxy Composite Prepregs," *J. Appl. Polym. Sci.* **30**, 289-296 (1985).

26. S. C. Lin, B. J. Bulkin, and E. M. Pearce, "Epoxy Resins. III. Application of Fourier Transform IR to Degradation Studies of Epoxy Systems," *J. Polym. Sci.: Polym. Chem. Ed.* **17**, 3121-3148 (1979).

27. K. C. Cole et al., "Comparison of Infrared Spectroscopic Methods for the Quantitative Analysis of Epoxy Resins Used in Carbon-Epoxy Composite Materials," *Appl. Spectrosc.* **42**, 761-769 (1988).

28. N. R. Smyrl, E. L. Fuller, and G. L. Powell, "Monitoring the Heterogenous Reaction of LiH with H_2O and CO_2 by Diffuse Reflectance Infrared Fourier Transform Spectroscopy," *Appl. Spectrosc.* **37**, 38 (1983).

29. E. L. Fuller, Jr. and N. R. Smyrl, "Chemistry and Structure of Coals; Diffuse Reflectance I.R. Spectroscopy Equipment and Techniques," *Fuel* **64**, 1143 (1985).

30. E. L. Fuller, Jr. et al., *Development of Diffuse Reflectance Infrared Spectroscopy Techniques and Theory for Surface Analysis*, *Y/DK-396*, Martin Marietta Energy Systems, Inc., Oak Ridge Y-12 Plant, 1985.

31. G. L. Powell et al., "The Barrel Ellipsoid Infrared Sampling Accessory for Remote Diffuse Reflectance and Emission Measurements," p. 1199, in Proceedings of *The Pittsburgh Conference in New York*, Abstract Book, Applied Spectroscopy Society, March 5-9, 1990.

32. M. A. Grayson and C. J. Wolf, "Low-Temperature Thermal Decomposition of an Epoxy Resin," *J. Polym. Sci.: Polym. Chem. ed.* **22**, 1897 (1984).

Internal Distribution

1. M. R. Cates
2. B. J. Frame
3. J. L. Frazier
4. J. G. Hubrig
5-14. C. J. Janke
15. W. S. Key
16. J. D. Muhs
17. R. E. Norris
18. H. E. Philpot
19. L. G. Powell
20. J. T. Shaffer
21. N. R. Smyrl
22. F. J. Smith
23. W. E. Smith
24. T. A. Vineyard
25. E. A. Wachter
26. D. A. Waters
27. R. E. Ziegler
28. Applied Technology Library
29. Central Research Library
30. Y-12 Technical Library
31. ORNL Patent Section
32-33. Laboratory Records Department
34. Laboratory Records - RC

External Distribution

35. M. B. Fennell, Code 35440, Marine Corps Air Station, Naval Aviation Depot, Cherry Point, NC 28533-5030
36. L. E. Radford, Code 35450, Marine Corps Air Station, Naval Aviation Depot, Cherry Point, NC 28533-5030
37. L. Scott, Code 840A, Marine Corps Air Station, Naval Aviation Depot, Cherry Point, NC 28533-5030
38. P. Campos, Code 5321, Navair Engineering Center, SESD, Lakehurst, NJ 08733
39. Doug Perl, Code 343, Naval Aviation Depot, North Island, San Diego, CA 92135
40. R. A. Retta, Code AIR-51412, Naval Air Systems Command, Washington, DC 20361-5140
41. Assistant Manager, Energy Research and Development, P.O. Box 2001, Oak Ridge, TN 37831-8600
42-43. Office of Scientific and Technical Information, P.O. Box 62, Oak Ridge, TN 37831